EJA

European Journal of Anatomy

Volume 26 - Number 3 May 2022

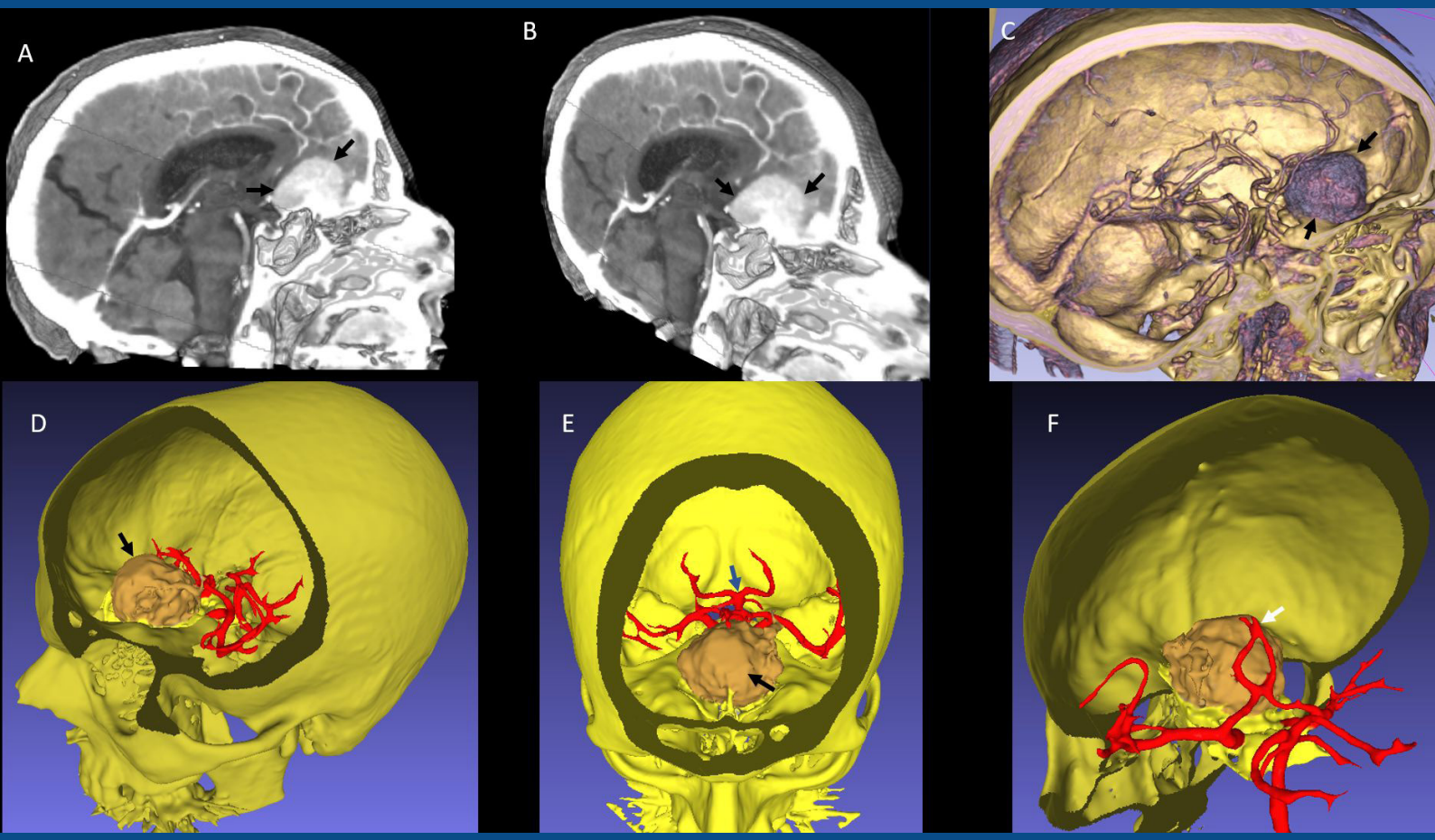

Indexed in:

CLARIVATE
- JCR:2020
- Q4 (21/23)
- I.F. J.C.I.: 0.19

DIALNET

EMBASE / Excerpta Medica

SCOPUS
- SJCR: 2020
- Q4 (31/39)
- I.F.: 0.162

Emerging Sources Citation Index

LATINDEX. Catálogo v1.0 (2002-2017)

Official Journal of the Spanish Society of Anatomy

www.eurjanat.com

EJA
European Journal of Anatomy

Volume 26 - Number 3 May 2022

Does altmetric score affect the impact factor of anatomy journals?

Asrın Nalbant

University of Bakırçay, Department of Anatomy, Faculty of Medicine, İzmir, Turkey

SUMMARY

The impact of a scientific article is measured by the impact factor (IF) of the journal in which it was published and the number of citations. The real impact is causing delays as citations happen over time. The Altmetric score originated as a measure of the digital dissemination of a scientific article across multiple social platforms**.** Our study aims to determine whether the Altmetric scores are related to the journal impact factor and the number of citations in the anatomy literature. The top 10 most cited articles were determined for the 15 anatomy journals with the highest impact factor in 2014, 2017 and 2019. Citation counts and Altmetric scores were recorded for each article. The relationship between the Altmetric score and 2019, 2017 and 2014 citation numbers were evaluated. It was also evaluated in correlation with the 2020 impact factor. At the same time, it was determined whether the articles had anatomical content or not.

In 2014, Altmetric scores did not correlate with citation number (r = 0.368, P = 0.177) and journal impact factor (r = 0.43, P = 0.52). In 2017, there was significant positive correlation between Altmetric scores and citation number (r = 0.914, P = 0.000), as well as between Altmetric scores and journal impact factor (r = 0.038, P = 0.003). Also significant positive correlation between 2017 Altmetric scores and 2019 impact factor (r = 0.065, P = 0.021). This study is the first to link traditional bibliometric measurements with newer digital dispersion measurements for anatomy publications. The Altmetric score correlates only weakly with citation numbers in the anatomy literature. However, the increase in the number of citations or the impact factor of the journals in which articles on anatomy are published shows that anatomy studies can be effective.

Key words: Altmetric score – Social media – Anatomy – Impact factor

INTRODUCTION

In order to determine the quality, distribution and impact of scientific research, the number of article citations and the impact factor of the journal in which the article is published are traditionally used methods (Nocera et al., 2019). The ubiquity of the Internet and social media in our daily lives has brought information to the public in its dissemination. Social media platforms continue to expand how information is shared, distributed, encountered and responded to in society. Various platforms such as Twitter, Facebook, blogs, Reddit and others, and online video sharing offer new opportunities for academic medical researchers

Corresponding author:
Asrın Nalbant. University of Bakırçay, Department of Anatomy, Faculty of Medicine, 35667 Seyrek/ Menemen, İzmir, Turkey. Phone: +90 232 493 00 00-1256; Fax: +90 0 232 844 71 22. E-mail: asrin.nalbant@bakircay.edu.tr - Orcid ID: 0000-0002-8538-3076.

Submitted: December 2, 2021. **Accepted:** February 1, 2022

https://doi.org/10.52083/UXMV4266

to expand their literature to the community (Priem et al., 2010). New bibliometric measurements using these platforms allow faster research dissemination and impact determination, unlike historical methods of citation count and journal impact factor calculations that may delay this process (Bornmann and Leydesdorff, 2014).

The extent of scientific research dissemination in the public sphere can be analyzed using the Altmetric attention score (AAS) (Elmor, 2018). AAS is the weighted number of all the research article's attention in the automatically calculated electronic media, including news sources and social media. It is a way of assessing the extent to which scientific research breakthroughs have spread to society. Its analysis provides an opportunity to gauge the public's relationship with a scientific field (Dagar and Falcone, 2021).

Recent research has analyzed the AAS of various medical and surgical subspecialties (Barakat et al., 2018; Patel et al., 2018; Nocera et al., 2019; Punia et al., 2019; Jia et al., 2020). A systematic review suggests that research studies' mentions of social media are associated with an increasing number of citations (Bardus et al., 2020). Similarly, a randomized controlled study found that tweeted articles received higher citations, with rates 9.5 times higher than articles randomized to the non-tweeted group (Luc et al., 2020; Hayon et al., 2019). This interest in the study of AAS in medicine reflects the reputation of a research study as a measure for assessing its impact on public access and academic impact.

To our knowledge, there are no previous studies in the anatomy literature comparing the relationships between traditional publication recognition bibliometry and Altmetric scores, including citation count and journal impact factor. This study aims to determine the correlation between these metrics to assess whether they are interchangeable measures of article influence and impact.

MATERIALS AND METHODS

We identified the 15 journals with the highest impact factor in Anatomy in 2014, 2017 (using Journal Citations Reports) (Clarivate, n.d.) (Clarivate, 2019. Journal citation report) and 2019 (using each journal website). While Journal Citation Reports utilizes the traditional impact factor to measure journal influence based on citable documents over two years, Scopus utilizes Citescore, which evaluates a 3-year citation window of all published document types. The results from searches the top 15 anatomy journals: *Human Brain Mapping, Frontiers in Neuroanatomy, Brain Topography, Brain Structure and Function, American Journal of Physical Anthropology, Journal of Anatomy, The Anatomical Record, Annals of Anatomy, Anatomical Sciences Education, American Journal of Surgical Pathology, Clinical Anatomy, Cell Tissues Organs, Journal of Histochemistry and Cytochemistry, American Journal of Human Biology, Anatomical Science International.*

All the original research articles published in these journals were extracted and tabulated. We used Dimensions (Digital Science & Research Solutions Inc.) to identify the AAS of included articles. We accessed this information to identify the top-10 most cited articles for 15 journals from January to December 2014. The same procedure was then used to identify the top-10 most cited articles from 2017 and 2019 for each of the journals above in order to account for changes in the Altmetric scoring system, shifts in the popularity and utilization of different social media platforms, and the overall advancement of the digital landscape of scientific research. The impact factor was assessed using Journal Citation Reports for each of the 15 journals in 2014, 2017 and 2019. The Altmetric score was recorded using the Altmetric bookmarklet for each of the 450 overall articles evaluated.

Statistics for this study were performed with SPSS V20. Kolmogorov–Smirnow test was used to control whether data were dispersed usually. Descriptive statistics were expressed as mean±SD for the continuous variables. Nonparametric analyses were applied, as the data were not normally distributed. Significant findings were interpreted using a predetermined P-value threshold of <.05. Mann Whitney U test was used to compare the articles according to their anatomy content. The correlation between the variables studied was determined using the

Spearman correlation coefficient (r), whereas the coefficient of determination (R2) was used to determine the proportion of variance in the data accounted for by the correlations discovered. This statistical analysis and methodological procedure were primarily derived from prior research that analyzed the correlation between the Altmetric score and citations in pediatric surgery and urology literature (Chang et al., 2019; Nocera et al., 2019).

RESULTS

Altmetric scores were recorded for the top 10 most-cited articles published in 2014 from each of the top 15 anatomy journals identified via Journal Citation Reports (Table 1). Hence, a total of 150 articles were analyzed from 2014. Citation count and journal impact factor showed a significant strong positive correlation in the 2014 cohort (r = 0.795, P <0.0001 for impact factor, Fig. 2). Altmetric scores were not associated with citation number for articles published in 2014 (r = 0.368, P = 0.177) and journal impact factor for manuscripts published in the same year (r = 0.032, P = 0.052; Fig. 1). This finding suggests that citation count and journal impact factor in the papers published in the 15 anatomy journals evaluated in 2014 are not strongly predicted by those articles' Altmetric scores.

The journals were also analyzed individually to determine a correlation coefficient between citation count and Altmetric score (Table 2). In 2014, only two journals out of the 15 analyzed had significant correlations between their articles' citation number and Altmetric scores. The journals with significant negative and positive associations between these variables included Anatomical Sciences Education (r = - 0.68, P = 0.02), American Journal of Surgical Pathology (r = 0.76 P = 0.01).

Altmetric scores were compared to citation count, and journal impact factor in 2017. Altmetric scores were significantly correlated with citation number for articles published in 2017 (r = 0.914, P = 0.000). Journal impact factor was also significantly correlated with Altmetric scores in the same group of articles evaluated from 2017 (r = 0.038, P = 0.003, Fig. 1). Citation count and journal impact factor showed a significant strong positive correlation in the 2017 cohort (r=0.724, P= 0.000. Fig. 2). The journals from 2017 were analyzed individually to determine a correlation coefficient between citation count and Altmetric score (Table 2). Only one of the 15 journals showed a significant correlation between the number of citations of their articles and the 2017 article Altmetric score. These journal with significant positive associations included Journal of Histochemistry and Cytochemistry (r = 0.67; P = 0.03).

Altmetric scores were compared to citation count, and journal impact factor in 2019. Altmetric scores were significant strong positive correlated with citation number for articles published in 2019 (r = 0.614, P = 0.000). Journal impact factor was also significantly correlated with Altmetric scores in the same group of articles evaluated from 2019 (r = 0.20, P = 0.01 Fig. 1). Citation count and journal impact factor showed a strong, positive correlation in the 2019 cohort (r=0.561, P= 0.000, Fig. 2). The journals from 2019 were analyzed individually to determine a correlation coefficient between citation count and Altmetric score (Table 2). No significant correlation was found in any of the journals between the number of citations of their articles and the 2019 article Altmetric score.

Comparisons between the Altmetric score and citation data in 2014, 2017 and 2019 vs journal impact factor in 2017, 2019 and 2020 were additionally performed. Altmetric score not associated with journal impact factor 2017 for articles published in 2014 (r=0.036, P = 0.43). Altmetric score significantly correlates with 2019 impact for articles published in 2017 (r= 0.65, P = 0.02). Altmetric score not associated with journal impact factor 2020 for articles published in 2019 (r= -0.011, P = 0.89, Fig. 1). In 2014 Citation count and journal impact factor in 2017 showed a significant strong positive correlation (r=0.728; P= 0.000). Journal impact factor in 2019 was also significantly correlated with citation count in the 2017 (r=0.657; P=0.000). Also journal impact factor in 2020 was significantly correlated with citation count in the 2019 (r=0.518; P=0.000, Fig. 2).

Table 1. Categorization of anatomy journal bibliometric and altmetric data.

Journal	Citations (Median [Range]) 2014	Altmetrics Score (Median [Range]) 2014	Journal Impact Factor (2014)	Citations (Median [Range]) (2017)	Altmetrics Score (Median [Range]) (2017)	Journal Impact Factor (2017)	Citations (Median [Range]) 2019	Altmetrics Score (Median [Range]) 2019	Journal Impact Factor (2019)	Journal Impact Factor (2020)
Human Brain Mapping	143.5 (104-350)	7 (0-365)	6.05	79 (60-498)	18.5 (9-323)	5.14	56.5 (42-86)	10 (5-66)	4.42	5.38
Frontiers in Neuroanatomy	60 (38-85)	3 (0-124)	3.18	37 (24-74)	2 (0-906)	3.37	19.5 (17-28)	5 (2-14)	3.29	3.85
Brain Topography	0 (0-59)	0 (0-5)	3.26	22 (12-119)	1 (0-24)	2.71	16.5 (10-123)	1 (0-144)	2.76	3.02
Brain Structure and Function	84.5 (62-151)	1 (0-11)	3.75	35 (30-59)	2 (1-36)	4.18	27 (22-42)	27 (0-43)	3.30	3.27
American Journal of Physical Anthropology	40 (27-77)	7.5 (0-169)	2.42	34 (23-56)	24 (2-2787)	2.96	16.5 (13-44)	25 (0-356)	2.41	2.35
Journal of Anatomy	45.5 (39-69)	11.5 (1-38)	2.43	24 (19-49)	4 (0-19)	2.61	32 (17-74)	6 (0-117)	2.03	2.61
The Anatomical Record	51.5 (33-68)	1.5 (0-76)	1.77	24 (18-30)	1 (1-50)	1.46	18 (17-45)	3.5 (0-950)	1.63	2.06
Annals of Anatomy	20.5 (13-38)	0.5 (0-111)	1.87	15 (11-33)	0 (0-19)	2.08	10.5 (9-45)	0 (0-7)	2.39	2.69
Anatomical Sciences Education	46 (33-83)	0 (0-5)	2.45	23 (16-123)	0 (0-33)	3.49	23.5 (19-44)	3.5 (1-41)	3.76	5.95
American Journal of Surgical Pathology	113.5 (90-172)	7.5 (4-50)	6.53	74 (56-168)	27.5 (3-214)	6.40	47 (42-67)	6.5 (1-35)	6.16	6.39
Clinical Anatomy	23 (20-38)	0.5 (0-6)	1.58	7 (12-26)	1 (0-3)	2.21	19 (15-62)	2.5 (0-20)	1.97	2.41
Cell Tissues Organs	21.5 (18-51)	0 (0-3)	2.42	13 (8-28)	0 (0-16)	1.43	7 (5-11)	0 (0-8)	2.06	2.48
Journal of Histochemistry and Cytochemistry	50.5 (35-200)	1.5 (0-7)	2.59	22.5 (13-56)	1.5 (0-13)	2.91	8.5 (7-77)	2.5 (1-23)	2.19	4.3
American Journal of Human Biology	55 (27-56)	5.5 (0-313)	1.99	35 (16-66)	6 (0-129)	1.70	19.5 (13-45)	14 (0-54)	1.56	1.93
Anatomical Science International	15.5 (11-20)	0 (0-6)	0.99	10 (6-32)	0 (0-1)	1.34	7 (6-18)	0 (0-3)	1.51	1.74

Comparisons between the Altmetric score and citation data in 2014, 2017, and 2019 were performed. From the same 15 anatomy journals selected for evaluation, a listing of the ten most cited articles in each journal in years (n = 450) was compiled. Altmetric scores and citation numbers for these articles were recorded. The cumulative citation count in 2017 was 5558 compared to the 8633 citations in 2014, representing a 35.6 % decrease. The cumulative citation count in 2019 was 3863 compared to the citations in 2017, representing a 21.5% decrease.

The cumulative Altmetric score in 2017 was 6330 compared to the 2135 cumulative total in 2014, representing a 133.7% increase. The cumulative Altmetric score in 2019 was 4247 compared to the Altmetric score in 2017, representing a 32.9% decrease. While the median value of the number of citations in 2017 was 43, 25 in 2014, this value was 19 in 2019. The median value of the Altmetric score in 2017 was 1 in 2014, 1.5 in 2017, and 4 in 2019.

According to the results of this comparison, we compared whether the first 15 articles of the

journals we included in the study were articles with anatomy content. While 70 of the articles in 2014 were content anatomy, 80 articles were not content anatomy. In 2017, 60 articles were content anatomy, 90 were not, and in 2019, 61 articles were content anatomy, and 89 were not. In comparing whether the first ten articles included in the study included anatomy in 2014, 2017 and 2019, there was a decrease in the correct anatomy content from 2014 to 2019.

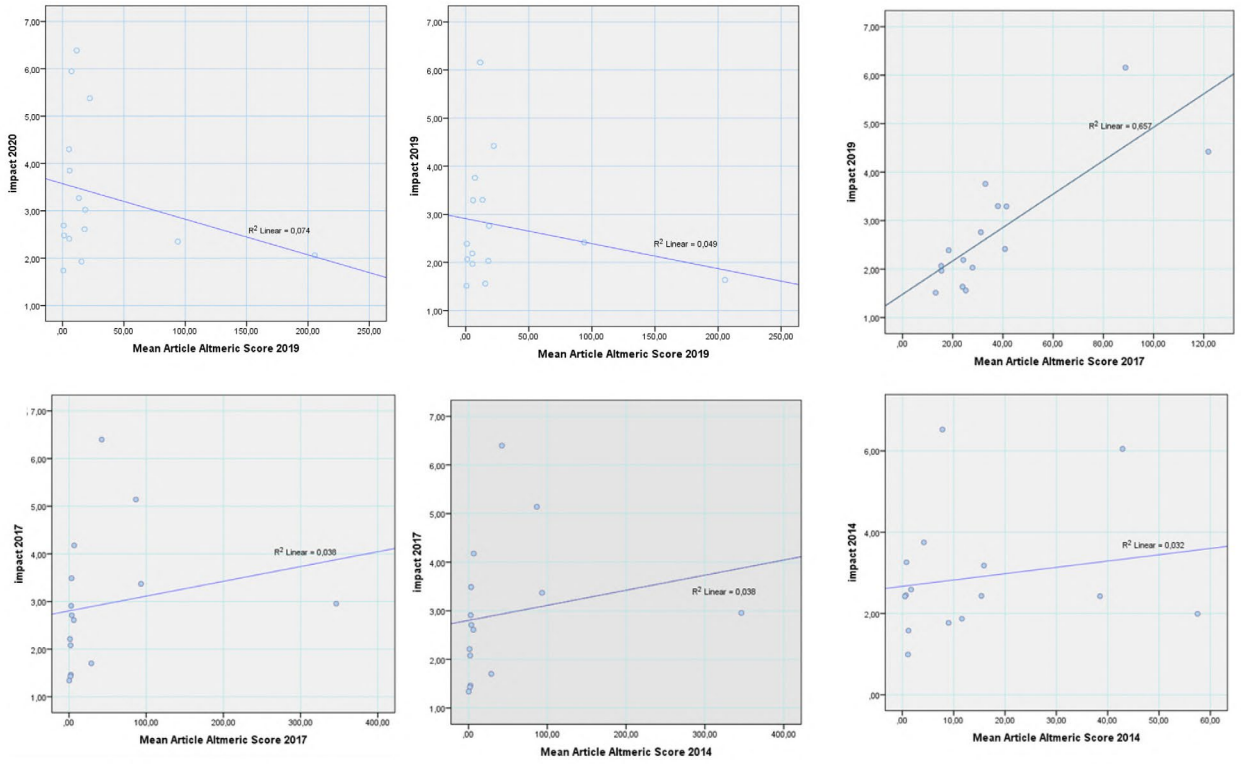

Fig. 1.- Comparisons between the Altmetric score and impact factor in 2014, 2017, 2019 and 2020.

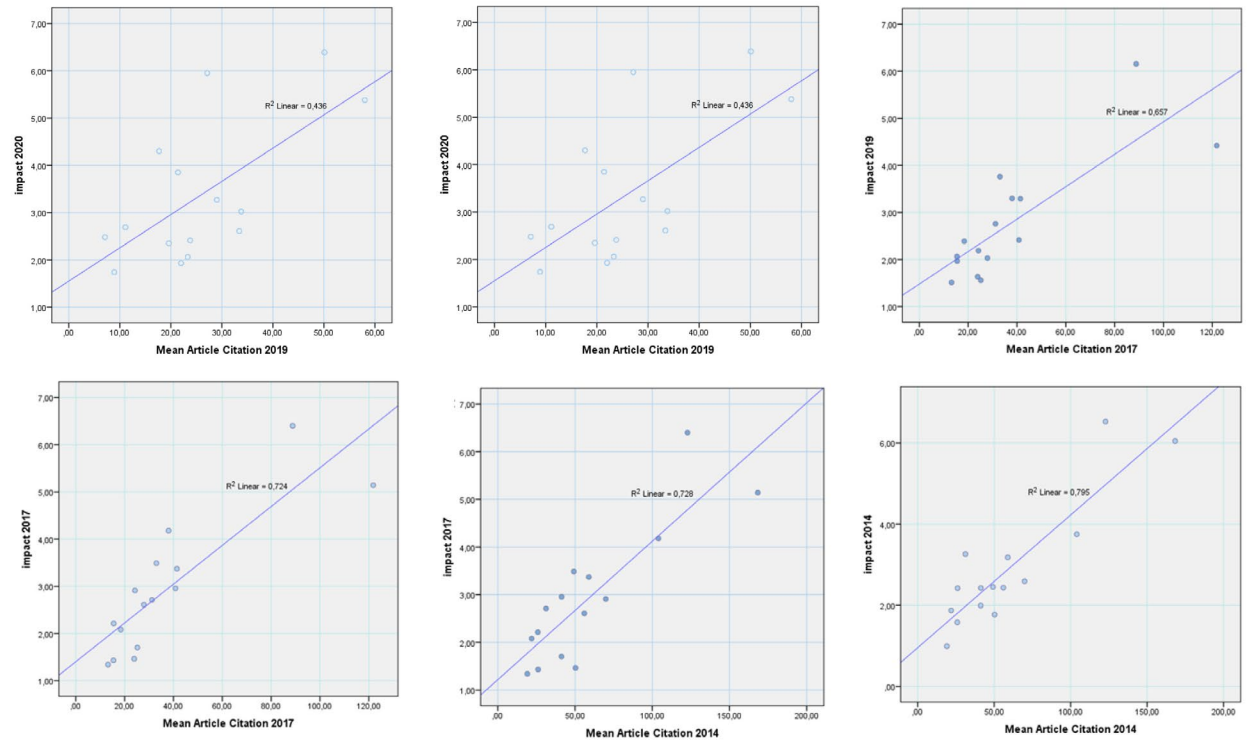

Fig. 2.- Comparisons between the citation and impact factor in 2014, 2017, 2019 and 2020.

Table 2. Summary of comparisons between bibliometrics and altmetrics for the journals of study in 2014, 2017 and 2019.

Journal	Correlation coefficient between number of citations and altmetric score (2014)	P value (2014)	Correlation coefficient between number of citations and altmetric score (2017)	P value (2017)	Correlation coefficient between number of citations and altmetric score (2019)	P value (2019)
Human Brain Mapping	0.43	0.21	0.04	0.90	-0.29	0.40
Frontiers in Neuroanatomy	0.21	0.55	-0.21	0.55	-0.45	0.18
Brain Topography	0.32	0.36	0.11	0.75	0.33	0.34
Brain Structure and Function	-0.09	0.76	-0.01	0.97	0.24	0.49
American Journal of Physical Anthropology	-0.07	0.84	-0.21	0.55	0.57	0.08
Journal of Anatomy	-0.16	0.65	0.03	0.91	-0.16	0.64
The Anatomical Record	-0.38	0.26	0.21	0.54	-0.02	0.95
Annals of Anatomy	0.00	0.98	-0.59	0.07	-0.32	0.36
Anatomical Sciences Education	-0.68	0.02*	0.52	0.11	0.23	0.52
American Journal of Surgical Pathology	0.76	0.01**	0.60	0.06	0.18	0.61
Clinical Anatomy	0.51	0.13	-0.38	0.27	0.59	0.07
Cell Tissues Organs	-0.06	0.85	-0.06	0.84	0.10	0.78
Journal of Histochemistry and Cytochemistry	0.24	0.50	0.67	0.03*	0.46	0.17
American Journal of Human Biology	0.29	0.41	0.03	0.93	0.60	0.06
Anatomical Science International	-0.19	0.58	0.22	0.52	-0.06	0.86

Correlation is significant at the *p <0.05; ** p <0.00

While there was no significant difference in comparing the anatomy content of the articles with the Altmetric score, article citations in 2014, a significant difference was found between the number of journal citations and impact factor for these years.

In the comparison made for 2017, there was no significant difference between journal citation and journal impact factor, but a significant difference was found between anatomy content in article citation and Altmetric score.

In the comparison made for 2019, a significant difference was found only between the number of journal citations and the anatomy content (Table 3).

When the articles in 2014 were examined, it was determined that the most cited articles for each of the 15 journals were the anatomy-based studies with morphometric measurements. In particular,

Table 3. Comparison of the anatomical content of the articles and the altmetric score, citation and impact factors.

Number of anatomy content articles (n) / year	Altmetric score 2014 (p)	Citation number of article 2014 (p)	İmpact factor 2014 (p)	Citation number of journal 2014 (p)	Altmetric score 2017(p)	Citation number of article 2017 (p)	İmpact factor 2017 (p)	Citation number of journal 2017 (p)	Altmetric score 2019 (p)	Citation number of article 2019 (p)	İmpact factor 2019 (p)	Citation number of journal 2019 (p)
N=70 yes N=80 no 2014	0.15	0.42	0.00**	0.01*	-	-	-	-	-	-	-	-
N=60 yes N=90 no 2017	-	-	-	-	0.00**	0.03*	0.28	0.08	-	-	-	-
N=61 yes N=89 no 2019	-	-	-	-	-	-	-	-	0.20	0.34	0.10	0.02*

Significant at the *p <0.05; ** p <0.00.

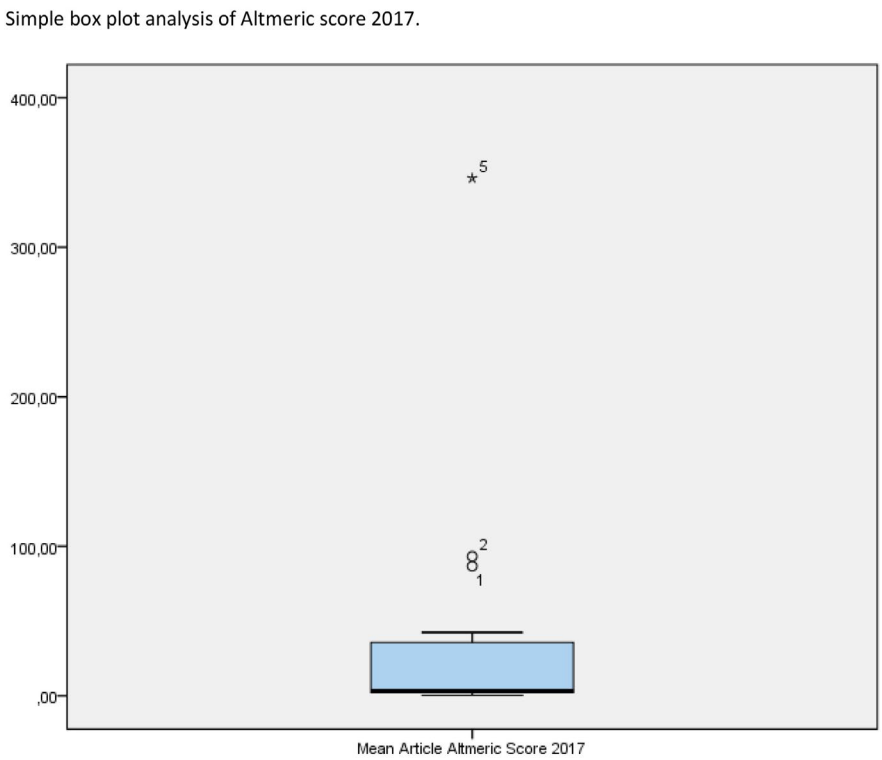

it was determined that studies with anatomy related to a disease or syndrome received more citations, while gross anatomy studies did not receive as many citations. When the articles in 2017 and 2019 were evaluated according to their citations, it was determined that the articles less contained anatomy. At the same time, it was observed that the journals that published gross anatomy studies included studies with histological and genetic content in these years, and it was determined that the number of citations in the articles of these journals decreased. Again in these years, it was observed that the articles with the highest citations were generally those without gross anatomy but with anatomy content.

DISCUSSION

To our knowledge, this is the first study to provide an in-depth statistical analysis of the relationship between Altmetrics and traditional bibliometrics of this scale in the anatomy literature. A weak positive correlation was demonstrated between the Altmetric score and citation number in the 2014 and 2017 cohorts. While the 2014 cohort only demonstrated a significant correlation between journal impact factor and citation count, the 2017 cohort demonstrated a significant correlation between Altmetric score with citation count and journal impact factor 2017 and 2019. The significant correlation of the Altmetric score of 2017 to the 2019 impact factor suggests that it is due to the more effective use of social media in recent years. But no significant correlation of the Altmetric score of 2019 to the 2020 impact factor. This result may suggest that another criterion may be determinative instead of the Altmetric score.

The increasing influence and societal uptake of various social media forms influence how research is distributed and encountered. The influence of this technology is demonstrated in our evaluation of the total Altmetric score in both the 2014 and 2017 cohorts. The total Altmetric score among 150 articles in 2017 was over three times more than the total Altmetric score among the same number of articles in 2014.

Social media is now on the agenda in academic studies, and some studies may even become a periodic subject of social media. The increase in the Altmetric scores of the articles in 2017 compared to 2014 is that social media is used more frequently and covers almost every field. In 2019, the Altmetric scores of the articles were lower than in other years. However, the number of citations for 2019 is equally low. Here, the citation

and Altmetric score may change according to the elapsed time.

The most cited articles were targeted and included in the study without considering their Altmetric scores were 0 points. Although these articles were read in Mendeley, an Altmetric score has not yet been formed because they are not included in social media (Twitter, Facebook, news outlet, blog, etc.).

These studies are influenced by the content of the journals and the subject of the article. In 2017, there were articles with many citations but an Altmetric score of 0. According to the research results, in 2017, when the journals reached the highest Altmetric score, the journals and articles that scored 0 were mostly anatomy education, tissue studies and model studies. This result can be interpreted as the fact that the public finds this information complex in the studies above and that this information is at a very advanced level, which is more of an interest to the academic community.

According to other studies on this subject, we can state that the journals used in our study are distributed homogeneously, because the journals in this study were not only gross anatomy but also journals covering the branches of neuroscience, radiology, anatomy education, microscopic anatomy and clinical anatomy. When we looked at the journals one by one in the study results, we saw that the articles of journals dealing with neuroscience had a higher Altmetric score. Analysis has led us to comment that neuroscience is more up-to-date and more remarkable, and therefore more spread on social media. The least Altmetric score was seen in educational journals. It was found that this journal showed a significant negative correlation between the Altmetric score and the number of citations in 2014. Our study showed us that articles on anatomy education did not attract much attention on social media.

Of the 15 journals evaluated, only 2 in 2014 and 1 in 2017 demonstrated significant correlations when analyzed individually. This finding may reflect differences in the methodologies behind Altmetrics and traditional bibliometrics or different approaches to article dissemination among individual journal authors and subscribers. Results suggest that Altmetrics alone may not be a good surrogate for article citations.

We can think that the decrease in citation numbers of the articles that have been cited the most in journals over the years may be due to the fact that the articles contain less anatomy. In 2014, when the most citations were received, the studies were usually human studies with anatomy content, and the lowest citation articles were histological and genetic studies. In line with these results, anatomy comes to the fore. In the same way, the same interpretation can be made for other years.

The articles with the highest Altmetric scores are mostly neuroscience-related. When we look at the neuroscience articles in general, it is also remarkable that the neuroscience articles with the anatomy content have high Altmetric scores. The common point of the two articles with the highest Altmetric scores belonging to two different journals in the study is that they contain new information about species (humans and carnivores). Apart from this, the fact that the articles evaluated within the scope of the study have higher Altmetric scores in studies containing human anatomy can be interpreted as increasing the effect when the studies are based on anatomy.

In this case, we can argue that the high number of articles with anatomy content in the top 15 most cited journals in 2014, when it was the highest impact factor, affected the journal citation and impact factor. In 2017 and 2019, the Altmetric score and citation number of articles did not affect the journal, and the number of citations and impact factors of the journals decreased with the fact that the top 15 models included fewer anatomy articles in their content. As a result, we can say that when journals generally publish studies with anatomy content, they are advantageous in terms of impact factor and number of citations.

In 2019 found that the Altmetric score was generally higher in articles where morphometric studies were paired with clinical findings: this and similar histological, genetic, pathological. Gross anatomy studies alone did not have the same effect in the evaluated articles. The fact that the studies had low Altmetric scores can be

interpreted as these issues are more of interest to researchers and have effectiveness in scientific platforms.

Our study has notable limitations. Our evaluation of each journal included the top-10 most cited articles. However, although some articles had fewer citations and a higher Altmetric score than the most cited article, they were omitted because they did not comply with the study method. The articles included in the study; Given that they represent a small minority of published research papers, it should be compared and discussed with further studies to assess whether these results can be generalized to studies with less visibility and impact. Despite the limitations above, our study is the first of its kind in anatomy. After that, studies in anatomy journals can be done on which subjects and with which methods the Altmetric score will be increased.

Today, the spread of research and its reach to more readers have increased with the Internet. For this reason, it brings to mind the question of whether actively used social media can affect the impact factors of studies. The question arises whether the effectiveness of a study should be measured by sharing it too much on social media and reaching more people, or whether it should be continued with the classical methods we know. Considering that social media does not have qualified criteria in evaluating studies, can it be accepted as a reliable and accurate representation method of the effect of the Altmetric score? Or which social media platforms will be considered eligible for this assessment? Therefore, further research is needed to evaluate the relationships between Altmetrics and traditional bibliometric measures to elucidate the relevance of Altmetrics in research analytics (O'Connor et al., 2017).

CONCLUSION

The Altmetric scoring system provides a more inclusive and rapid measurement of research impact than traditional metrics. However, this modernized system currently lacks data and large-scale studies to replace citation count and journal impact factor as the sole measure of article dissemination. More research is needed to evaluate the relationships between Altmetrics and traditional bibliometric measures to elucidate Altmetrics' relevance in research analytics.

According to the study results, an increase in the impact factor or the number of citations of the journals that publish the articles containing anatomy may facilitate the acceptance of anatomy studies by the journals. Future studies should help understand the impact of social media's relationship with anatomy research and its tools to disseminate new information.

REFERENCES

ALTMETRİC BOOKMARKLET. Available at: https://www.altmetric.com/products/free-tools/bookmarklet.

BARAKAT AF, NİMRİ N, SHOKR M, MAHTTA D, MANSOOR H, MOJADİDİ MK, MAHMOUD AN, SENUSSİ M, MASRİ A, ELGENDY IY (2018) Correlation of altmetric attention score with article citations in cardiovascular research. *J Am Coll Cardiol*, 72(8): 952-953.

BARDUS M, EL RASSİ R, CHAHROUR M, AKL EW, RASLAN AS, MEHO LI, AKL EA (2020) The use of social media to increase the impact of health research: systematic review. *J Med Internet Res*, 22(7): e15607.

BORNMANN L, LEYDESDORFF L (2014) Scientometrics in a changing research landscape: bibliometrics has become an integral part of research quality evaluation and has been changing the practice of research. *EMBO Rep*, 15: 1228-1232.

CHANG J, DESAİ N, GOSAİN A (2019) Correlation between altmetric score and citations in pediatric surgery core journals. *J Surg Res*, 243: 52-58.

DAGAR A, FALCONE T (2021) Altmetric scores analysis reveals a high demand for psychiatry research on social media. *J Psych Res*, 298: 113782.

DIGITAL SCIENCE & RESEARCH SOLUTIONS INC., n.d. Re-imagining discovery and access to research: grants, publications, citations, clinical trials, patents and policy documents in one place. [WWW Document]. URL https://www.dimensions.ai/.

ELMOR SA (2018) The altmetric attention score: what does it mean and why should I care? *Toxicol Pathol*, 46: 252-255.

HAYON S, TRİPATHİ H, STORMONT I, DUNNE M, NASLUND M, SİDDİQUİ M (2019) Twitter mentions and academic citations in the urologic literature. *Urology*, 123: 28-33.

JİA JL, NGUYEN B, MİLLS DE, POLİN DJ, SARİN KY (2020) Comparing online engagement and academic impact of dermatology research: an altmetric attention score and plumx metrics analysis. *J Am Acad Dermatol*, 83: 648-650.

JOURNAL CITATION REPORTS, Clarivate Analytics. Available at: https:// incites.clarivate.com.

LUC JGY, ARCHER MA, ARORA RC, BENDER EM, BLİTZ A, COOKE DT, HLCİ TN, KİDANE B, OUZOUNİAN M, VARGHESE JR TK, ANTONOFF MB (2020) Does tweeting improve citations? One-year results from the TSSMN prospective randomized trial. *Ann Thorac Surg*, 111(1): 296-300.

NOCERA AP. BOYD CJ, BOUDREAU H, HAKİM O, RAİS-BAHRAMİ S (2019) Examining the correlation between altmetric score and citations in the urology literature. *Urology*, 134: 45-50.

O'CONNOR E, NASON G, O'KELLY F, MANECKSHA R, LOEB S (2017) Newsworthiness vs scientific impact: are the most highly cited urology papers the most widely disseminated in the media? *BJU Int*, 120: 441-454.

PATEL RB, VADUGANATHAN M, BHATT DL, BONOW RO (2018) Characterizing highperforming articles by altmetric score in major cardiovascular journals. *JAMA Cardiol*, 3: 1249-1251.

PRİEM J TD, GROTH P, NEYLON C (2010) Altmetrics: A manifesto. Altmetrics, 2010. Available at: http://altmetrics.org/manifesto

PUNİA V, AGGARWAL V, HONOMİCHL R, RAYİ A (2019) Comparison of attention for neurological research on social media vs academia: an altmetric score analysis. *JAMA Neurol*, 76: 1122-1124.

Determining gestational age in the early fetal period: A comparison of morphometrical parameters

Omar D. Cortes-Enriquez, Victor M. Beltran-Aguilar, Ana L. Yee-De Leon, Norberto Lopez-Serna

Embryology Department, Faculty of Medicine of the Autonomous University of Nuevo Leon, Nuevo León, Mexico

SUMMARY

Estimation of fetal age is an important component of prenatal evaluation. The measure of the Crown-Rump Length (CRL) by ultrasound is one of the most frequently used methods to determine it. However, in certain pathologies, this measure could lose accuracy, and other measures should be taken to evaluate fetal age and to determine the normal growth of the conceptus. The main objective of this research was to compare different morphometric parameters with CRL in normal human fetuses to determine which of them has a stronger correlation with gestational age to be a useful measure when CRL could not be appropriately evaluated. We measured 10 different morphometric parameters and the weight in 120 human fetuses product of abortion that had externally normal morphology, and a Pearson´s Correlation test was made with each of the parameters with the gestational age determined using the CRL.

Each of the 10 parameters had a significantly strong correlation with CRL. However, some of them have a stronger correlation and should be preferred when CRL is not available. If available, fetal age should be estimated using an ultrasound technique and measuring the CRL. Nevertheless, if an alteration in one of the structures affects its measure, a different parameter should be used. The limitations of each parameter should be noticed before using them.

Key words: Gestational age – Fetal development – Fetal structures – Morphogenesis – Fetal weight

INTRODUCTION

Over the years, different types of measurements have been used to estimate fetal age. Due to its accessibility, ideally, these measurements should be obtained through the use of ultrasound, a low-cost technology, available in most hospitals, which is harmless during pregnancy. The measurement of the crown-rump length is considered the gold standard, as well as the most accurate method for calculating fetal age (Hadlock, 1990). However, in certain situations where the morphology of the fetus is affected due to certain pathologies, some methods of calculation of fetal age may not be accurate (Sherwood et al., 2000). It is known, for example, that the accuracy of measuring biparietal diameter is more likely to be affected by different maternal and fetal factors compared to head circumference (Johnsen et al., 2004).

Corresponding author:
Omar Daniel Cortes Enriquez. Embryology Department of the Faculty of Medicine of the UANL, Francisco I. Madero Av. And Jose E. Gonzalez Av. Mitras Centro, 64000, Monterrey, Nuevo Leon, Mexico. Phone: 52 (81) 8329 4187. E-mail: omardcortes@outlook.com

Submitted: November 8, 2021. **Accepted:** February 5, 2022

https://doi.org/10.52083/HSLZ4758

Furthermore, different non-pathological variables can also affect the growth of the structures that are used for measurement, and therefore not be as reliable, as the measurement of the abdominal perimeter due to the rapid growth of the abdomen in intrauterine life. As a result, it is necessary to search for alternatives and evaluate their precision.

Research comparing traditional measurement methods to obtain fetal age is quite scarce, since current tendencies include looking for new and modern techniques to estimate fetal age, however not always available (Minier et al., 2014a; 2014b; Pomier et al., 2019). It is necessary to compare the traditional methods in order to find out which is the most accurate in cases where the gold standard cannot be used and no modern technologies to perform these measurements are available.

A pair of studies were made using Multiple Slide Computed Tomography (MSCT) technology, which found that it is possible to calculate the fetal age by evaluating the deciduous tooth gems or the mandible, obtaining a reliable result compared to the measurement of the femoral diaphyseal length (Minier et al., 2014a; 2014b). However, calculating the fetal age with this method may not always be possible, particularly in cases where an MSCT is not available. In another study, authors concluded that orbital measurement using a 3D CT scan could provide a reliable measurement of fetal age, particularly in fetuses with trisomy 21, but this method also becomes unfeasible in cases where the equipment is not available (Pomier, 2009). The measurement of the basilar portion of the occipital bone was also found to be a useful and reliable option for estimating fetal age. Nevertheless, their observations focused on estimating fetal age in fetuses that are the product of abortion, and it is not possible to take this measure in utero by ultrasound (Nagaoka et al., 2012). Likewise, it has been argued that the histological study of the kidney can also be a reliable tool to estimate fetal age (Kumar and Pillay, 1996). Out of the morphological measures, the quantification of surfactant factor produced by type 2 pneumocytes by immunohistochemistry can be used to estimate fetal age, yet both methods are only functional in cases where fetal age is studied in fetuses outside the uterus (Betz et al., 1992).

About the measuring of the ear, several studies have acknowledged the measurement of the external ear as an indicator for either detecting chromosomal abnormalities or determining the fetal age of the product. Sivan et al. (1983) first examined ear length on newborns, determining a parameter to classify small and low set of ears, which was correlated with diagnosing syndromes in pediatric patients.

Chitkara et al. (2000) measured the pinna by sonography, and then developed a nomogram in which the ear was compared to gestational age, and the linear regression found r = 0.96, hence suggesting a high correlation between both variables.

Another study aimed to examine fetal ear length in products with aneuploidy, and not only it was found that these had significantly shorter ears, but also that its length was disproportionate with the biparietal diameter, another measurement used to approximate fetal size (Yeo et al., 2003).

The importance of traditional measurements relies on the fact that they can be calculated in the uterus through an ultrasound, a technology that has a worldwide distribution and is available to the majority of the population. A more accurate gestational age diagnosis using ultrasound could be performed with information about the precision of these measurements.

MATERIALS AND METHODS

This research followed the directions of the Helsinki Declaration and was approved by our institutional ethics committee, with approbation number EB21-00001. A total of 120 human fetuses with normal external morphology and with ages from 12 to 20 weeks of gestation (WOG) were measured using 10 morphometrical parameters; the weight were also determined to compare which of them has a stronger correlation with the gestational age estimated measuring the Crown-Rump Length (CRL) (Paten,1982). The parameters are described, and a graphic description is shown in Fig. 1. The sample size was taken under our laboratory availability of human fetuses.

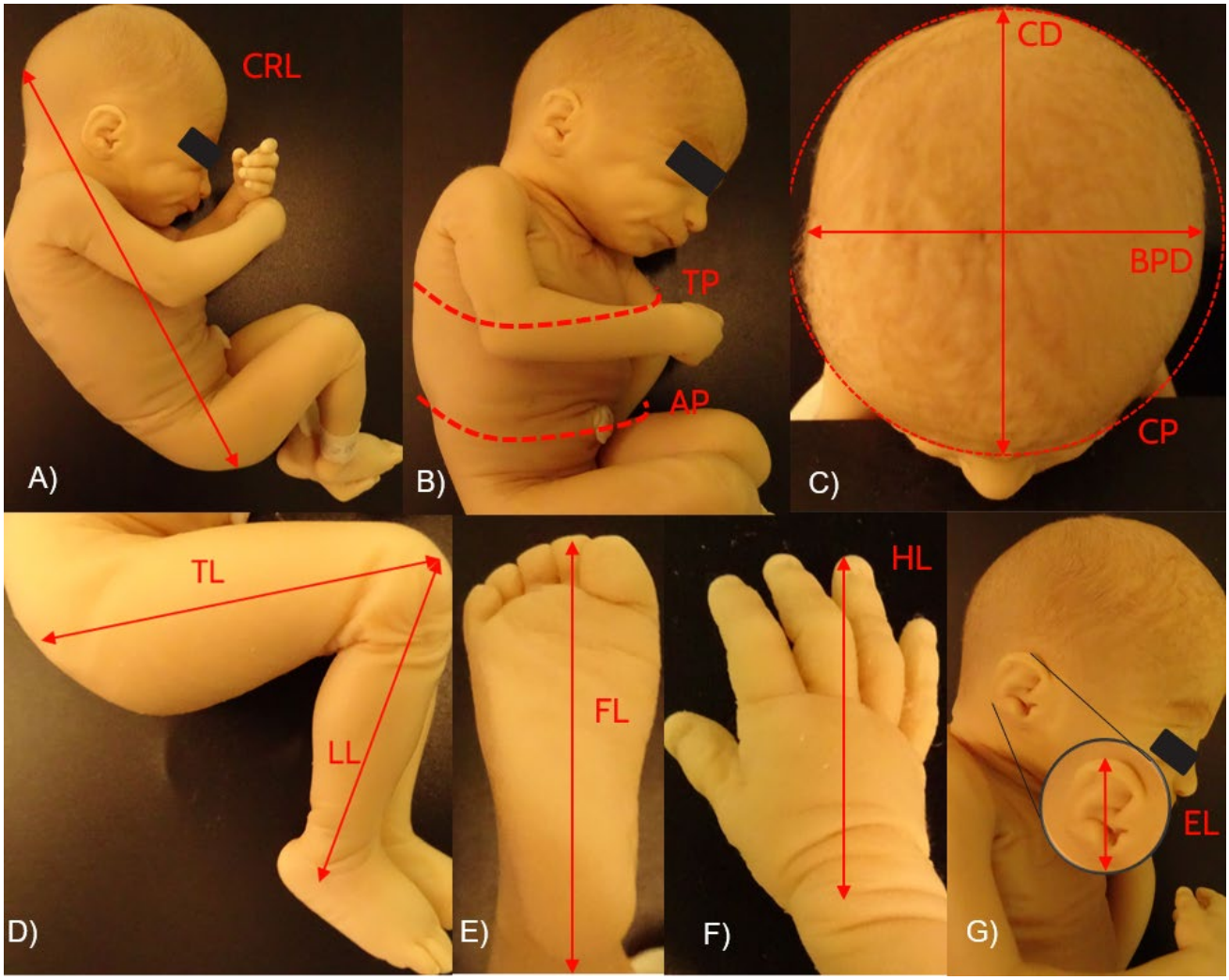

Fig. 1.- Morphometrical parameters to estimate fetal age in a fetus of 20 Weeks of Gestation (WOG). CRL: Crown-Rump Length. TP: Thoracic Perimeter. AP: Abdominal Perimeter. CD: Cephalic Diameter. BPD: Biparietal Diameter. CP: Cephalic Perimeter. TL: Thigh Length. LL: Leg Length. FL: Foot Length. HL: Hand Length. EL: Ear Length.

The Crown-Rump Length (CRL) was measured from the most prominent part of the occiput to the most prominent part of the rump. Thoracic Perimeter (TP) was measured at the level of the nipples. The abdominal Perimeter (AP) was measured around the level of the umbilical cord. Cephalic Diameter (CD) was measured from the sinciput to the occiput. Biparietal Diameter (BPD) was measured as the distance from both parietal bones in the fetus. Cephalic Perimeter (CP) was measured at the level above the eyebrows of the fetus. Thigh Length (TL) was measured from the hip joint to the knee joint. Leg Length (LL) was measured from the knee joint to the ankle joint. Foot Length (FL) was measured from the heel to the most prominent toe. Hand Length (HL) was measured from the wrist joint to the middle finger. Finally, Ear Length (EL) was measured from the helix to the lobule.

A data set was made using the Microsoft Excel 365 Software, and information was processed using the IBM SPSS 24 software. We calculated each measure's mean and standard deviation for each week of gestation from 12 to 20 WOG. This gestational age was previously determined by measuring the Crown-Rump Length (CRL) defined as the preferred measure to estimating fetal age. After corroborating the normal distribution of data with a Kolmorov-Smirnoff test, a Pearson's Correlation test was made from each of the measures and the weight with the CRL to evaluate which had the strongest correlation with this measure.

RESULTS

Results from the mean and standard deviation for each measure at each week of gestation from 12 to 20 WOF are summarized in Table 1.

Table 1. Measures of morphometrical parameters. Each measure is represented as the mean (±SD). HL: Hand Length. LL: Leg Length. FL: Foot Length. TL: Thigh Length. CD: Cephalic Diameter. CRL: Crown-Rump Length. CP: Cephalic Perimeter. TP: Thoracic Perimeter. AP: Abdominal Perimeter. BPD: Biparietal Diameter. EL: Ear Length.

WOG	WEIGHT (gr)	HL (mm)	LL (mm)	FL (mm)	TL (mm)	CD (mm)	CRL (mm)	CP (mm)	TP (mm)	AP (mm)	BPD (mm)	EL (mm)
12	35.75 (5.72)	11.0 (1.41)	17.0 (1.41)	12.5 (0.70)	27.00 (0.00)	57.5 (7.77)	77.5 (0.70)	88.00 (5.65)	73.00 (9.89)	65.00 (16.97)	56.00 (2.82)	6.5 (0.70)
13	54.19 (12.82)	13.62 (1.40)	21.88 (3.21)	15.00 (1.41)	29.88 (2.93)	62.66 (4.89)	92.66 (4.15)	97.33 (8.1)	84.37 (10.56)	75.28 (12.29)	62.50 (4.75)	7.22 (0.91)
14	72.92 (7.94)	15.16 (0.98)	25.00 (2.44)	17.85 (1.57)	35.57 (2.76)	70.00 (3.51)	103.28 (3.98)	108.85 (6.17)	94.42 (6.07)	88.85 (7.22)	66.33 (3.98)	8.50 (0.50)
15	151.24 (41.64)	19.90 (2.42)	36.70 (73.33)	24.22 (2.77)	47.30 (5.85)	92.77 (10.47)	124.11 (8.00)	133.11 (41.80)	128.11 (17.84)	119.88 (18.64)	82.50 (9.20)	11.33 (2.33)
16	208.91 (47.54)	21.28 (2.74)	37.50 (7.80)	27.00 (3.33)	49.81 (6.15)	93.31 (14.41)	133.18 (5.92)	153.36 (14.26)	138.95 (14.44)	136.85 (13.19)	89.91 (4.99)	11.16 (1.02)
17	279.61 (61.04)	25.00 (2.17)	45.21 (4.51)	31.21 (2.52)	55.69 (3.78)	108.68 (12.43)	146.59 (5.47)	159.90 (35.83)	143.04 (32.61)	135.73 (37.41)	100.63 (8.53)	13.45 (1.50)
18	344.19 (65.40)	25.96 (2.76)	47.84 (7.36)	34.88 (2.61)	59.80 (6.74)	111.08 (20.93)	160.12 (8.89)	155.87 (58.59)	163.22 (26.06)	153.59 (24.39)	112.62 (27.15)	15.68 (1.70)
19	421.51 (95.12)	29.86 (3.20)	53.06 (6.87)	38.68 (3.59)	67.06 (6.54)	125.64 (13.16)	171.35 (8.57)	201.78 (22.48)	184.50 (12.43)	177.50 (14.53)	118.90 (6.59)	17.54 (1.29)
20	408.02 (92.95)	31.75 (4.52)	51.50 (5.09)	38.25 (3.05)	63.00 (7.28)	127.71 (7.56)	176.42 (11.54)	201.42 (17.39)	176.66 (11.41)	171.33 (10.51)	121.50 (4.94)	18.32 (2.82)

All of the measured parameters show an increasing pattern as the gestational age increases. However, not all of the measures show a constant increment, as some of them showed periods of greater growth and periods with smaller increments in their size. This is graphically represented in Fig. 2, where the CRL pattern among the studied period is compared with the rest of the parameters measured. In this graphic, CRL is represented with a continuous black line, and it can be observed that, as described by previous authors, it represents the measure with the most constant increment during this period of gestation.

Table 2 shows the results of the Pearson´s Correlation test from each of the measured

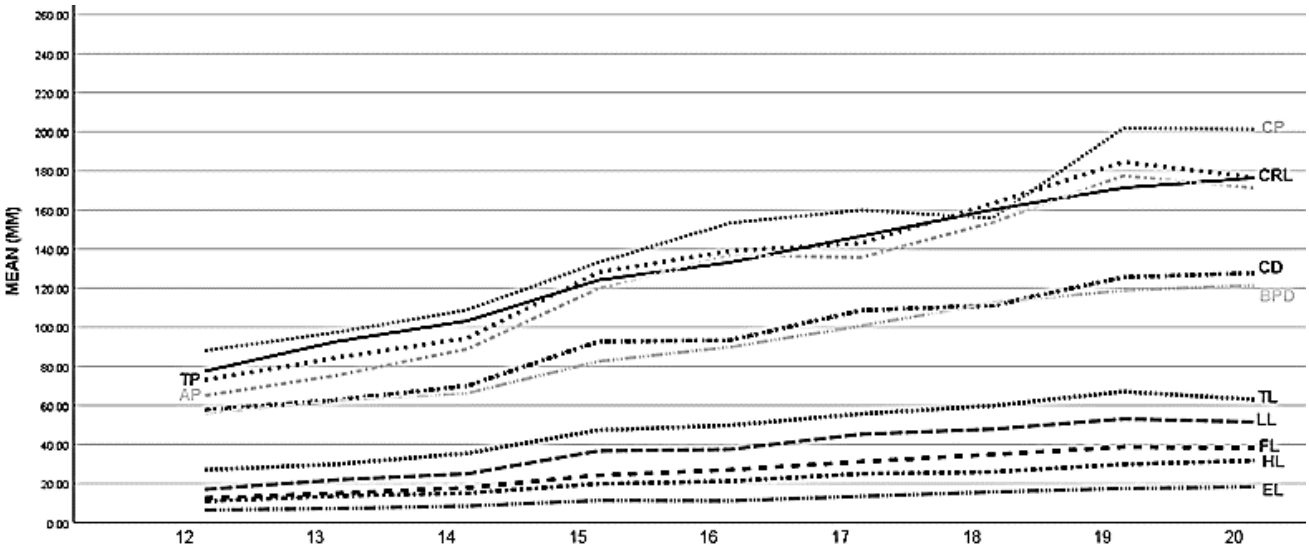

Fig. 2.- Growth pattern of the measured parameters. The CRL shows the most constant increasing pattern.

parameters with the CRL, and, as is shown, all of them have a strong correlation with this measure. Foot Length (FL) and the Biparietal Diameter (BPD) have the next most constantly increasing pattern with the stronger correlation with the CRL. This table could be used as a guide to select a parameter to determine gestational age when CRL could not be used, and this parameter should be selected in the presented order for the accuracy of the age estimation.

Table 2. Pearson´s correlation of each of the measured parameters with the CRL. All of the measures were significant with a p-value <0.01.

MORPHOMETRIC PARAMETER	PEARSON´S CORRELATION TEST
CROWN- RUMP LENGHT (CRL)	1
FOOT LENGHT (FL)	0.997
BIPARIETAL DIAMETER (BPD)	0.996
HAND LENGHT (HL)	0.995
LEG LENGHT (LL)	0.993
CEPHALIC DIAMETER (CD)	0.992
THORACIC PERIMETER (TP)	0.991
TIGHT LENGHT (TL)	0.99
ABDOMINAL PERIMETER (AP)	0.989
EAR LENGHT (EL)	0.989
WEIGHT	0.985
CEPHALIC PERIMETER (CP)	0.973

DISCUSSION

Estimating fetal age is an important part of prenatal evaluation, as it can be a marker of normal development. If possible, fetal age should be determined using non- invasive methods such as the use of different measures through an ultrasound technique. One of the most used measures is the Crown-Rump Length (CRL), which is a constant parameter that strongly correlates with fetal age. We described, as previous authors, that CRL could be the most useful parameter to determine gestational age, since it has significant increases over each week of development, enough to discriminate from one another, making it the most accurate measure (Hadlock, 1990). However, it could be affected by different pathologies that affect its measured components (Sherwood et al., 2000). For example, a patient with anencephaly or cranioschisis would show a smaller length that would not correlate with fetal age properly. On the other hand, a patient with hydrocephaly could show a larger length that also would not be correct (Johnsen et al., 2004). In these cases, a different parameter could be used for estimating fetal age, like the measure of the Foot Length (FL), a simple measure that has shown to strongly correlate with the estimation by CRL. Notice that each of the parameters have their limitations, and they should be considered before using them for the purpose of determining fetal age: for example, the abdominal perimeter is highly influenced by the liver development and the presence or absence of the physiological gut herniation, and thus it should not be used in the period where this herniation takes place. Ear Length (EL), a recently studied structure for determining fetal age, showed a strong correlation with age determined by CRL, however smaller than that from other parameters (Chitkara et al., 2000). However, these structures have an important role when other structures are affected, and their position could be also used as a marker of adequate development (Yeo et al., 2003). Further research should be done to define the normal range for each of the parameters, as this could vary for different characteristics as gender and ethnicity.

ACKNOWLEDGEMENTS

The authors sincerely thank those who donated their bodies to science so that anatomical research and teaching could be performed. Results from such research can potentially increase scientific knowledge and can improve patient care. Therefore, these donors and their families deserve our highest respect.

REFERENCES

BETZ P, NERLICH A, WILSKE J, WIEST I, KUNZE C, PESCHEL O, PENNING R (1992) Determination of fetal age by immunohistochemical estimation of surfactant-producing alveolar type II cells. *Forensic Sci Int*, 53(2): 193-202.

CHITKARA U, LEE L, EL-SAYED YY, HOLBROOK RH, BLOCH DA, OEHLERT JW, DRUZIN ML (2000) Ultrasonographic ear length measurement in normal second- and third- trimester fetuses. *Am J Obstet Gynecol*, 183(1): 230-234.

HADLOCK FP (1990) Sonographic estimation of fetal age and weight. *Radiol Clin North Am,* 28(1): 39-50.

JOHNSEN SL, RASMUSSEN S, SOLLIEN R, KISERUD T (2004) Fetal age assessment based on ultrasound head biometry and the effect of maternal and fetal factors. *Acta Obstet Gynecol Scand*, 83(8): 716-723.

KUMAR KU, PILLAY VV (1996) Estimation of fetal age by histological study of kidney. *Med Sci Law*, 36(3): 226-230.

MINIER M, DEDOUIT F, MARET D, VERGNAULT M, MOKRANE FZ, ROUSSEAU H, ADALIAN P, TELMON N, ROUGE D (2014a) Fetal age estimation using MSCT scans of the mandible. *Int J Legal Med*, 128(3): 493-499.

MINIER M, MARET D, DEDOUIT F, VERGNAULT M, MOKRANE FZ, ROUSSEAU H, ADALIAN P, TELMON N, ROUGE D (2014b) Fetal age estimation using MSCT scans of deciduous tooth germs. *Int J Legal Med*, 128(1): 177-182.

NAGAOKA T, KAWAKUBO Y, HIRATA K (2012) Estimation of fetal age at death from the basilar part of the occipital bone. *Int J Legal Med*, 126(5): 703-711.

PATTEN BM (1982) Age, growing and changes in external chape of the body. In: *Patten´s Human Embryology*. Mc Graw-Hill, USA, pp 74-66.

POMMIER S, ADALIAN P, GAUDART J, PANUEL M, PIERCECCHI-MARTI MD, LEONETTI G (2009) Fetal age estimation using orbital measurements: 3D CT-scan study including the effects of trisomy 21. *J Forensic Sci*, 54(1): 7-12.

SHERWOOD RJ, MEINDL RS, ROBINSON HB, MAY RL (2000) Fetal age: methods of estimation and effects of pathology. *Am J Phys Anthropol*, 113(3): 305-315.

SIVAN Y, MERLOB P, REISNER SH (1983) Assessment of ear length and low set ears in newborn infants. *J Med Genet*, 20(3): 213-215.

YEO L, GUZMAN ER, ANANTH CV, WALTERS C, DAY-SALVATORE D, VINTZILEOS AM (2003) Prenatal detection of fetal aneuploidy by sonographic ear length. *J Ultrasound Med*, 22(6): 565-576.

A thorough cadaveric investigation of coronary ostia and its relationship with sinotubular junction

Swati Bansal[1], Rajiv Jain[2], Virendra Budhiraja[3], Shveta Swami[4], Rimpi Gupta[5], Mehak Sikka[6]

[1,3-6]Department of Anatomy, Kalpana Chawla Government Medical College, Karnal, Haryana, India
[2]Department of Medicine, Nemi Chand Medical College, Israna, Haryana, India

SUMMARY

Coronary arteries take origin from the sinus of Valsalva present at the aortic root bounded by a circumferential ridge called sinotubular junction (STJ). Developmentally, the location and morphology of these ostia may vary, and can cause variations in origin of coronary arteries and further complications in any interventional cardiac procedure. This has made it necessary to find the variation in number and location of ostia, their size, shape and relation with surrounding structures. The present study included 40 formalin-fixed cadaveric hearts. The average diameter of the right coronary ostium (RCO) was 3.1 mm and the left coronary ostium (LCO) was 4.2 mm. With regard to the shape of the ostium, the RCO was described as circular in 92.5% (37/40), horizontally elliptical in 7.5% (3/40) of cases. The LCO was circular in 90% (36/40), horizontally elliptical in 5% (2/40) of cases. The RCO was located below STJ in 65% cases (26/40), at STJ in 22.5% (9/40) and above STJ in 22.5% (9/40) cases. LCO were below STJ in 50% (20/40), at STJ in 27.5% (11/40) and above STJ in 22.5% (9/40) cases. Multiple ostia in single aortic sinus were recorded in 24.4 % of cases. The study of the location, shape and morphometry of coronary ostia is essential for any cardiac interventional procedures done for diagnostic and therapeutic evaluation.

Key words: Left coronary artery – Ostia – Right coronary artery – Sinus – Sinotubular – Tubular

ABBREVIATIONS:

LCO - left coronary ostium

RCO - right coronary ostium

CO - coronary ostia

STJ - sinotubular junction

INTRODUCTION

Coronary arteries are functional end arteries irrigating the heart, arising from the coronary ostia, which are two in number, located in the sinus of Valsalva, also known as aortic sinuses. These aortic sinuses are three in number located distal to the aortic valve at the root of the ascending aorta. The right coronary artery arises from the anterior aortic sinus, left from the left posterior aortic sinus, and the remaining third sinus is known as non-coronary sinus, because no coronary artery arise from that. The junction between aortic

Corresponding author:
Dr. Swati Bansal. Department of Anatomy, Medical college Block, Kalpana Chawla government medical college, Karnal, 132001, Haryana, India. Phone: +91-9416909881. E-mail: bansal.swati64@gmail.com

Submitted: January 18, 2022. **Accepted:** February 7, 2022

https://doi.org/10.52083/NVVY6522

sinuses and aorta is called sinotubular junction (STJ). Usually, the coronary ostia (CO) are located within the sinuses below STJ. However, the ostium may sometimes present at and above this circumferential ridge. Today, with the changes in living and working style, cardiac prognosis is proven to be worse, especially in young adults, and death occurs because of myocardial ischemia. So routine medical checkups must include coronary angiography. So as for purposes of diversity every cardiologist should have sound anatomical knowledge of normal, as well as variant topography of CO. The position and shape of CO and its relationship with STJ is valuable for any interventional as well as surgical cardiovascular procedure, such as coronary catheterization. After going through previous studies, the authors found that the studies were either angiographic studies or the studies conducted in populations of different countries, so data on Indian population are scarce. So, it is crucial for clinicians to know the pattern of these variations in selected demographic data. Further, the present study can add a range to the previous data for reference in designing of catheters in accordance with the requirements of the Indian population. So, this has motivated us to study the variant location, shape, size of coronary ostia and its relationship with STJ in Indian population.

MATERIALS AND METHODS

This study is a descriptive cross-sectional study. A total of 40 heart specimens preserved in 10% formalin were procured for the study in the dissection hall of the Anatomy Department from the cadavers used for routine undergraduate teaching. The heart specimens were both from male and female cadavers with a mean age of 60 years. Micro dissection was done on the heart to expose both coronary arteries and to remove the fat layer from epicardium so as to get a clear view of arteries. Then, the ascending aorta was transversely cut 2.5 cm above the level of origin of the coronary arteries. After getting a clear view of all the aortic leaflets and ostia, a longitudinal incision was given on the posterior wall of the noncoronary sinus. Then, the aortic root was opened like a book, and the following measurements were taken with the help of a 0.01 mm sensitive digital vernier caliper (Fig. 1):

1. Shape of CO.
2. Diameter of CO.
3. Location of CO in relation with STJ.
4. Height of cusps and ostium from bottom of sinus.
5. Location of ostium in relation with upper margin of aortic cusps.
6. Presence of any accessory ostia.
7. Location of ostium in relation with valve commissures.

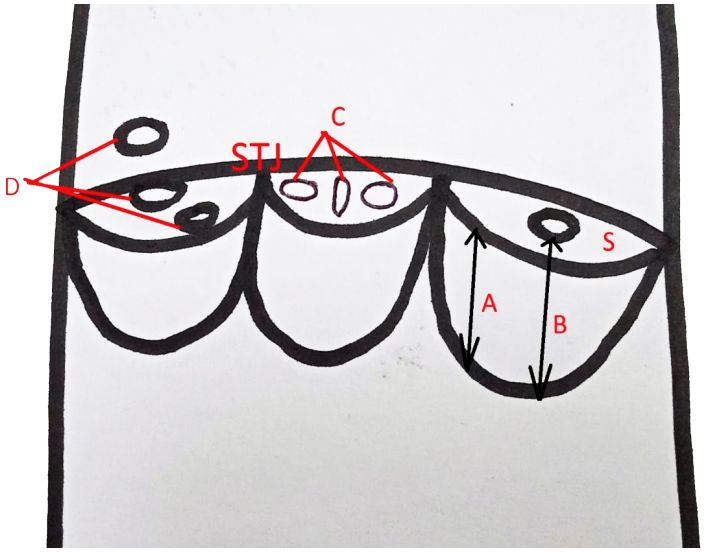

Fig. 1.- A and B: Distance of upper margin of aortic cusp and ostium from bottom of sinus. S: aortic sinus. C: different shapes of CO. D: location of ostium in relation with STJ.

Any cadaveric hearts with gross cardiomegaly and death because of any cardiac reason were excluded from the study. The measurements were double-checked by other authors so as to avoid any subjective bias. The results were tabulated in Microsoft Excel, and then statistical analysis was done by a data analysis tool.

RESULTS

Shape: As seen from Table 1, the shape of CO varied from circular, horizontally elliptical to vertically elliptical in appearance. Predominantly, the shapes of the ostia were circular. And none of the right and left ostia were found vertically elliptical in shape (Figs. 1 and 2).

Table 1. Shape of left and right coronary ostium.

Author (year)	Sample size (n)	Population	Right ostia (%)			Left ostia (%)		
			Circular	Horizontally elliptical	Vertically elliptical	Circular	Horizontally elliptical	Vertically elliptical
Present study	40	India	92.5	7.5	-	90	5	-

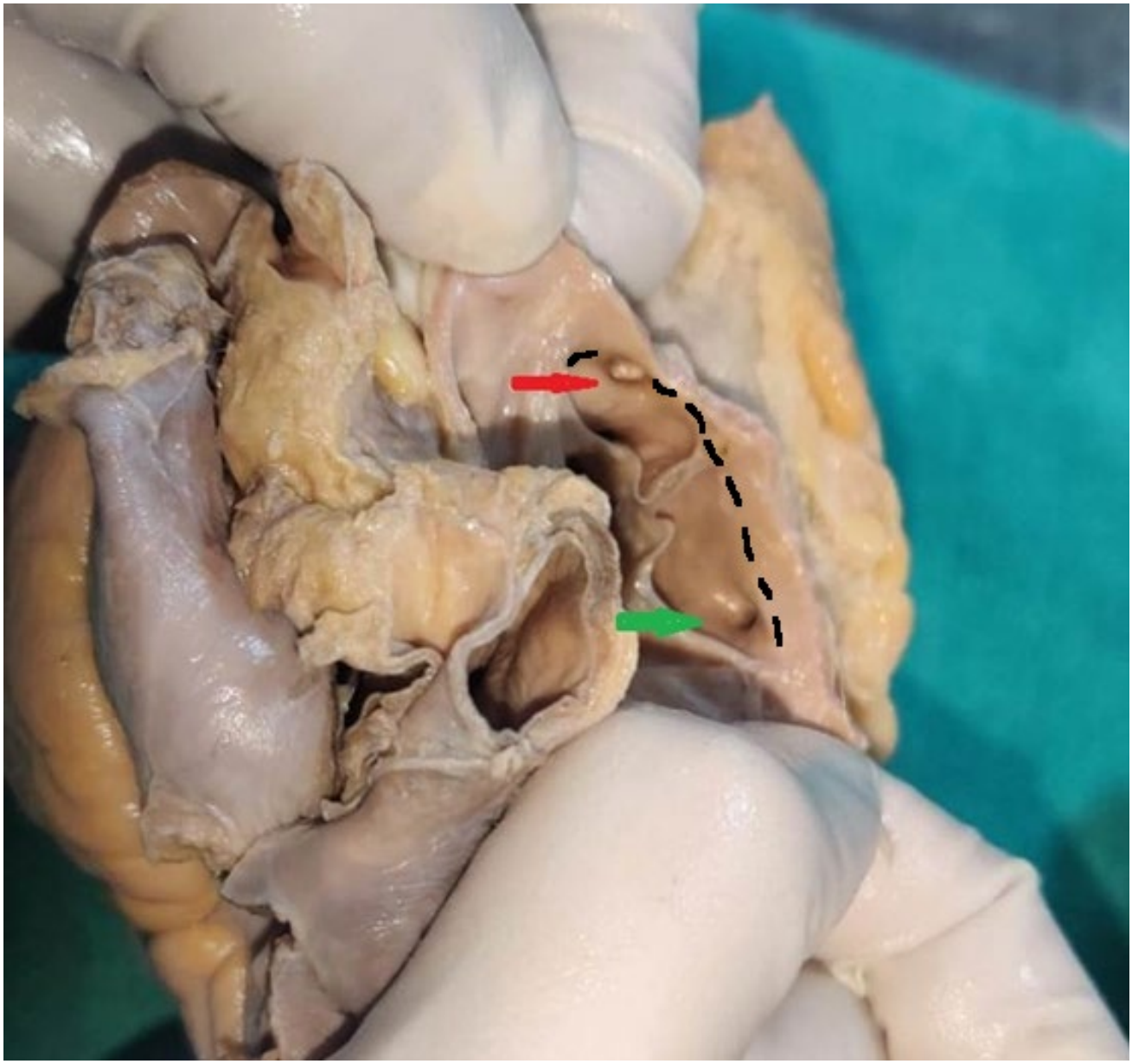

Fig. 2.- Red arrow: LCO, circular, centrally located, at STJ. Green arrow: RCO circular, below STJ, near commissure towards right.

Diameter: The mean diameter of LCO is 4.2 mm and that of RCO was 3.1 mm and when t-test was applied on the mean values; the difference was statistically significant (Table 2).

Relation to STJ: As shown in Table 3 and Figs. 2, 3, 4, CO showed variation in vertical placement. The most preferred location of both CO was sinus in nature.

Height of upper margin of the cusp and ostium from bottom of sinus: the average height of the upper margin of the cusp of the anterior aortic sinus from the bottom was 10.69±0.98 mm and that of the left posterior sinus was 10.82±0.99 mm. The average distance of the ostium from the bottom of the sinus in case of RCO was 13.44±1.3 mm, and that of LCO was 13.84±1. 2 mm (Table 4).

Location of the ostium in relation with upper margin of aortic cusps: in the present study, we found both the ostia were present above the upper margin of the respective cusps.

Table 2. T-test: paired two sample for mean.

	RCO	LCO
Mean	3.140769	4.2
Variance	0.25337	0.433695
Observations	40	40
Pearson Correlation	0.475318	
Hypothesized mean difference	0	
Degree of freedom	38	
t Stat	10.8464	
P(T<=t) one-tail	1.7E-13	
t Critical one-tail	1.685954	
P(T<=t) two-tail	3.4E-13	
t Critical two-tail	2.024394	

Table 3. Positions of CO with respect to STJ.

	Below STJ (n/%)	At STJ	Above STJ
Right coronary ostia	26(65)	9(22.5)	5(12.5)
Left coronary ostia	20(50)	11(27.5)	9(22.5)

Fig. 3.- Red arrow: Horizontally elliptical left ostium, centrally placed below STJ.

Fig. 4.- Red arrow LCO, circular, centrally placed above STJ.

Table 4. Measurement of height of aortic cusp and ostium from the bottom of sinus.

	Height of the cusp from bottom of the sinus		Height of the ostium from bottom of the sinus	
	Average	Range (mm)	Average	Range (mm)
Right	10.6992	8-12	13.44575	9-15
Left	10.8282	9-14	13.847	8-16

Location of the ostia with reference to commissures: out of 40 RCO, 80% (32/40) were located in the center of the respective sinus, only 17.5% (7/40) were towards the commissure on the right. In case of LCO, all the ostia were located in the center of the respective sinus with a frequency of 97.5% (39/40); only 2.5% (1/40) were located towards the commissure on the left (Figs. 5, 6).

Accessory ostia: accessory ostia were found in 24.4% cases only in the anterior sinus, and no such ostia were found in the left sinus (Figs. 5, 6).

DISCUSSION

The present study was conducted in a series of 40 hearts. In all the specimens, it was found that there were three aortic sinuses within their respective aortic cusps. The cusps of the aortic valve were connected with each other at the commissures, and on the inner side of the aorta a clear ridge was seen above the commissures, which indicate STJ. The CO location could vary from sinus to tubular and sinotubular junction, as shown in (Fig. 1). The location of CO is crucial for interventional cardiologists during catheter manipulation in procedures like angioplasty, angiography, or transcatheter aortic root valve replacement (Kulkarni and Paranjpe, 2015). In the present study, the left ostia were below STJ in 50% (20/40), at STJ in 27.5% (11/40) and above STJ in 22.5% (9/40) cases. The findings of this study correlate with values of Indian studies done by Nalluri et al. (2016) and Agrawal et al. (2018), who observed LCO relation with STJ in 52%, 39%, 9% and 64%, 32%, 4% respectively. However, the values did not correlate with the Indian study done by Kaur et al. (2012), who found it 78%, 15%, 7% with STJ. This discrepancy could be explained

Fig. 5.- Arrow A and B indicating accessory ostia and arrow C indicates RCO near commissure towards right.

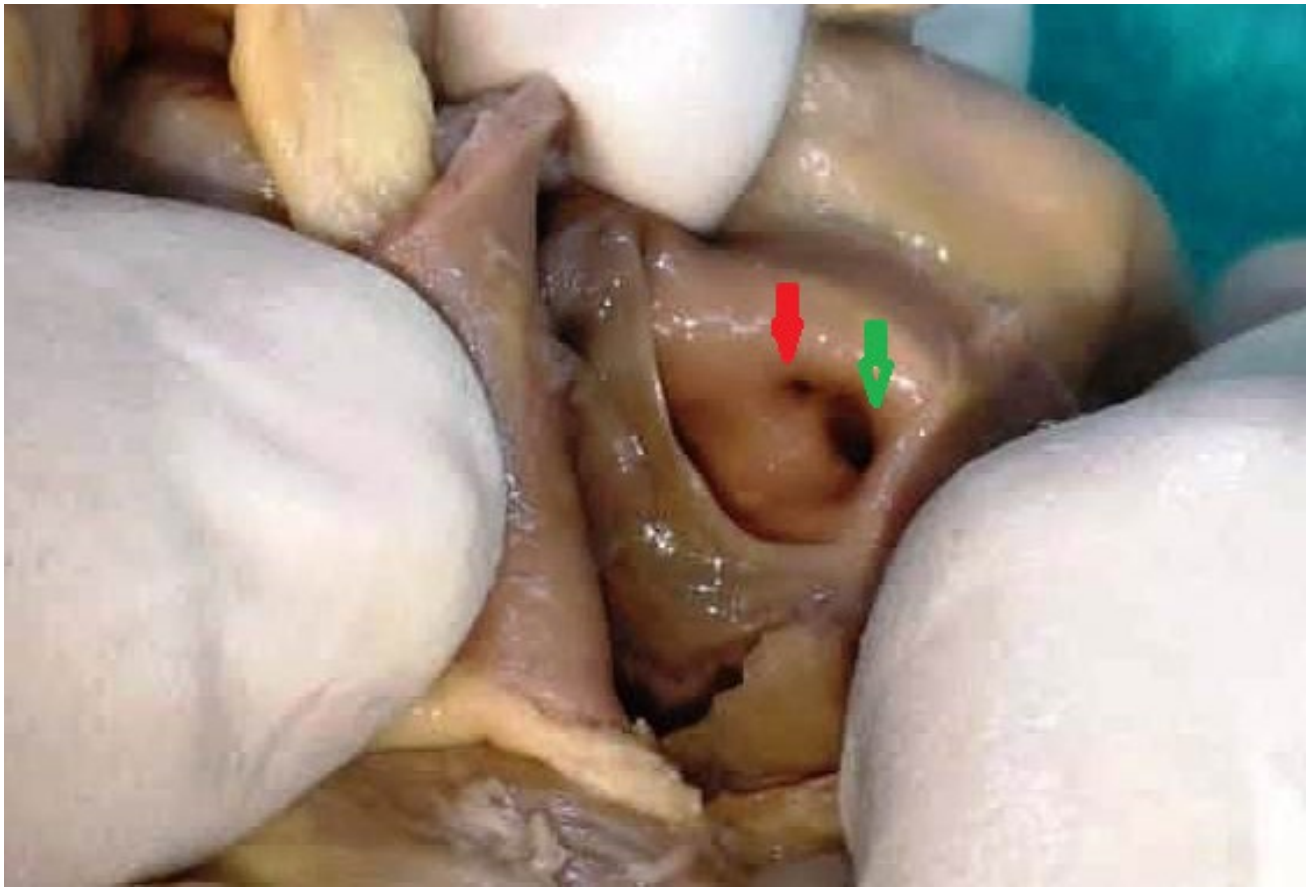

Fig. 6.- Red arrow indicating accessory ostium and green arrow towards RCO circular, near commissure towards right.

by the fact that in some cases, even when the ostia were above the level of commissures, the sinotubular ridge arched over the ostial opening rather than being straight. The difference in the findings described above might be due to overlooking the arched pattern of the sinotubular ridge. Moreover, when the results of the present study were compared with previous studies done by Pejkovic et al. (2008), Kosar et al. (2009), Govsa et al. (2010) and Nasr Tahlawi (2018), as shown in Table 5, it did not correlate, because of the impact of different geographical and racial background. RCO were present below STJ in 65% (26/40), at STJ in 22.5% (9/40) and above STJ in 2.5% (5/40) cases. The findings of this study correlate with values of Indian studies done by Nalluri et al. (2016), who observed RCO relation with STJ in 65%, 24%, 11%, and Agrawal et al. (2018) recorded in 78%, 10%, 12%. However, the values did not correlate with the Indian study done by Kaur et al. (2012), who found it in 83%, 14%, 3% with STJ, and Luckrajh et al. (2019) and Pejkovic et al. (2008) records were 88%, 12%, 0% and 19%, 71%, 10% respectively, as shown in Table 5. Regarding high origin of the coronary arteries, Kim et al. (2006) and Montaudon et al. (2007) stated that, if coronary artery origin was more than 1 cm above STJ, it was considered to be a high take-off, and within 1 cm above STJ it is normal. The failure rate of coronary catheterization was higher in patients having a coronary ostium above STJ. These ectopic coronary arteries frequently have slit like orifices and a tangential proximal course along the aortic wall, on which they lie, loosely attached to the aortic tissue. The right coronary artery is the most frequently ectopic artery, but the left coronary artery (or separately, the left anterior descending and circumflex artery) may also originate ectopically (Nishi et al., 2010). High take-off coronary arteries may link with sudden cardiac death, myocardial ischemia and increased risk of atherosclerosis. As far as myocardium perfusion was concerned, wherever CO might be located it did not affect coronary flow, according to Joshi et al. (2010); but, in case of aortic valve dysfunction. when aortic valve might flatten upon ostium in maximum systolic pressure, CO located above STJ would be functionally advantageous.

In the present study, the accessory ostia were noticed only in the right sinus in 24.4% cases, and no such ostia were noticed in the left sinus. These accessory ostia were circular in shape, smaller in size as compared to main ostium (Figs. 5, 6). As such, no independent artery was arising from these minute ostia. Wherever in anterior sinuses accessory ostia were present, the main ostium was found to be shifted near the commissure. The presence of multiple ostia within the coronary sinuses with or without original variations of the coronary arteries might be due to the growth of the coronary arteries into the aorta from the peritruncal ring of coronary vasculature, not grow out of the aorta (Fiss, 2007). Moreover, Udaya Sankari et al. (2011) added that this process involves apoptotic changes by the molecular mechanism through vasculoendothelial and fibroblast growth factors, where these factors stimulate the vasculogenesis and angiogenesis. However, the presence of multiple openings within AAS was explained as a result of the absorption

Table 5. Position of CO and its relationship with STJ.

Author (year)	Sample size	Population	RCO relation to STJ (%)			LCO relation to STJ (%)		
			Above	At	Below	Above	At	Below
Pejkovic et al. (2008)	150	Austria	10	71	19	60	18	22
Kosar et al. (2009)	700	Turkey	0.14	0.71	-	-	-	-
Kaur et al. (2012)	77	India	3	14	83	7	15	78
Govsa et al. (2010)	100	Turkey	3	13	78	13	29	58
Nalluri et al. (2016)	80	India	11	24	65	9	39	52
Agrawal et al. (2018)	50	India	12	10	78	4	32	64
Nasr and Tahlawi (2018)	60	Saudi Arabia	3.3	16.7	80	6.3	20	73.3
Present study	40	India	12.5	22.5	65	22.5	27.5	50

of the bulbous cordis into both ventricles during the heart folding by Stankovic and Jesic (2004). As far as diameter of CO was concerned, in the present study the mean diameter of RCO was 3.14±0.25 and that of LCO was 4.2±0.43. These compare favorably with other studies done by Kulkarni and Paranjpe (2015), Bhimalli et al. (2011), Cavalcanti et al. (2003) and Kaur et al. (2012) as shown in Table 6. Table 2 shows that the difference in the mean was statistically significant between LCO AND RCO diameter with p-value less than 0.05 at 95% confidence interval. Using the t-test, t statistic observed is greater than t critical, hence the mean diameters of LCO and RCO differ significantly. The diameter of the CO needs to be considered in the designing of equipment such as catheters for coronary angiography, coronary perfusion cannulas for the administration of cardioplegic solution and stents for aorto-ostial lesions, according to Kaur et al. (2012). This may ensure optimal results and avoid retrograde aortocoronary dissection (Dombe et al., 2013). The present study samples were irrespective of gender, but previous studies by Nasr and Tahlawi (2018) and Mobin et al. (2021) had shown no statistically significant difference in the parameters studied among male and female. In the present study, a circular shape ostium was found in 92.5% of RCO and 90% of LCO, whereas 7.5% of RCO and 5% of LCO were horizontally ellipsoid in shape. And none of the CO were vertically ellipsoid in shape. When the results of the present study were compared with data available in the literature, it did not correlate favorably (Table 7). This might be because of different racial and geographic backgrounds. The knowledge of the shape of the ostium is important while inserting and manipulating catheters in procedure like angiography, angioplasty (Kulkarni and Paranjpe, 2015).

According to the literature, there were cases reported of sudden death in young individuals and on autopsy CO found to be slit-like. Slit-like ostia are often associated with acute angulations of the

Table 6. Comparison of mean diameter of CO with other studies.

Studies	RCO	LCO
Kulkarni and Paranjpe (2015)	2.5 ± 1.0	2.8 ± 1.0
Bhimalli et al. (2011)	2.38 ± 1.33	3.17 ± 0.34
Cavalcanti et al. (2003)	3.46 ±0.94	4.75 ±0.93
Kaur et al. (2012)	3.9 ± 1.0	4.6 ± 1.0
Ortale et al. (2005)	5.0 ± 0.9	
Kohler et al. (1981)	3.833	4.833
Ballesteros and Ramirez (2008)	3.58 ± 0.59	
Present study	3.14±0.25	4.2±0.43

Table 7. Shows different shapes of CO and comparison with previous studies.

Author (year)	Sample size (n)	Population	Right ostia (%)			Left ostia (%)		
			Circular	Horizontally elliptical	Vertically elliptical	Circular	Horizontally elliptical	Vertically elliptical
Luckrajh et al. (2019)		South Africa	52	24	24	30	60	5
Kulkarni & Paranjpe (2015)	90	India	16	76	7	23	73	10
Govsa et al. (2010)	100	Turkey	60	-	-	55	-	-
Present study	40	India	92.5	7.5	-	90	5	-

initial part of the coronary artery, and predispose individuals to ischemia of the myocardium by Garg and Tiwari (2000). As far as horizontal placement of ostium was concerned, it might be located in the center of the sinus or slightly to the left or the right near the commissure. In the present study, 80% of RCO were in the center, and 17.5% near the commissure towards the right. In case of LCO, in 97.5% cases they were located in the center, and in 2.5% of cases it was towards the commissure on the left. There was paucity of literature for the data regarding variation in horizontal placement of the ostium. Knowledge of variation in the horizontal location of the ostia is important while doing Jatene's procedure of catheterisation. During catheterisation, the aortic valvular leaflet may be damaged if the ostium is located close to the leaflet. The average distance of the right ostium and the cusp from the bottom of the sinus in the present study was 10.6 mm and 13.44 mm, and that of the left cusp and ostium was 13.84 mm and 10.8 mm, which was almost equal on both the sides (Table 4). The aforesaid parameter was noted by few authors, such as Joshi et al. (2010), Jatene et al. (1999), and in all the studies RCO was placed higher than LCO. But in contrast, LCO was placed a little higher than RCO by Nalluri et al. (2016). It needs further study to find which one is higher in location. An abnormal localization of the coronary ostium is important in performing aortotomy incision for aortic valve exposure, preparing a coronary button in root replacement, and approaches for aortic root enlargement. Preoperative diagnosis of such coronary abnormalities is also important for surgical correction of congenital heart diseases, such as tetralogy of Fallot and transposition of great arteries. The limitation of the present study on variations in coronary ostia is due to the small sample size irrespective of age and gender difference.

CONCLUSION

The present study elucidates that the diameter of LCO was bigger than RCO; a circular shape and sinus location was predominant in both the ostia. The height of both the ostia was found equal from the bottom of respective sinus. The accessory ostia showed a maximum of two in number, were minute in size and only in right anterior aortic sinus. And important finding was that, wherever accessory ostia were present, the main ostia were shifted near the commissure. This anatomical study will help cardiologists and interventional surgeons to enhance their knowledge in variations of coronary ostia. This awareness will help to reduce the morbidity and mortality associated with coronary artery interventions.

ACKNOWLEDGEMENTS

The authors sincerely thank those who donated their bodies to science so that anatomical research and teaching could be performed. Results from such research can potentially increase scientific knowledge and can improve patient care. Therefore, these donors and their families deserve our highest respect.

REFERENCES

AGRAWAL R (2018) Anatomical study of coronary ostia in cadaveric human heart. *GJRA,* 7(3): 23-25.

BALLESTEROS LE, RAMIREZ LM (2008) Morphologic expression of the left coronary artery: a direct anatomical study. *Folia Morphol,* 67(2): 135-142.

BHIMALLI S, DIXIT D, SIDDIBHAVI M, SHIROL VS (2011) A study of variations in coronary arterial system in cadaveric human heart. *World J Sci Technol,* 1(5): 30-35.

CAVALCANTI JS, DE MELO NC, DE VASCONCELOS RS (2003) Morphometric and topographic study of coronary ostia. *Arq Bras Cardiol*, 81(4): 359-362.

DOMBE D, ANITHA T, KALBANDE S, NARESH T (2013) Clinically relevant morphometric and topographic analysis of coronary ostia. *Int J Curr Res Rev,* 5: 6.

FISS DM (2007) Normal coronary anatomy and anatomic variations. *Appl Radiol,* 36: 14-26.

GARG N, TIWARI A (2000) Primary congenital anomalies of the coronary arteries: a coronary arteriographic study. *Int J Cardiol*, 74: 39-46.

GOVSA F, CELIK S, AKTAS EO, AKTAS S, KOCAK A, BOYDAK B, SEN F (2010) Anatomic variability of the coronary arterial orifices. *Anatolian J Cardio,* 10.

JATENE MB, MONTEIRO R, GUIMARAES MH, VERONEZI SC, KOIKE MK, JATENE FB (1999) Aortic valve assessment. Anatomical study of 100 healthy human hearts. *Arq Bras Cardiol*, 73: 75-86.

JESHIKA SL, LUCKRAJH, KAPIL SS, LELIKA L (2019) An anatomical investigation of the coronary ostia and its relationship to the sinotubular junction within a select South African population. *Eur J Anat*, 23(3): 159-165.

JOSHI SD, JOSHI SS, ATHAVALE SA (2010) Origins of the coronary arteries and their significance. *Clinics* (Sau Paulo), 65(1): 79-84.

KAUR D, SINGH K, NAIR N, KALRA AS (2012) Morphology and morphometry of coronary ostia in South Indian adult human cadaveric hearts. *Int J Biol Med Res,* 3: 2169-2171.

KIM SY, SEO JB, DO KH, HEO JN, LEE JS, SONG JW, CHOE YH, KIM TH, YONG HS, CHOI SI, SONG KS, LIM TH (2006) Coronary artery anomalies: classification and ECG-gated multi-detector row CT findings with angiographic correlation. *Radiographics*, 26: 317-333.

KOHLER F, BLESS H, PITTNER PM (1981) Postmortem radiological studies of human ostia. *Rofo,* 134(5): 476-482.

KOSAR P, ERGUN E, OZTURK C, KOSAR U (2009) Anatomic variations and anomalies of the coronary arteries: 64-slice CT angiographic appearance. *Diagn Interv Radiol*, 15: 275-283.

KULKARNI JP, PARANJPE V (2015) Topography, morphology and morphometry of coronary ostia – a cadaveric study. *Eur J Anat,* 19: 165-170.

LUCKRAJH SJ, SATYAPAL SK, LAZARUS L (2019) An anatomical investigation of the coronary ostia and its relationship to the sinotubular junction within a select South African population. *Eur J Anat*, 23(3): 159-165.

MOBIN N, BASAVANAGOWDAPPA H, MADHU B (2021) A cross sectional study of anatomical variations of coronary ostia in the adult human hearts and its clinical significance. *JCDR*, 15(2): AC05-AC09.

MONTAUDON M, LATRABE V, IRIART X, CAIX P, LAURENT F (2007) Congenital coronary arteries anomalies: review of the literature and multidetector computed tomography (MDCT)- appearance. *Surg Radiol Anat,* 29: 343-355.

NALLURI HB, MOHAMMED AA, LEELA V (2016) Anatomic variability of coronary ostia in adult human cadaveric hearts. *Int J Anat Res*, 4(1): 1321-1325.

NASR AY, TAHLAWI MEL (2018) Anatomical and radiological angiographic study of the coronary ostia in the adult human hearts and their clinical significance. *Anat Cell Biol*, 51: 164-173.

NISHI H, MITSUNO M, TANAKA H, RYMOTO M, FUKUI S, MIYAMOTO Y (2010) High anomalous origin of the right coronary artery associated with aortic stenosis: a word of caution. *Ann Thorac Surg,* 89(3): 961-963.

ORTALE JR, MECIANO J, PACCOLA AM (2005) Anatomados ramos lateral, diagonal e anterosuperior noventriculo esqerdo do curacao humano. *Rev Bras CirCardiovas*, 20: 149-158.

PEJKOVIC B, KRAJNC I, ANDERHUBER F (2008) Anatomical variations of coronary ostia, aortocoronary angles and angles of division of the left coronary artery of the human heart. *J Int Med Res,* 36: 914-922.

STANKOVIC I, JESIC M (2004) Morphometric characteristics of the conal coronary artery. *MJM,* 8: 2-6.

UDAYA SANKARI T, VIJAYA KUMAR J, SARASWATHI P (2011) The anatomy of right conus artery and its clinical significance. *Recent Res Sci Technol*, 3: 30-39.

CT angiographic study of hepatic arteries variants in Iranian subjects

Asgar Moghani[1], Fatemeh Azemati[2], Amir Abdolmaleki[3], Mohammad Rezapour[1], Bahman J. Kondori[3,4]

[1] Student Research Committee, Baqiyatallah University of Medical Sciences, Tehran, Iran

[2] Department of Biology, School of Basic Sciences, Science and Research Branch, Islamic Azad University, Tehran, Iran

[3] Department of Anatomical Sciences, Faculty of Medicine, Baqiyatallah University of Medical Sciences, Tehran, Iran

[4] Baqiyatallah Research Center for Gastroenterology and Liver Diseases (BRCGL), Baqiyatallah University of Medical Sciences, Tehran, Iran

SUMMARY

This retrospective study aimed to assess the anatomical variations of hepatic arteries (HAs) in Iranian subjects referred to the Baqiyatallah Hospital (Tehran, Iran) as a reference medical center. The presence of anatomical variations such as hepatic arteries (HA) is approved among different societies. Classification of common patterns and probable variants of HA seems necessary in preoperative precautions of hepatosurgeries. Multidetector computed tomography angiography scans were prepared from the patients referred to the Baqiyatallah Hospital from January 2019 to January 2020. Inclusion and exclusion criteria were assessed, and all patterns of hepatic arterial supply were evaluated in 240 cases based on Michels' classification of HA. Following the assessment of 240 patients, HA variants with aberrant origin (types of II-VIII) were detected in 55 cases (22.92%). Besides, no patients were reported as types of XI and X variants (n=0). Also, no relationship was found between the HA and gender. Detection of common patterns along with abnormal variations of HA variants is necessary for hepatosurgical procedures. We found that 22.92% of Iranian patients referred to the Baqiyatallah hospital represented HA variation which must be considered in hepatic surgeries.

Key words: Variation – Hepatic artery – Computed tomography – Abdominal angiography

INTRODUCTION

Different hepatic functions are affected by the liver perfusion arteries, including HA and portal vein, which supplies 25% and 75% of the liver, respectively. Due to the critical role of HA in the preservation of the vital status of the liver, these arteries should be considered in various hepatosurgery processes. The celiac trunk (CT), as an essential branch of the aortic artery is responsible for blood supply to the essential organs such as spleen, stomach, and liver. Three main branches are divided from CT, including left gastric artery (LGA), splenic artery (SA), and common hepatic artery (CHA). Finally, the CHA is divided into two main branches, right HA (RHA) and left HA (LHA), which are responsible for the blood supply to the right and left lobes of liver, respectively (León et al., 2021). These

Corresponding author:
Bahman Jalali Kondori. Department of Anatomical Sciences, Faculty of Medicine, Baqiyatallah University of Medical Sciences, Tehran, Iran.
E-mail: Bahmanjalali2010@gmail.com

Submitted: January 15, 2022. **Accepted:** February 14, 2022

https://doi.org/10.52083/LYEA4587

arterial branches of the liver are sometimes divided from other sources than CHA, which are considered HA variants. The importance of angiography examination and identification of these variants prior to surgery is necessary for safe hepatosurgeries.

According to concepts of anthropology, HA has different variants in each country. Systematic examination of HA variants was first performed by Michels on autopsies (1966). Michels introduced 10 types of classification of HA as an accepted criteria for other investigations (Michels, 1966). In 2021, Imam et al., after examination of anatomical variations of HA, concluded that despite the presence of unclassified variants of the hepatic artery in different communities, this study also requires further in-depth evaluation due to the different unclassified patterns and HA variations requires further examinations in other countries (Imam et al., 2021). The most common classification of normal and variant hepatic arteries is based on Michels' guidelines. Ten different types of HA have been reported originated from a gastric artery or even from the superior mesenteric artery (SMA). Also, in this type of classification, accessory hepatic arteries were found following corpus dissection (Imam et al., 2021).

Multidetector computed abdominal tomography angiography is a technique used to visualize arterial and venous vessels throughout the body. This imaging protocol is widely used in the study of HA branches and their variants (Zaki et al., 2020).

Since there is no comprehensive study examining the prevalence of HA in the Iranian population, we aimed to investigate the typical anatomical structure and variants of HA in Iranian patients referred to Baqiyatallah Hospital as a reference medical center, using Multidetector computed tomography abdominal angiography technique and based on Michels' criteria. The results of this study can determine the types and prevalence of HA variations in Iranian society for safer hepatosurgeries.

MATERIALS AND METHODS

Patients collection and inclusion/exclusion criteria

All adult patients (18-80 years) referred to the Baqiyatallah hospital (Tehran, Iran) with abdominal pathologies were selected for primary screening of HA patterns from January 2019 to January 2020. Baqiyatallah hospital, as a reference medical center for hepatogasteric pathologies, was considered for data collection. Following preparation of multidetector computed tomography (MDCT) angiography (SOMATOM Sensation 16, Siemens, Germany), low-quality images, dissatisfied patients with the experiment, and the individuals with previous experience of HA surgery were excluded. Finally, a total of 240 patients were entered into the study. All administrative protocols were applied under the supervision of the Research Committee of Baqiyatallah University of Medical Sciences (Ethics Code: IR.BMSU.REC.1399.395), and the patients' medical records also remained confidential and undisclosed.

Protocol of MDCT procedure

A topography scan was performed following patient preparation and basic routine arrangements from the diaphragmatic region to the pubic symphysis. Using the Timing Bolus technique, the time required for the contrast agent to reach the CT was calculated. The thickness of images was defined as 7mm, and other device settings were provided as follows; 120 KV and Mas 320. Appropriate volume (1cc/kg) of Visipaque 320 mg contrast medium using an injector (speed of 4-6 ml/s) was injected through the cubital vein. The obtained axial images were entered into the workstation, and sagittal, coronal, three dimensional (3D) reconstructions were provided (Kalra et al., 2008).

Image interpretation and Michels` classification

The prepared images were analyzed independently by two expert radiologists. Celiac axis anatomy was evaluated, including LGA, SA, and CHA. Also, SMA was assessed to detect possible variations of aberrant arteries. HA variations

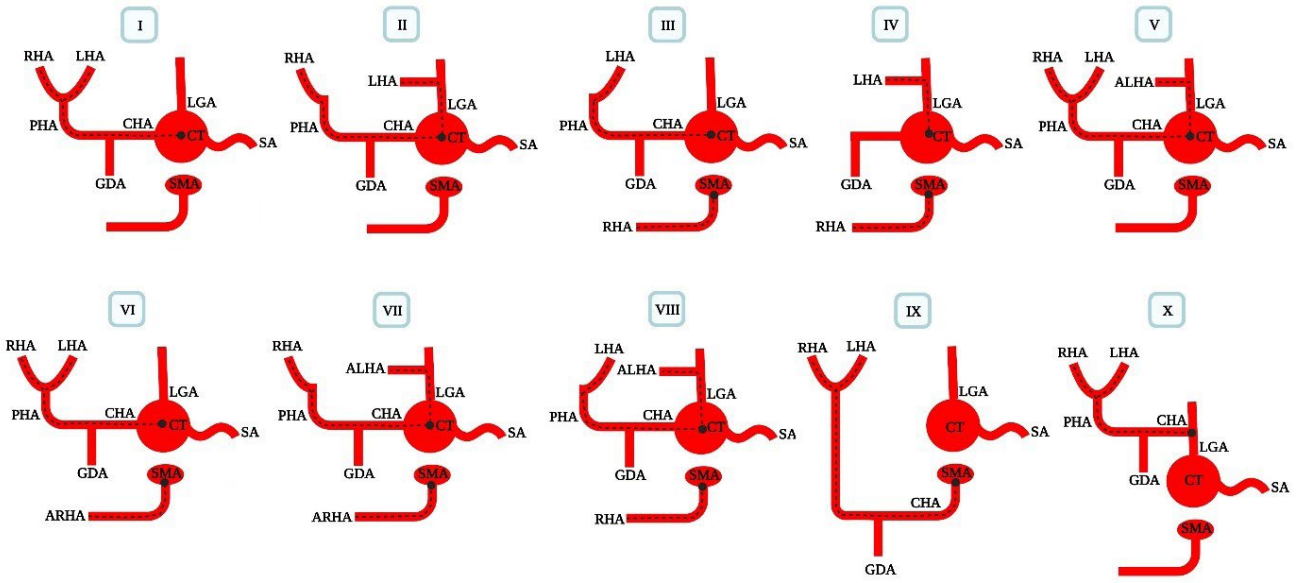

Fig. 1.- Ten patterns of hepatic artery variants according to the Michel`s classification. CT: celiac trunk, LGA: left gastric artery, SA: splenic artery, CHA: common hepatic artery, GDA: gastroduodenal artery, PHA: proper hepatic artery, RHA: right hepatic artery, and LHA: left hepatic artery.

were categorized for all images according to the Michels' guideline including: I. normal anatomy of HA, II. LHA originated from LGA, III. RHA originated from SMA, IV. LHA originated from LGA, and RHA originated from SMA, V. accessory left hepatic artery (ALHA) originated from LGA, VI. accessory right hepatic artery (ARHA) originated from SMA, VII. ALHA originated from LGA and ARHA originated from SMA, VIII. ALHA originated from LGA and RHA originated from SMA, IX. CHA originated from SMA. Finally, X. CHA originated from LGA (Fig. 1). The probable relationship between the prevalence of HA variations and male and female genders was evaluated and reported.

Statistical analysis

The statistical analysis among the prevalence of HA variation and gender was assessed using the Chi-squared χ^2 Test. Whole analyses were performed using SPSS™ software (v. 22, IBM Corporation NY, USA). The significant level was considered $p<0.05$.

RESULTS

Following consideration of inclusion/exclusion criteria, 240 (of 320 adult individuals) patients referred to the Baqiyatallah hospital were selected for CT, and it`s arterial branch variations. Demographic findings represented that the mean age of the patients was 45±3 years. Also, no significant ($p<0.05$) alteration was detected among the type of HA variants and the gender of patients (Table 1). All cases were found in the category of Michels` classification, and no new unclassified HA variations were detected.

In the field of assessment of origination of CHA, these types of variations were only found in IV, IX and X types. Respectively, no CHA was originated from CT (type IV), and also CHA was originated from SMA (type IX), and LGA (type X). In this study, no variants of CT and CHA were reported in types of IX and X. Besides, in our findings, 1.66% of cases had no CHA. In these cases, the RHA and LHA were originated from SMA and LGA, respectively (Table 1, Fig. 2).

According to the Michels' classification for assessment of RHA and ARHA variations, abnormal origination of RHA or the presence of ARHA were detected in variant types of III, IV, VI, VII, VIII, IX, and X. Totally, 8.32% of cases had abnormal origin of RHA and ARHA was detected in 7.07% of patients. In HA, the RHA variant of III (5.83%), IV (1.66%), and VIII (0.83%) were originated from SMA, while in types of VI (6.66%) and VII (0.41%), the presence of ARHA was detected (Table 1, Fig. 2).

Following assessment of LHA and ALHA, the aberrant origin of LHA was found derived from LGA in variation types of II (5%) and IV (1.66%).

Table 1. Frequency of types of hepatic artery variations according to the Michel`s classification. Data were presented in percentage. N=100. Type I: normal anatomy, type II: left hepatic artery from left gastric artery, type III: right hepatic artery from superior mesenteric artery, type IV: left hepatic artery from left gastric artery and right hepatic artery from superior mesenteric artery, type V: accessory left hepatic artery from left gastric artery, type VI: accessory right hepatic artery from superior mesenteric artery, type VII: accessory left hepatic artery from left gastric artery and accessory right hepatic artery from superior mesenteric artery, type VIII: accessory left hepatic artery from left gastric artery and right gastric artery from superior mesenteric artery, type IX: common hepatic artery from superior mesenteric artery, type X: common hepatic artery from left gastric artery.

Variant Types	I	II	III	IV	V	VI	VII	VIII	XI	X
Frequency (n/%)	185 77.08%	12 5%	14 5.83%	4 1.66%	6 2.5%	16 6.66%	1 0.41%	2 0.83%	0 0%	0 0%
Relationship with genders	p=0.32	p=0.18	p=0.09	p=0.17	p=0.07	p=0.09	p=0.08	p=0.20	p=0.31	p=0.14

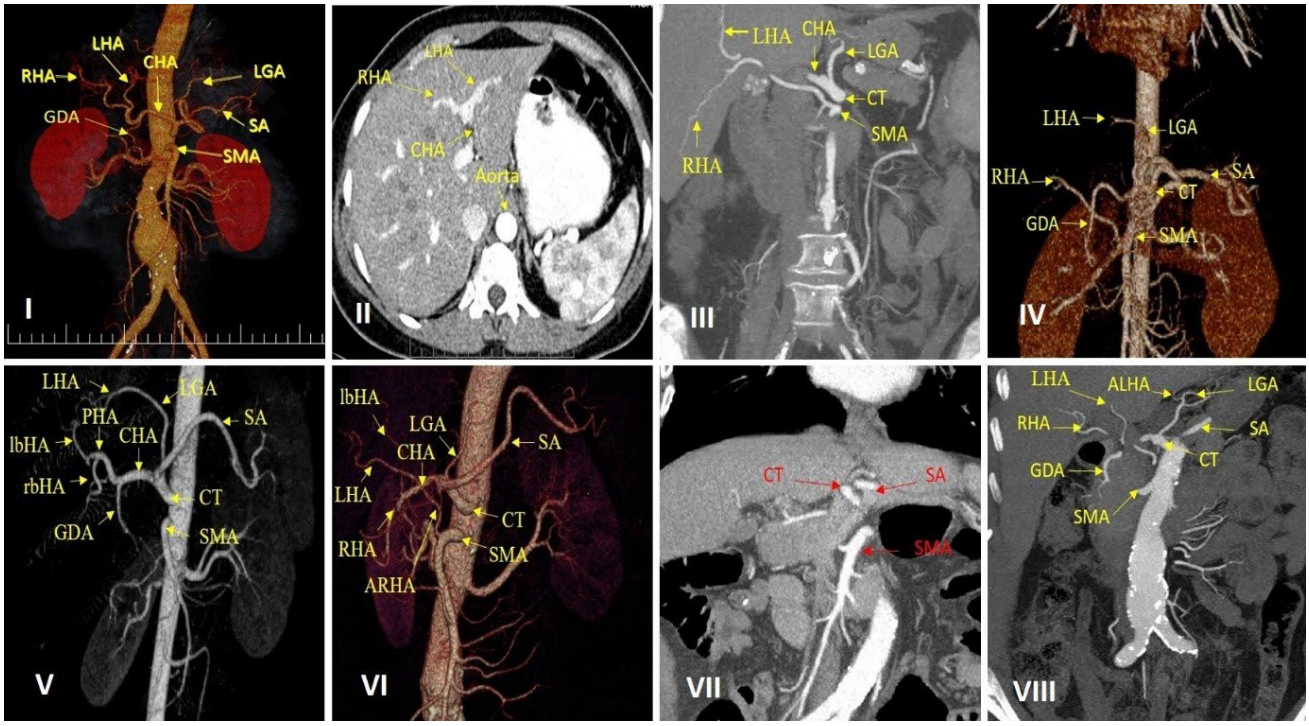

Fig. 2.- CT angiography images of hepatic artery variants in patients referred to Baqiyatallah hospital. CT: celiac trunk, LGA: left gastric artery, SA: splenic artery, CHA: common hepatic artery, GDA: gastroduodenal artery, PHA: proper hepatic artery, RHA: right hepatic artery, and LHA: left hepatic artery.

Also, no LHA was detected in type VII (0.41%). In types of V (2.5%), VII (0.41%), and VIII (0.83%), the left lode of the liver was also supplied by ALHA, as an additional artery originated from LGA. Totally, 6.66% of cases had an aberrant origin of LHA, and 2.91% had an extra artery for the left lobe of the liver in the form of ALHA (Table 1, Fig. 2).

DISCUSSION

According to the anatomical differences of HA among the countries and the need for determination of the prevalence of HA variants in Iranian society as one of the necessary arrangements for a safe hepatosurgery, we conducted an original retrospective study. Totally, we found that in 22.92% of the Iranian population, the HA is prone to variation, while 77.08% of individuals had a typical form of vascular pattern of HA. In a comprehensive investigation, Johnson coworkers assessed the prevalence of Hepatic artery anomalies in unselected patients undergoing computed tomography (CT) of the abdomen. 309 CT angiographic studies performed over 2 years were selected and assessed according to the Michels guideline. They found that 63.4% of individuals had conventional vascular anatomy, and the remaining represented variation in European countries (Johnson et al., 2013).

In this study, 1.66% of patients lacked the CHA branch. In these cases, the right and left hepatic arteries were derived from the SMA and LGA, respectively. Examination of DICOM images

showed that in the absence of RHA separated from CHA; this artery is probably originated from SMA. Besides, this artery is isolated from LGA in the absence of LHA originating from CHA. Parallel to our findings, Juszczak and coworkers assessed the unusual pattern of CT in 350 cases using MDCT images. As we found, they also reported the rare cases of variation in CT, especially the absence of CHA. They concluded that, although the absence of CHA is rare, it should be considered an essential issue in heapatosurgical procedures (Juszczak et al., 2021). Cankal et al. explicitly examined the variants of CT and HA in 200 patients using assessment of Multi-slice computed tomography images. CHA was found in 4% of cases in study of Cankal, which showed a significant difference in the frequency distribution of this variation in Turkish society compared to Iran; in our study population, no sample was found for type IX, but in Cankal` s study, 1.5% of the Turkish population represented CT with no CHA branch. In these cases, CHA was derived from the SMA (Cankal et al., 2021).

The RHA is one of the main clinical and surgical arteries due to its involvement in gallbladder blood supply, as well as the major part of the right lobe of liver (Mugunthan et al., 2016). In our findings, 8.32% of cases had an aberrant origin of RHA. In this cases, the blood supplies of right lobe and gallbladder were provided through SMA as an alternative blood supply. Mugunthan et al. assessed the probable variation of RHA in 60 adult cadavers (Mugunthan et al., 2016). Although in most cases, the typical origin of RHA was reported by Mugunthan, et al., but approximately in 13% of cadavers, the aberrant origin of RHA was found. Choi et al. (2021) in a comprehensive study on 5625 patients using computed tomography and digital subtraction angiographic images, evaluated the anatomic variations of hepatic arteries. They found the prevalence of aberrant RHA and LHA approximately 15%. Our study found this value as 8.32% and 6.66% for RHA and LHA, respectively. Finally, they reported that, if there was a variation in the hepatic artery (right or left), the accompanying variation in the other related hepatic artery is possible (Choi et al., 2021). In this study and based on Michels' guideline, the ARHA was originated from SMA in 7.07% of patients. In serval articles, this sub-arterial branch (ARHA) was derived from the GDA (Yamashita et al., 2015) or CHA (Polguj et al., 2010).

Another critical artery blood supply to the left lobe of the liver is LGA involved in hepatic artery reconstruction during liver transplantation (Yilmaz et al., 2021), esophagogastric, and gasterectomy (Shinohara et al., 2007). Our findings represented that 6.66% of all cases have aberrant origin of LHA. Also, we found that all cases of aberrant LHA were derived from LGA. In a meta-analysis study in 2020, the global prevalence of LHA was estimated 13.52%, in comparison with 6.66 in our study for the Iranian population (Cirocchi et al., 2020). Futara and coworkers analyzed HA variations on Ethiopians 110 postmortem cadavers comprehensively. Considerably, there was no LHA variation originating from LGA in Ethiopian populations, whereas in the same population, this artery was isolated from other arterial branches such as SA, CHA, and CT (Futara et al., 2001). Besides, in Iranian population in the present study, LHA was only originated from LGA.

It would be worth mentioning that the highest percentage of HA variations was observed in type VI, indicating that an extra branch of ARHA was originated from SMA. Besides, a lower percentage of HA variation was found in the XI and X types.

We also found no considerable relationship between the prevalence of HA variants and gender. Fatih Cankal and coworkers evaluated the prevalence of CT, HA, and their collateral branches using Multi-Slice Computed Tomography. They found no considerable differences among the prevalence of HA variants and genders in the turkey population (Cankal et al., 2021). This concept was also considered by Farghadani et al. in the field of assessment of anatomical variation of the celiac axis and its arterial branches using multidetector computed tomography angiography technique. As we found no considerable changes, they also stated the non-significant association among the male or female genders and the prevalence of CT variants (Farghadani et al., 2016).

CONCLUSION

The results of this novel study showed that most people of the Iranian society have a liver with a typical arterial pattern. Interventional radiologists and hepatobiliary surgeons practicing in Iran must be cognizant of these differences in order to minimize morbidity and mortality during invasive procedures. It is recommended that this research protocol be conducted in other communities as well in order to reach a global conclusion in this regard.

ACKNOWLEDGEMENTS

We are grateful to the Student Research Committee, Baqiyatallah University of Medical Sciences, for their financial support (Grant number: 99000471).

ETHICS APPROVAL AND CONSENT TO PARTICIPATE

All assessments were conducted in accordance with ethical principles and under the supervision of the University's Ethics Committee (Ethic NO: BMSU.REC.1399.395).

REFERENCES

CANKAL F, KAYA M, GUNER MA (2021) Evaluation of celiac trunk, hepatic artery variations, and their collateral arteries by multi-slice computed tomography. *Sisli Etfal Hastanesi tip bulteni*, 55(2): 217-223.

CHOI TW, CHUNG JW, KIM HC, LEE M, CHOI JW, JAE HJ, HUR S (2021) Anatomic variations of the hepatic artery in 5625 patients. *Radiol Cardiothoracic Imag*, 3(4): e210007.

CIROCCHI R, D'ANDREA V, AMATO B, RENZI C, HENRY BM, TOMASZEWSKI KA, RANDOLPH J (2020) Aberrant left hepatic arteries arising from left gastric arteries and their clinical importance. *Surgeon*, 18(2): 100-112.

FARGHADANI M, MOMENI M, HEKMATNIA A, MOMENI F, BARADARAN MAHDAVI MM (2016) Anatomical variation of celiac axis, superior mesenteric artery, and hepatic artery: Evaluation with multidetector computed tomography angiography. *J Res Med Sci*, 21: 129-129.

FUTARA G, ALI A, KINFU Y (2001) Variations of the hepatic and cystic arteries among Ethiopians. *Ethiopian Med J*, 39(2): 133-142.

IMAM A, KARATAS C, MECIT N, AFAK K, YILDIRIMOGLU T, KALAYOGLU M, KANMAZ T (2021) Anatomical variations of the hepatic artery: a closer view of rare unclassified variants. *Folia Morphol*, doi: 10.5603/FM.a2021.0024. Online ahead of print.

JOHNSON PB, CAWICH SO, ROBERTS P, SHAH S, GARDNER MT, GORDON-STRACHAN G, PEARCE NW (2013) Variants of hepatic arterial supply in a Caribbean population: A computed tomography based study. *Clinic Radiol*, 68(8): 823-827.

JUSZCZAK A, CZYŻOWSKI J, MAZUREK A, WALOCHA JA, PASTERNAK A (2021) Unusual variations in the branching pattern of the coeliac trunk and their clinical significance. *Folia Morphol*, 80(2): 283-289.

KALRA MK, SAINI S, RUBIN GD (2008) *MDCT: from protocols to practice*: Springer Science & Business Media.

LEÓN RAE, AGUIRRE GB, CORONADO VT, SÁNCHEZ DA, NAVA MCI, ZAMUDIO MD, PINEDA-MARTINEZ D (2021). Variations of the celiac trunk in Mexican population by MDCT angiography. *Eur J Anat*, 25(1): 57-64.

MICHELS NA (1966) Newer anatomy of the liver and its variant blood supply and collateral circulation. *Am J Surg*, 112(3): 337-347.

MUGUNTHAN N, KANNAN R, JEBAKANI CF, ANBALAGAN J (2016) Variations in the origin and course of right hepatic artery and its surgical significance. *J Clin Diagnos Res*, 10(9): AC01-AC04.

POLGUJ M, GABRYNIAK T, TOPOL M (2010) The right accessory hepatic artery; a case report and review of the literature. *Surg Radiol Anat*, 32(2): 175-179.

SHINOHARA T, OHYAMA S, MUTO T, YANAGA K, YAMAGUCHI T (2007) The significance of the aberrant left hepatic artery arising from the left gastric artery at curative gastrectomy for gastric cancer. *Eur J Surg Oncol*, 33(8): 967-971.

YAMASHITA K, HASHIMOTO D, ITOYAMA R, OKABE H, CHIKAMOTO A, BEPPU T, BABA H (2015) Accessory right hepatic artery branched from gastroduodenal artery. *Surg Case Rep*, 1(1): 90.

YILMAZ S, AKBULUT S, KUTLUTURK K, USTA S, KOC C, AYDIN C, BASKIRAN A (2021) Using the recipient's left gastric artery for hepatic artery reconstruction in living donor liver transplantation. *Liver Transplant*, 27(6): 923-927.

ZAKI S, ABDELMAKSOUD A, KHALED B, KADER IA (2020) Anatomical variations of hepatic artery using the multidetector computed tomography angiography. *Folia Morphol*, 79(2): 247-254.

A study on the morphometric analysis of glenoid cavity of scapula using a polymerizing acrylic mould

Vaithianathan Gnanasundaram[1], Hannahsugirthabai Rajilarajendran[2], Thotakura Balaji[3]

[1] Department of Anatomy, Chettinad Hospital and Research Institute, Chettinad Academy of Research and Education, India
[2] Department of Anatomy, Chettinad Hospital and Research Institute, Chettinad Academy of Research and Education, India
[3] Department of Anatomy, Chettinad Hospital and Research Institute, Chettinad Academy of Research and Education, India

SUMMARY

The shoulder joint is the most commonly dislocated joint in the body. Several conditions can cause shoulder disability, like avascular necrosis, rotator cuff tear, or fractures. Therefore, patients are advised to consider shoulder joint replacement surgery as a long-term remedy. Glenoid component loosening is a long-term complication seen in arthroplasty. Biomechanics of the reconstructed glenohumeral joint need a better understanding, so that the reason behind glenoid component loosening can be identified. The goal of this study is to record and analyze the various parameters using a mould. In this study, 106 scapulae with intact glenoid were included in the study. Acrylic moulds were measured with a vernier caliper.

The values were found to be symmetrical with respect to the right and left sides. New parameters which were studied include the thickness of the mould. The mean values at T1, T2, T3 were 2.95±0.75 mm, 2.67±0.74 mm, 2.26±0.55 mm respectively. The statistical significance was observed with the parameters. P-value was 0.002, 0.001 and 0.001 between Surface area - AP1, SI - AP and AP1 - T1 respectively. The dimensions which were from a mould give an added information about the depth of glenoid component, used for total shoulder arthroplasty.

Key words: Glenoid cavity – Acrylic mould – Surface area – Diameters – Arthroplasty

INTRODUCTION

The shoulder joint has more mobility at the cost of stability (Blache et al., 2017). The glenoid cavity is the main component in the formation of the shoulder joint. Its shallowness allows for movements in all axes (Sandstrom et al., 2015). The glenoid labrum increases its depth to a certain degree (Almajed et al., 2021). Several conditions can cause shoulder disability like avascular necrosis, rotator cuff tear, or fractures, and patients are advised to consider shoulder joint replacement surgery as a long-term remedy (Orfaly et al., 2007). The morphology of the glenoid cavity is highly variable. The shape of the cavity, if we consider previous studies,can be classified into oval, pear-shaped, and inverted-comma-

Corresponding author:
Dr Hannahsugirthabai Rajilarajendran. Department of Anatomy, Chettinad Hospital and Research Institute, Chettinad Academy of Research and Education, IT Highway, Kelambakkam, Chennai, Tamil Nadu, India 603103. Phone: +918300945188 / +919710403803.
E-mail: drrajianat@gmail.com

Submitted: November 8, 2021. **Accepted:** February 28, 2022

https://doi.org/10.52083/ATJJ6704

shaped (Mamatha et al., 2011). Alignment of the humerus and the glenoid articular surfaces is one of the predisposing factors for glenohumeral joint instability, which is one of the predisposing factors for rotator cuff pathology (Brewer et al., 1986). Diversified shapes of the glenoid cavity have been described with respect to the notched anterior glenoid rim (Prescher and Klumpen, 1997). The presence of a notch defines the shape of the glenoid cavity. The depth of the notch increases from oval to inverted-comma shape. It has been found that if the notch is distinct then the glenoid labrum is not fixed to the bony margin of the notch, but bridges the notch itself. This could make the shoulder joint less resistant to dislocating forces (Prescher and Klumpen, 1997). Variations in the dimensions of various parameters of the glenoid cavity have been studied before. The surface area and depth of the cavity in dry scapula are the new metrics evaluated to obtain further knowledge that could be of use for the surgeons in total shoulder arthroplasty (TSA).

In 1972, Neer used a single glenoid component size, which was completely made of polyethylene, during the first TSA cases (Neer, 1974). The present study designs a new method in acquiring morphometric data with the help of a glenoid mould. The mould gives much more insight on the dimensions of the prosthesis, which involves giving more depth by inclusion of parameters and helps improve efficacy in shoulder arthroplasty.

MATERIALS AND METHODS

The study was carried out in 106 dry scapulae of unknown age and sex. Side was determined, 52 belonging to the right and 54 belonging to the left glenoid. Only fully developed dry glenoid cavities without porosities were selected for the morphometric analysis. Moulding material (Dental products of India, Mumbai, India), an acrylic repair material used in dentistry, was taken along with cold mould seal. Sliding calipers were used for measurements.

The surface of the glenoid cavity was cleaned and dried. The mould material was added on the glenoid cavity and allowed to solidify. The solid moulds were removed from the glenoid cavity for analysis using vernier caliper. Parameters used for the analysis were:

Shape of the glenoid cavity: the shape of the cavity was taken with pencil tracing in white paper. Three different shapes based on the tracings were obtained. They were classified as a) oval shape, b) pear shape, and c) inverted-comma shape (Fig. 1).

Superoi diameter (SI): this was measured between the points A and B, extending from the highest point in the superior margin to the lowest point in the inferior margin of the glenoid cavity (Fig. 2).

Antero-posterior diameter (AP1): this was measured between the points C and D, extending from the anterior glenoid margin to the posterior glenoid margin. The line segment CD represents the maximum breadth of the glenoid cavity.

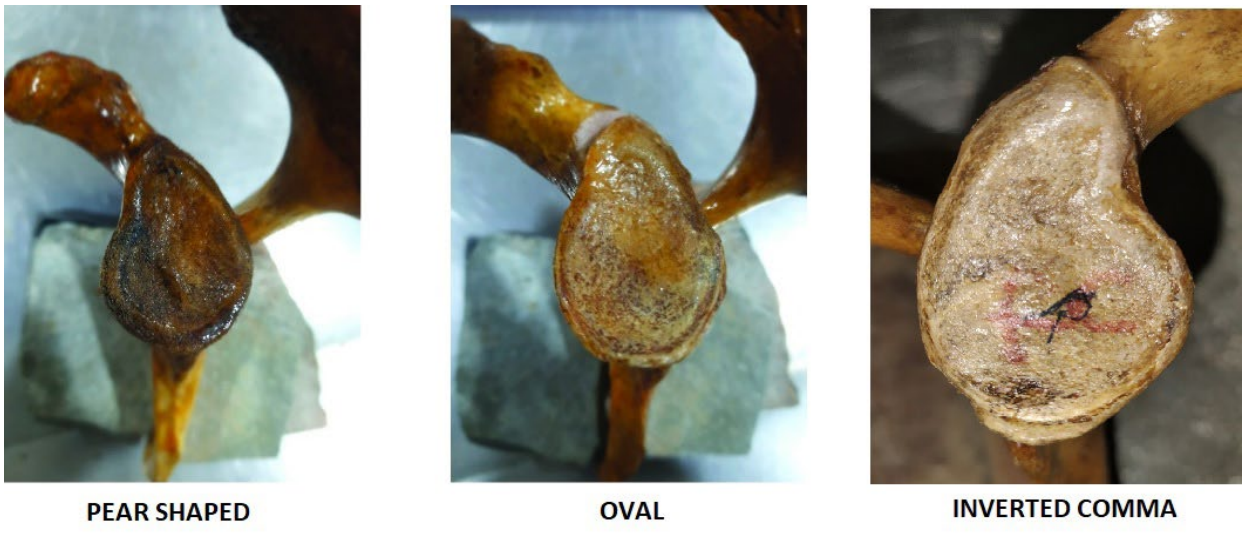

Fig. 1.- Shape of glenoid cavity. Shapes classified as a) Pear shape b) oval shape c) Inverted comma shape.

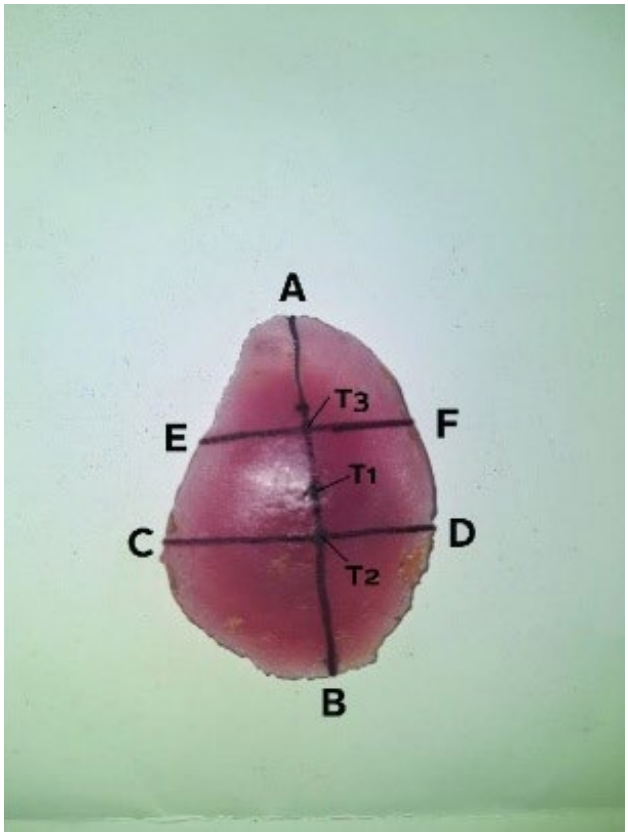

Fig. 2.- Diameters of glenoid mould. AB – Supero-Inferior diameter (SI). CD - Antero Posterior diameter (AP1). EF - Antero Posterior diameter (AP2). T1 – Thickness at midpoint between the points A and B. T2 - Thickness at midpoint between the points C and D. T3- Thickness at midpoint between the points E and F.

Antero-posterior diameter (AP2): this was measured between the points E and F, a horizontal line drawn at the midpoint between the points A and T1.

Surface area: outline tracing of the cavity was taken in graph sheet and measured in cm^2.

Thickness (T1): the thickness of the mould was measured at the midpoint taken between the points A and B, which corresponds to the mid-equator of the glenoid.

Thickness (T2): the thickness of the mould was measured at the midpoint taken between the line segment CD intersecting the line segment AB.

Thickness (T3): the thickness of the mould was measured at the midpoint taken between the line segment EF intersecting the line segment AB.

All measurements were made using a vernier caliper and the unit of measurement was millimeter. IBM SPSS software was used in order to find any statistical significance. The parameters were analyzed using unpaired sample t-test.

RESULTS

In the study which included 106 dry scapula the various metrics were tabulated with respect to side.

Supero-inferior (SI) and AP1 diameter presented symmetry in values of right and left glenoid. The right glenoid diameter in AP 2 was slightly higher than the left (Table 1).

Table 1. Comparison of diameters between the sides.

Sl. No	Observation	SI diameter (mm)		AP1 diameter (mm)		AP2 diameter (mm)	
		Right	Left	Right	Left	Right	Left
1	Range	27.3 to 36	27.1 to 36.3	17.3 to 28.4	18.5 to 28	12.3 to 20.5	11.9 to 18.9
2	Mean ±SD	31.65 ±2.32	31.78 ±2.56	22.91 ±2.86	22.99 ±2.48	16.10 ±2.11	15.69 ±1.62

Thickness at T1 and T2 presented the right-side marginally higher than the left-side values. In T3, the left side was slightly thicker than the right (Table 2).

Table 2. Comparison of thickness between the sides.

Sl. No	Observation	T1 (mm)		T2 (mm)		T3 (mm)	
		Right	Left	Right	Left	Right	Left
1	Range	1.5 to 4.3	1.4 to 5.1	1.4 to 4.3	1.8 to 4.6	1.1 to 3.5	1.2 to 3.3
2	Mean ±SD	2.90 ±0.79	2.99 ±0.76	2.64 ±0.76	2.70 ±0.73	2.33 ±0.62	2.23 ±0.47

The mean of the surface area of the right glenoid was 6.56±1.13 cm^2, and the left glenoid was 6.76±1.23 cm^2, which showed left dominance (Table 3).

Table 3. Comparison of surface area between the sides.

Sl.No	Observation	Right (cm^2)	Left (cm^2)
1	Range	3.5 to 8.5	4.5 to 9.5
2	Mean±SD	6.56±1.13	6.76±1.23

Out of 18 inverted-comma-shaped glenoids, 8 belonged to the right and 10 to the left side. In 58 pear-shaped glenoids, 30 were right and 28 were left. Oval shape was found in 14 right and 15 left glenoids (Table 4).

Table 4. Comparison of shapes between the sides.

Number of bones	Shape of glenoid	Incidence of shape	Right	Left
18	Inverted comma	16.98%	7.55%	9.43%
58	Pear	54.72%	28.30%	26.42%
30	Oval	28.30%	13.21%	15.09%

The shape and thickness were evaluated for statistical significance using IBM-SPSS software. $P \leq 0.05$ was considered statistically significant. Confidence interval for the difference in means was 95%.

In Pearson correlation, statistical correlation was not found between sides and diameters. The correlation between other values reported significance at various levels: p-value was 0.002 between surface area and AP1, 0.001 between SI and AP1, 0.001 between AP1 and T1, and 0.002 between AP1 and T2 levels (Table 5).

Table 5. Statistical correlations between parameters (Table showing p-value and 95% confidence interval between the parameters). *significant at p<0.05

	Side	Surf Area (cm^2)	SI	AP1	AP2	T1	T2	T3
Side		0.538	0.841	0.435	0.909	0.679	0.737	0.507
Surf Area (cm^2)	0.538		0	0.002	0	0.166	0.187	0.381
SI	0.841	0		0.001*	0	0.133	0.148	0.267
AP1	0.435	0.002*	0.001*		0	0.001*	0.002*	0
AP2	0.909	0	0	0		0.115	0.16	0.127
T1	0.679	0.166	0.133	0.001*	0.115		0	0
T2	0.737	0.187	0.148	0.002*	0.16	0		0
T3	0.507	0.381	0.267	0	0.127	0	0	

Irrespective of shape, significance was found at T1 and T2 with p-values 0.04 and 0.008 respectively (Table 6).

Table 6. Statistical correlations between shape and thickness (95% confidence interval and p-value). *significant at p<0.05

Thickness	T1	T2	T3
Shape	0.04*	0.008*	0.207

DISCUSSION

The study which was carried out with a mould closely resembled a glenoid component used in shoulder arthroplasty. The measurements made in this study differs from other studies in that the glenoid cavity measurements were taken from a mould, whereas various authors did it in dry scapulae, or by radiographic measurements in living subjects. The study included new parameters which were not studied by other authors. The metrics of the present study were compared with those of other studies for differences and similarities.

The present study showed inverted-comma shape in 16.98%, pear shape in 54.72%, and oval shape in 28.30% of all glenoid cavities. In the present study, inverted-comma shape was found in 7,55% of right-sided scapulae and 9,43% of left-sided scapulae presented with inverted-comma shape. None of the studies were close to the results compared to present study. The closest results were registered by El-Din and Ali (2015), which recorded the values at 16.25% on the right and 20% on the left side. Another study similarly close to the present values was done by Neeta Chhabra et al. (2015), which showed 22% on the right and 13% on the left side. Pear shape was predominantly the shape seen in most glenoid cavities. El-Din and Ali (2015), whose study came close to the present study, has reported with 35% on the right and 27.5% on the left side as against 28.30% on the right and 26.42% on the left in our present study. With respect to oval shape, the study by Rajput et al. (2012) reported 16% on the right and 15% on the left; and Neeta Chhabra et al. (2015), with 30.90% on the right and 32.40% on the left side. Our study presented with 13.21% on the right and 15.09% on the left side. The findings in this study were comparatively low. The studies by Prescher et al. (1997) have shown that, when

the glenoid notch is distinct, the glenoid labrum is loosely attached at the notch and can be a factor for anterior dislocation. Checroun et al. (2002) demonstrated a mismatch between glenoid and glenoid components regarding their shape. Our results compared the shape and thickness to help understand that shape alone was not the standout factor in glenoid component designing. (Table 7).

Table 7. Comparison of studies (shape of glenoid cavity).

Authors	Total no. of specimens	Pear shaped (%)	Inverted comma shaped (%)	Oval shaped (%)
Mamatha et al.	Right - 98	46	34	20
	Left - 104	43	33	24
Rajput et al.	Right - 43	49	35	16
	Left - 57	46	39	15
El-Din and Ali	Right - 80	35	16.25	48.75
	Left - 80	27.5	20	52.5
Neeta Ch-habra et al.	Right - 55	47.28	21.82	30.9
	Left - 71	54.92	12.68	32.4
Present study	Right - 52	28.30%	7.55%	13.21%
	Left - 54	26.42%	9.43%	15.09%

In the present study, the supero-inferior diameter of 31.65±2.32 mm on the right and 31.78±2.56 mm on the left were recorded. The studies which were closest in values were recorded by Mamatha et al. (2011), and Rajput et al. (2012). The mean values in those studies were at 34.76 mm, 33.67 mm on the right side and 34.43 mm, 33.92 mm on the left side respectively. The values in Neeta Chhabra et al. (2015) were 38.46 mm, 39.03 mm on the right and the left sides respectively were much higher compared to the present study. Churchill et al. (2001), Frutos et al. (2002), and Ozer et al. (2006) recorded the diameters based on sex in contrast to the present study, which was based on side. Their mean values stood at 37.5 mm, 36.08 mm, 38.71 mm on the male scapula, and 32.6 mm, 31.7 mm, 33.79 mm on the female scapula respectively (Table 8).

The mean antero-posterior 1 diameter in the present study was 22.91±2.86 mm, 22.99±2.48 mm on the right and the left side respectively. There seems to be no significance in size difference between the right and the left side, as was reported in the present study. Except for Mamatha et al. (2011), other studies reported the right glenoid to be broader in diameter than the left side. The study by Mamatha et al. (2011) was quite close to the present , with values of 23.35 mm on the right and 23.02 mm on the left. The average of both sides was 22.95±2.64 mm, which was quite similar to female glenoids, as reported by Ozer et al. (2006) and Frutos et al. (2002), in which the values were found to be 22.31 mm and 22.72 mm respectively. In the present study, the left-side diameter was quite close to what was found by a study by Rajput et al. (2012), in which the value was 22.92 mm (Table 9).

Table 8. Comparison of studies (supero-inferior diameter).

Authors	Total no. of specimens	Mean SI diameter (mm)
Churchill et al.	Male: 200	37.5
	Female: 144	32.6
Frutos	Male: 65	36.08
	Female: 38	31.7
Ozer et al.	Male: 94	38.71
	Female: 92	33.79
Mamatha et al.	Right: 98	33.67
	Left: 104	33.92
Rajput et al.	Right: 43	34.76
	Left: 57	34.43
Neeta Chhabra et al.	Right - 55	38.46
	Left - 71	39.03
Present study	Right - 52	31.65
	Left - 54	31.78

Table 9. Comparison of studies (antero-posterior 1 diameter).

Authors	Total no. of specimens	Mean AP1 diameter (mm)
Churchill et al.	Male: 200	27.86
	Female: 144	23.6
Frutos	Male: 65	26.3
	Female: 38	22.31
Ozer et al.	Male: 94	27.33
	Female: 92	22.72
Mamatha et al.	Right: 98	23.35
	Left: 104	23.05
Rajput et al.	Right: 43	23.3
	Left: 57	22.92
Neeta Chhabra et al.	Right – 55	25.04
	Left – 71	24.85
Present study	Right – 52	22.91
	Left – 54	22.99

The mean antero-posterior 2 diameter recorded in this study was 16.10±2.11 mm on the right, and 15.69±1.62 mm on the left glenoid. The diameters reported by Mamatha et al. (2011), 16.27 mm and 15.77 mm on the right and left side respectively, were in accordance with the present study. Iannotti et al. (1992) reported a higher diameter of 23.77 mm against the mean diameter of 15.89 mm in our study. The studies carried out by Iannotti et al. (1992) and Churchill et al. (2001) showed that the values recorded were higher than the values in our study, carriedout in Indian scapulae, which is suggestive of difference in diameters among races. In the study by Rajput et al. (2012), with 15.10 mm right and 13.83 mm left glenoid, the right glenoid was broader than the left and the values were comparatively lower than in our study. Kavita et al. (2013) and Neeta Chhabra et al. (2015), with diameters of 16.8 mm (right), 15.77 mm(left) and 18.6 mm (right), 18.70 mm (left), suggested similarities in diameters of glenoid cavity irrespective of sides. Higher number of pear-shaped glenoid is attributed to much lower AP-2 diameter. The data from studies carried out by Mamatha et al. (2011), Rajput et al. (2012), and Neeta Chhabra et al. (2015) coincide with our study (Table 10).

Table 10. Comparison of studies (antero-posterior 2 diameter).

Authors	Total no. of specimens	Mean AP2 diameter (mm)
Iannotti et al.	140	23.77
Mamatha et al.	Right: 98	16.27
	Left: 104	15.77
Rajput et al.	Right: 43	15.1
	Left: 57	13.83
Kavita et al.	Right: 67	16.8
	Left: 62	16.3
Neeta Chhabra et al.	Right - 55	18.7
	Left - 71	18.6
Present Study	Right: 52	16.1
	Left: 54	15.69

The mean thickness at the midpoint between A and B on the right side was 2.90±0.79 mm, and on the left side 2.99±0. 76 mm. The mean thickness at the midpoint between C and D on right side was 2.64±0.76 mm and on left side 2.70±0.73 mm. The mean thickness at the midpoint between C and D on the right side was 2.33±0.62 mm and on the left side 2.23±0.42 mm. As far as we know, this is the first study of its kind to use a cast mould and measure the thickness of it. Previous studies on glenoid component concentrated in the longevity of the implant rather than its shape, size or thickness (Gonzalez et al., 2011).

The thickness of glenoid component plays a major role in giving the shoulder prosthesis its durability (Mamatha et al., 2011). The present study, which was done uniquely in a mould, reports parameters on the thickness of mould at three different points, which could be an aid in designing the glenoid component efficiently and in improving efficacy.

The mean surface area for the right glenoid was 6.56±1.13 cm^2, and for the left glenoid 6.76±1.23 cm^2. Homem et al. (2018) reported perimeter of right glenoid at 6.72 cm^2 and left glenoid at 9.63 cm^2.

Although statistical significance was found between the diameters and surface area in t-tests, it does not relate much in pathological changes altering the glenoid cavity and its rim to a certain degree. The available glenoid component in the market and dimensions of the glenoid cavity have to be taken into consideration in accordance with the demographic conditions (Mamatha et al., 2011). The goal of this study is to give an insight and advantage in designing the glenoid component by devising a replica through a mould.

To summarize, the presence of a glenoid notch was observed in 70% of glenoid cavities, with no difference in values between the sides. Marked symmetry was found in our study when compared to other studies, which had a difference in data between the right and left sides. 3D-imaging and patient specific instrumentation will have to be based on a profound knowledge of glenoid morphology (Zumstein et al., 2014). The most common long-term complication of TSA is glenoid loosening, which accounts for approximately 24% of all TSA complications (Gonzalez et al., 2011). We have devised a dataset with glenoid mould height, width, thickness and surface area.

This study provided new parameters to give an insight on the depth of the glenoid cavity by using a cold mould. The mould, although structurally different from actual glenoid component, provides knowledge for possible restructuring in designing of the glenoid component. A glenoid mould can serve a perfect module to study the component designing, which in turn can help the orthopedicians decide on the size of the component.

ACKNOWLEDGEMENTS

The authors sincerely thank those who donated their bodies to science so that anatomical research and teaching could be performed. Results from such research can potentially increase scientific knowledge and can improve patient care. Therefore, these donors and their families deserve our highest respect.

REFERENCES

ALMAJED YA, HALL AC, GILLINGWATER TH, ALASHKHAM A (2021) Anatomical, functional and biomechanical review of the glenoid labrum. *J Anat*, 00: 1-11.

BLACHE Y, BEGON M, MICHAUD B, DESMOULINS L, ALLARD P, DALMASO F (2017) Muscle function in glenohumeral joint stability during lifting task. *PLoS ONE,* 12(12): e0189406.

BREWER BJ, WUBBEN RC, CARRERA GF (1986) Excessive retroversion of the glenoid cavity: a cause of non-traumatic posterior instability of the shoulder. *J Bone Joint Surg Am*, 68(5): 724-731.

CHECROUN AJ, HAWKINS C, KUMMER FJ, ZUCKERMAN JD (2002) Fit of current glenoid component designs: an anatomic cadaver study. *J Shoulder Elbow Surg*, 11: 614-617.

CHURCHILL RS, BREMS JJ, KOTSCHI H (2001) Glenoid size, inclination,and version: An anatomic study. *J Shoulder Elbow Surg*, 10(4): 327-332.

EL-DIN WA, ALI MH (2015) A morphometric study of the patterns and variations of the acromion and glenoid cavity of the scapulae in Egyptian population. *J Clin Diagn Res*, 9(8): 8-11.

FRUTOS LR (2002) Determination of sex from the clavicle and scapula in a Guatemalan contemporary rural indigenous population. *Am J Forensic Med Pathol*, 23: 284-288.

GONZALEZ JF, ALAMI GB, BAQUE F, WALCH G, BOILEAU P (2011) Complications of unconstrained shoulder prostheses. *J Shoulder Elbow Surg*, 20(4): 666-682.

HOMEM JM, DEMAMAN AS, LACHAT D, ZAMARIOLI A, THOMAZINI JA, LACHAT JJ (2018) Anatomical and anthropological investigation of the articular surface of the human glenoid cavity in Brazilian corpses. *SM J Clin Anat*, 2(2): 1010.

IANNOTTI JP, GABRIEL JP, SCHNECK SL, EVANS BG, MISRA S (1992) The normal glenohumeral relationship. *J Bone Joint Surg*, 74(4): 491-500.

KAVITA P, JASKARAN S, GEETA (2013) Morphology of coracoids process and glenoid cavity in adult human scapulae. *Int J Anal Pharmac Biomed Sci*, 2(2): 19-22.

MAMATHA T, PAI SR, MURLIMANJU BV, KALTHUR SG, PAI MM, KUMAR B (2011) Morphometry of glenoid cavity. *Online J Health Allied Sci*, 10(3): 7.

NEER 2ND CS (1974) Replacement arthroplasty for glenohumeral osteoarthritis. *J Bone Joint Surg Am*, 56(1): 1-13.

NEETA CHHABRA, SURAJ PRAKASH, MISHRA BK (2015) An anatomical study of glenoid cavity: its importance in shoulder prosthesis. *Int J Anat Res*, 3(3): 1419-1424.

ORFALY RM, ROCKWOOD CA JR, ESENYEL CZ, WIRTH MA (2007) Shoulder arthroplasty in cases with avascular necrosis of the humeral head. *J Shoulder Elbow Surg*, 16(3 Suppl): S27-32.

OZER I, KAZUMICHI K, MEHMET S, ERKSIN G (2006) Sex determination using the scapula in medieval skeletons from east. *Anatolia Coll Antropol*, 302: 415-419.

PRESCHER A, KLUMPEN T (1997) The glenoid notch and it's relation to the shape of the glenoid cavity of the scapula. *J Anat*, 190(Pt3): 457-460.

RAJPUT HB, VYAS KK, SHROFF BD (2012) A study of morphological patterns of the glenoid cavity of scapula. *Nat J Med Res*, 2(4): 504-507.

SANDSTROM CK, KENNEDY SA, GROSS JA (2015) Acute shoulder trauma: what the surgeon wants to know. *RadioGraphics*, 35(2): 475-492.

ZUMSTEIN V, KRALJEVIC M, HOECHEL S, CONZEN A, NOWAKOWSKI AM, MULLER-GERBLM (2014) The glenohumeral joint - a mismatching system? A morphological analysis of the cartilaginous and osseous curvature of the humeral head and the glenoid cavity. *J Orthop Surg Res*, 13: 9-34.

Preliminary results of the first Spanish virtual body donation program. Usefulness in Anatomy, Morphological Sciences, and healthcare implications

José Aso Escario[1], José V. Martínez Quiñones[1], Ricardo Arregui[1], Fabián Consolini[1], Daniel Chaverri Fierro[2], María Llorens Eizaguerri[2], Manuel Gil Begué[3], Ana Nuez Polo[4], Salvador Baena Pinilla[5], Alberto Aso Vizán[6]

[1] Servicio de Neurocirugía. Hospital MAZ, Zaragoza, Spain

[2] Servicio de Cirugía Ortopédica y Traumatología, Hospital MAZ, Zaragoza, Spain

[3] Servicio de Calidad e Innovación, Hospital MAZ, Zaragoza, Spain

[4] Dirección Médica, Hospital MAZ, Zaragoza, Spain

[5] Cátedra de Anatomía Humana, Facultad de Medicina, Universidad de Zaragoza, Instituto de Medicina Legal de Aragón, Zaragoza, Spain

[6] Servicio de Cirugía Ortopédica y Traumatología, Hospital general de la Defensa, Universidad de Zaragoza, Spain

SUMMARY

The donation of human bodies for medical education purposes currently faces a shortage that could, in some way, limit the practical teaching of anatomy, aggravated in pandemic times.

Medical diagnosis has undergone a revolution due to the so-called "imaging techniques", which obtain digital files containing, totally or partially, a virtual copy of the body.

This enables a new type of donation that has been termed, in recent publications, "virtual body donation". According to this, a virtual body donation program, has been implemented, including a repository of digital samples, generated from image scans, provided by patients.

This article presents the program casuistry, analyzes the usefulness of this type of material, both from the educational and healthcare care points of view, and deals with some difficulties or problems in the constitution and management of these programs, as well as the solutions that could be implemented.

The program promotes an innovative form of teaching anatomy and related sciences (pathology, anthropology, and others). It also has advantages for the training of professionals in virtual dissection techniques and virtopsy. In addition, its usefulness in research appears to be unlimited in anatomy, anthropology, and other disciplines.

Virtual models, generated by these programs and organized as "object's repositories", extend

Corresponding author:
José Aso Escario. Hospital MAZ, Avenida de la Academia General Militar 74, 50015 Zaragoza, Spain. Phone: 976-748000, ext 1031; Fax: 976748044. E-mail: jaso@maz.es

Submitted: December 18, 2021. **Accepted:** February 19, 2022

https://doi.org/10.52083/PSJO9849

their usefulness timelessly and they can be indefinitely studied. The need to expand these virtual donations to a multicenter and cooperative implementation is emphasized, with the purpose of creating extensive digital object's repositories and including as many specimens as possible, both normal and pathological.

Key words: Body donation – Image analysis – 3D modelling – Virtopsy – Virtual dissection

LIST OF ABBREVIATIONS

VBD: Virtual body donation

VBDP: Virtual body donation program

VRO: Virtual repository of objects

DICOM: Digital Imaging and Communications in Medicine

DICOMDIR: File containing information of the DICOM files (series, instances, indexes and others)

PACS: Picture Archiving and Computer System

IAPT: Image analysis and processing techniques

3D: Three dimensions

CT: Computed Tomography

MRI: Magnetic Resonance Imaging

INTRODUCTION

Organ donation for healthcare purposes is the foundation of organ and tissue transplantation programs, the Spanish model being one of the most accredited worldwide (Matesanz, 2004). These programs have their own legal regulations (Ley 30/1979, 1979; Real Decreto 1723/2012, 2012).

However, if the objective of the donation is teaching or research, in Spain there is a lack of specific regulation. Usually, it is each school of medicine that establishes its own rules, being the written consent, signed while alive by the donor, the main rule that governs the relationship between the donor and the university (McHanwell et al., 2008).

Human body donation for teaching or research purposes provides a limited number of corpses, which could be scarce for some academic or research needs, as in Radiological Anatomy, for example. In the Third World, where often there is a low supply of cadavers, or where cultural or religious beliefs prevent whole-body donation, an effort to find other specimens in place of cadaveric donation should be made.

It would be also important to find a substitute for wet cadaveric materials during the Covid pandemic or other similar future epidemic threats.

During the last years the diagnosis in medicine has undergone a revolution with the development of "imaging techniques." Basically, these techniques acquire the virtual body of the patient, either totally or partially.

Based on this, a new donation possibility ("virtual body donation" -VBD) has been proposed for use in teaching or research. Characteristics, requirements, documentation, and legal regulation of such programs has been recently published (Aso et al., 2019).

Following the guidelines of this publication, a VBD program, including a repository of objects (VRO) made up of the specimens produced by the donations, has been implemented.

In the present paper, the experience, casuistry, and usefulness of this program are analyzed, both at a medical training and healthcare care levels, as well as the difficulties or problems inherent to such type of initiatives.

MATERIAL AND METHODS

Methodology

Informed consent

The methodology for the inclusion of patients in the VBD program begins with the informed consent. Normally, it is the doctor responsible for the patient who has the mission of explaining the program, giving him/her the information document, and signing, together with him/her, the authorization form for the donation.

This form follows the directives of the European Union on the rights of patients and regulations (Reglamento UE 2016/679, 2016) and includes

the necessary information about the donated material (Dicom files).

It is very important for the patient to know what is subject to donation. The patient is informed about the fundamentals of medical image, which include files that follow the DICOM protocol (Digital Imaging and Communications in Medicine), stored in the PACS (Picture Archiving and Computer System) (Napoli et al., 2003; NEMA, 2001).

A DICOM file can be viewed as a stack of images described by an index, called DICOMDIR. Each file includes a header, which contains data of the patient (Name, date of birth, weight, etc.), of the acquisition (type of imaging technique, place, Hospital, and others), as well as information on the images (i.e.: calibration, gray levels, bits per pixel, resolution) (Rorden, 2018).

Patients are also informed that these files content graphical data that can reproduce his/her appearance and other elements that can identify him/her, as well as personal information. Likewise, they are informed that the files will be treated using image analysis and processing techniques (IAPT) (Bankman, 2020) that allow, in turn, to obtain other new products like 3D models, both for visualizing and printing.

The patients are informed that the files and the new products of image processing will be treated anonymously, and that he/she may or may not consent to the inclusion of certain parts of the anatomy, such as the face, which could identify him.

The program includes an information dossier, and both this and the donation form have been approved by the Hospital's Ethics Committee.

Once the informed consent has been obtained, the following phase is started, generating the objects of interest.

General issues concerning the VBD (patients inclusion criteria, informed consent, database requirements, personal data protection, anonymity, and others, can be consulted in a recent publication (Aso et al., 2019), as well as other ethical and medicolegal aspects of the program.

Generation of objects

Actions on DICOM files, aimed to scientific purposes, are known as "image analysis and processing techniques" (IAPT).

Classically, they can be classified as follows:

- ***Techniques of image analysis***

  They operate on graphic files without modifying them, aimed at obtaining information on some characteristics of the object.

  Interactive inspection, measuring angles, distances, volumes, and indices, is an interesting example and can be done repeatedly and remotely. Euclidean or geometric morphometrics, are additional examples useful in anthropology or forensic medicine.

- ***Techniques of image processing***

  These are manipulative operations intended to modify some characteristics of the file. The result, even temporarily, is an image (a file) different from the one was taken from the start.

  The clearest example is the segmentation of regions of interest. This procedure isolates one anatomical part from the rest. Once separated, all kinds of inspections or measurements can be carried out on it.

  One of the main applications of segmentation is the selection of structures for their three-dimensional reconstruction.

  3D reconstructions merit a special review. Most programs that allow 3D reconstructions make it possible to generate and analyze models, either by their own software or by exporting to other three-dimensional environments (Autodesk 3DS Max, 2019; Javan et al., 2020). Basically, 3D reconstruction provides either volumes or isosurfaces.

  Table 1 shows the most important characteristics and differences between volumes and isosurfaces. In the isosurface, the object is only composed of a mesh of triangles arranged in one or several surfaces.

Table 1. Characteristics of 3D models.

Volume	Isosurface (Mesh)
Clouds of voxels with different shadows of grey	Meshes arranged by means of triangles joining the object points
Offer a very detailed imagen of the specimen	Only superficies of object are rendered
It is not possible to store the volumes	Can be stores as 3D formats (.obj,.stl,...)
Can be split or cut, being the section surface homogeneous	Can be cut or split, but its section shows only the plane or line when the surfaces were cut
We cannot give them physical properties	They can have physical properties

However, in the volume, all the anatomical elements are shown, represented by their respective voxel, each of which contains its specific properties (location, gray range, etc.).

Once cut, the surface of a volume section will show all the texture of the original tissues. In contrast, cutting an isosurface will show multiple planes and hollow areas between them.

Although the external appearance is very similar, the techniques applicable to the volume are much more extensive and deeper than to the isosurface, as can be understood since the latter only has planes of triangles.

In both cases, the quality of the reconstructions is immense, and techniques like the rendering of materials have been used with spectacular results (Dappa et al., 2016).

- ***Combined techniques***

  Both procedures (analysis and process) can be used in conjunction. Frequently, a processing task is firstly carried out and, afterwards, an analysis technique is applied to the result.

  Some examples are Registry, Fusion, Navigation, Augmented and Virtual Realities.

  Augmented reality is based on inserting virtual objects into a real-world environment (for example, 3D models). Virtual reality involves the inspection of a completely virtual environment. The use of augmented reality has been proposed as a complementary method to autopsy (Affolte et al., 2019).

  Other important procedure is 3D Printing, one of the most useful products in teaching and research (Javan et al., 2020), as well as in surgical planning, as will be discussed later.

IAPT procedures are possible by means of dedicated software. There are a variety of packages, many of them freeware or public domain, which can be useful (Inria teams, 2021; Schindelin et al., 2012; Roset et al., 2004; Yushkevich et al., 2006; Kikinis et al., 2014; Fogal et al., 2010; Heckel et al., 2009; Amorim et al., 2015; Cignoni et al., 2008).

The virtual objects generated by the IAPT are stored into an Object Repository (VRO).

It is one of the most interesting parts of the program and, probably, also one of the most useful for teachers, researchers, or other professionals with an interest in these techniques.

IAPT typically generate new elements from DICOM files. These elements can be: Flat images (two-dimensional), triplanar reconstructions, three-dimensional reconstructions in the form of volumes of isosurfaces (meshes). In turn, these elements can produce other objects through post-processing. For example: virtual anatomical preparations of muscles, bones, nerves, etc. (Fig. 1).

The management of the donation program and the repository of objects follows the guidelines previously published (Aso et al, 2019), including a Hospital Monitoring Committee and a computerized database for managing the specimens generated and stored in the VRO.

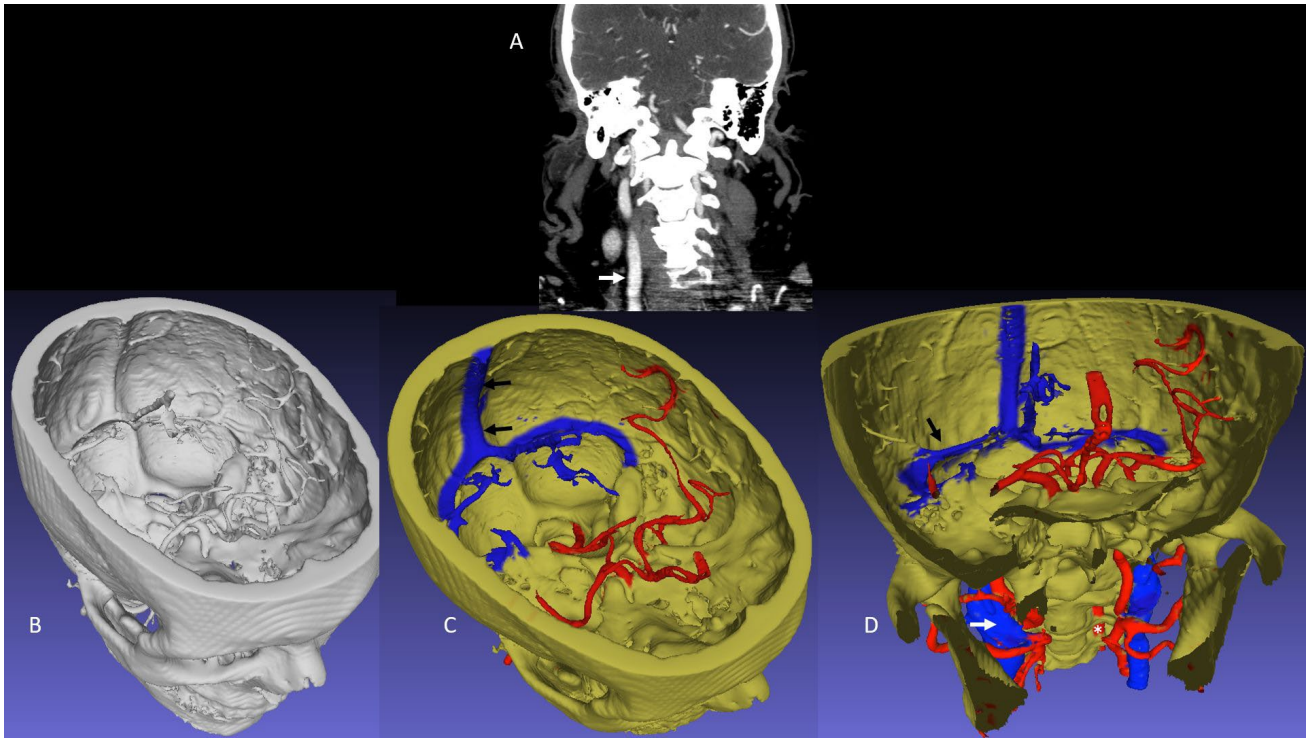

Fig. 1.- Craniocervical CT angiogram (**A**) in a patient with vertebral artery dissection. Images **B**, **C** and **D** are preparations made by the students from CT angiography, aimed to show the encephalic vascularization and its relationship with the bone. Black arrows show parts of venous circulation. White arrow in D points to jugular vein. These latter structures were segmented and depicted by students, as a part of their learning of cephalic circulation.

RESULTS

From January 2020 to June 2021, a total of 63 patients was included into the VRO: 44 men and 19 women. Acceptance of the donation has been excellent, accounting only one refuse, a foreign patient who, probably, did not understand the utility or purpose of the project, mainly due to a linguistic barrier.

Each donation, after IAPT procedures, has generated, in turn, a subset of objects that included:

- Three-dimensional models in the form of isosurfaces (mesh or meshes) (N=71)
- Videos of interaction with specimens (dissections of volumes, mainly, or of isosurfaces) (N=4)
- Flat or mapped images (imbibed with information using a dedicated software) (N=11).
- 3D printed objects (N=15)

The average number of objects generated by each patient was three, with a minimum of one and a maximum of 11.

A total of five final degree (Medical School) projects have been carried out using this procedure with very good results. The matters were related to interactive visualization of the models and geometric morphometrics. A subspecialty subject in bio-anthropology, physical and forensic, is regularly using the VRO for teaching in school of medicine, applied to sexual dimorphism identification, including both theoretical and practical learning.

Two investigation works are currently under way, related to reconstruction of historical skulls, based on indexed graphic cranial and CT-scout profile databases provided by VRO. Graphic similarities of skull can be identified, providing a method for reconstructing the cranial morphology and facial appearance, by using geometrics morphometrics techniques and multivariate statistics (principal component analysis, thin plate spline deformations and others).

One of the final degree projects, investigated, by means of a questionnaire, the acceptance of the interactive visualization of models among medical students. The results showed an enthusiastic assessment in 98% of them on the usefulness of

the method in practical teaching of the subject of Anatomy. Many students indicated the great advantage of being able to use the models in their place of study, studying them in a group, and of the possibility to telematic consult the teacher in real time about questions on the model, even after post-processing carried out by students themselves.

Another feature frequently referred was the need of formation in image processing techniques in the curriculum of the degree in Medicine, encouraging to implement learning activities on the subject.

From a healthcare point of view, the useful of interactive visualization of objects and managing of 3D printed models were revealed to be cardinal in presurgical planning. The procedure was tested in 8 cases, mostly related to spine and cranial interventions. Topographical identification of landmarks, planning of placing site, size of implant, and surgical obstacles avoidance were the most advantageous features.

Other important results were related to preoperative training of the entire surgery team. For the surgeons, drill essaying, cutting bone and tumors removal on 3D printed models were revealed to be excellent resources. X-Ray technicians were accustomed prior to the operation to the projections to be used in the operation. Nurses and auxiliars had the opportunity to anticipate surgical requirements or even seeing the surgical step-by-step prior the real intervention.

All these advantages were emphasized by personal involved in surgical actuations in an enthusiastic way.

DISCUSSION

Anatomy Teaching

The teaching of anatomy has been subject to great challenges since the advent of new technologies. Some of pioneer teaching strategies have been recently reviewed (Vázquez et al., 2007) and they appeared to be a powerful tool in both theorical and practical teaching. VBD can offer numerous resources to these teaching procedures, especially in practical approaches, i.e.: classrooms for virtual dissecting normal and pathological cases (Bolliger and Thali, 2015), virtual museums, and new visualization environments and procedures (Virtual and Augmented Realities) (Yushkevich et al., 2006).

At the same time, virtual donation notably increases the number of specimens and materials (virtual anatomical preparations from the post-processing of donations) that can be stored and reused indefinitely.

Another great advantage in pre-graduate teaching is that the student can have the specimen and perform with the preparations commissioned by the teacher. Since the model is indestructible because backup copies are available, the student can, interactive and repeatedly, rehearse different approaches until they find the one that best suits the requirements.

As an example, Fig. 2 summarizes the result of a conversion of a radiological model (CT in “A”). Firstly, to a grey scale 3D model (“B”) and, secondly, to a color solid model (“C” and “D”). This process was accomplished by a group of students assisted by the professor, learning the radiological anatomy (CT) of the case. They also acquired enough skill to prepare virtual models, being able to isolate, identify and depict the intracranial circulation. They were instructed to virtually remove the brain, and isolate (dissect) the intracranial mass (olfactory meningioma), as well to expose the entire Willis polygon. Afterwards, they presented the final model (solid 3D) with different cranial bone virtual removal enabling to see the separated (segmented) structures from various angles.

This procedure was very useful for the students in learning, for instance, the Willis polygon because it was an interactive practical lesson.

In turn, these models, generated by the students themselves, can become part of the VRO in the same way as in an Anatomic Museum (Fig. 1).

It was also found that work in group is favored, as to each student could prepare his/her own specimens, to later become part of a common project.

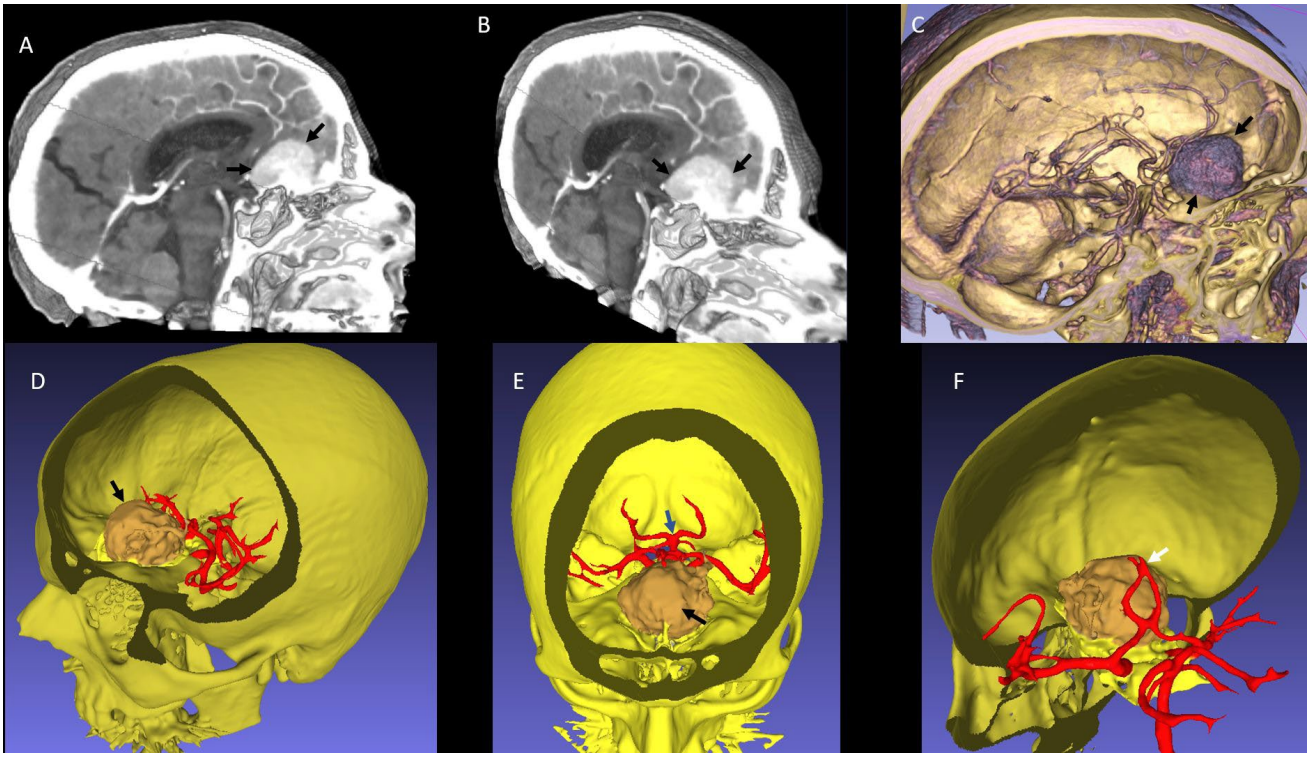

Fig. 2.- Differences between "Volume" and "Isosurface". The preparation corresponds to an olfactory meningioma (arrows in A, B, C and D). In **A** and **B** a rendered volume is presented. Note the different levels of gray that depicts the entire anatomy of brain and tumor. In the isosurface (**D**, **E** and **F**) several surfaces (composed by triangles) conform the object shape. Blue arrow in E and white arrow in F point to different parts of Willis polygon showing its relations with the mass.

One characteristic that appeared relevant was the need of learning and training in the use of IAPT techniques. In pre-graduate teaching, any discipline or sub-discipline that deals with training with these techniques was found.

Fundamentals of IAPT procedures includes the concept and structure of digital image, how it is organized on the servers, how to retrieve, store and work with it. Segmentation tasks, interactive visualization, reconstruction, and a long list of procedures, are part of IAPT procedures in which, both undergraduate and graduate students, should be trained.

Morphological Sciences Departments (Anatomy, in particular) are the ideal environment to perform this type of training.

Research

VBD programs create new sources and methods of research. DICOM files include mathematical information of the specimen, like calibrations, enabling accurate measurements, and references for the location of landmarks. Precise calculation of surfaces, volumes, index, densities and other magnitudes or relations are possible, even automatically.

Some new research techniques, such as geometric morphometrics, find in DICOM files an ideal medium for clinical investigation (Aso et al., 2018).

As an example, CT image databases were used to generate a graphical craniofacial consensus, allowing similarities to be found between living individuals and skeletal remains. This technique has been useful in the reconstruction or modeling of an unknown face from VBDP patients whose craniofacial geometric morphometry was like the problem case.

Clinical Teaching

Postgraduate teaching, in particular the training of residents, is easy with virtual models and allows, for example, to virtually test the reduction of fractures, or to simulate the use of new stabilization devices (implants, and others) in cases with pathology.

In the Hospital, the acceptance of this type of teaching has been enthusiastic, appearing

an interesting educative line to follow and consolidate.

Transversality of these systems must also be emphasized since they are not limited to applications in Medicine. Other professionals, like nurses, physiotherapists, occupational therapists, could benefit from the teaching and research applications of this programs. In the hospital, the reception of these teaching resources by these professionals has been excellent.

Healthcare

Around 75% of the cases, showed direct healthcare utility in surgical planning. As an example, two cases of pelvic fractures were presented, in which it was possible to presurgical essay both the operative technique as the implants on virtual objects and, specifically, on 3D printed models (Fig. 3). In one patient, suffering from a D11 crush fracture on a severe scoliosis, it was possible to repeatedly plan and rehearse on the virtual and printed model how to perform a percutaneous arthrodesis, with very good results (Fig. 4).

The usefulness of the method in planning percutaneous spinal arthrodesis in this case was evident, mainly to simulate the crowding of the towers for the percutaneous introduction of the screws, enabling to find the best way to place them comfortably in surgery. In another case, it helped to rule out a percutaneous approach, because such tower crowding made the technique impossible, opting for an open procedure.

Another additional case was a penetrating injury of the superior longitudinal venous sinus in which the surgical planning was established after reconstructing and printing the 3D model with segmentation of each of the parts.

3D printing goes beyond the mere reproduction of form. Different materials were tested until the finding of the best reproduction of bone characteristics. Once found the best material, its characteristics allowed to accurately simulate the trepanation, the milling, brocading, and bone cutting. All these maneuvers were found to be a perfect resemblance of the actual surgical ones (Fig. 5).

Likewise, the 3D printed objects should have radiological fidelity, enabling radiology to be used as an assistant in the essays on the printed model (Fig. 6).

Fig. 3.- 34-year-old male patient with pelvis fracture (AO classification 61C2.3) that progressed to pseudoarthrosis. **A**: Note the pseudoarthrosis of both ilio-pubic branches (red rings) with significant displacement. **B** and **C**: essaying the surgery on the 3D printed model. **D**: The plates are shaped and adapted to the model. **E**: Surgical approach. The plate is visible on the right side. Previous shaping of the plates allowed us to save significant surgical time. **F**: X-ray of the result.

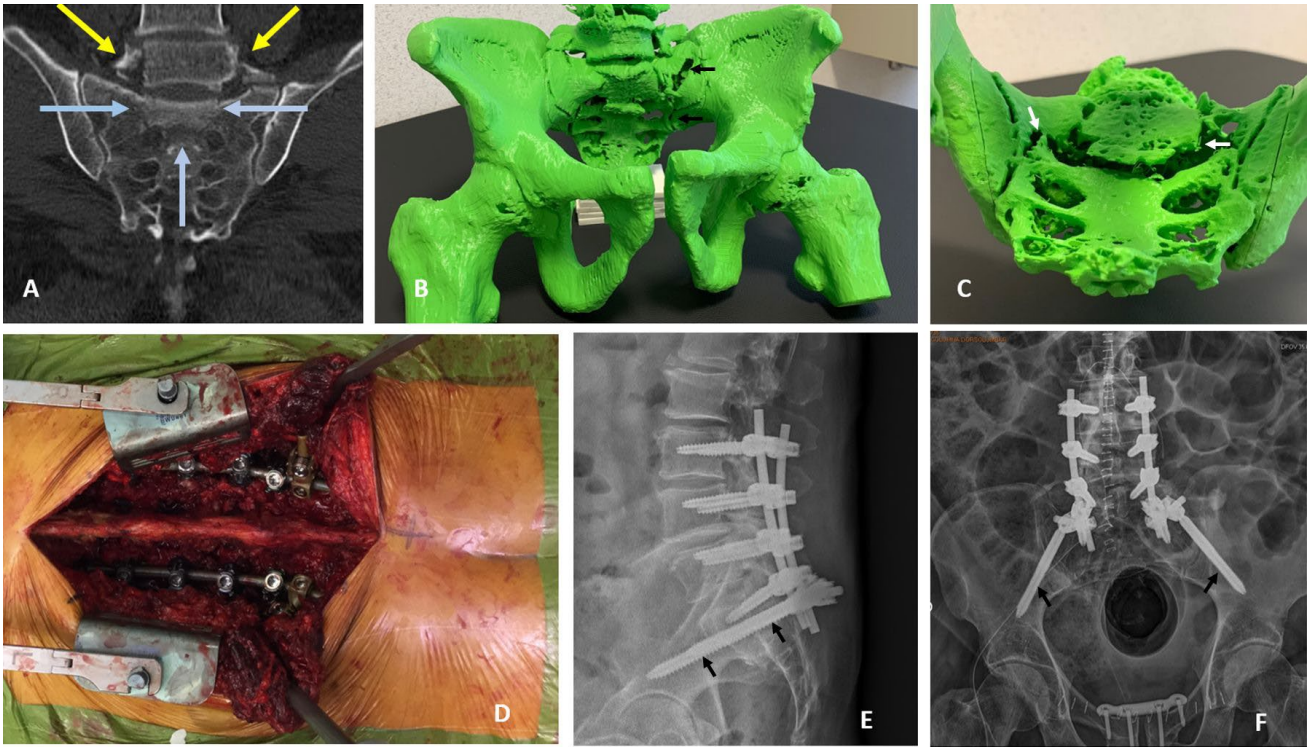

Fig. 4.- 60-year-old man with spinopelvic dissociation. **A**: the arrows mark the fracture of both transverse processes of L5 and the classic sacral "U-shaped" fracture. **B** and **C**: 3D printed model. **D**: intraoperative image showing L3-L4-L5-S1 instrumentation. **E** and **F**: radiological result. Arrows in B and C show fracture lines. A sacro-pelvic screw was placed (arrows in E and F). The insertion path and dimensions of this screw were previously planned and trained on the 3D printed model.

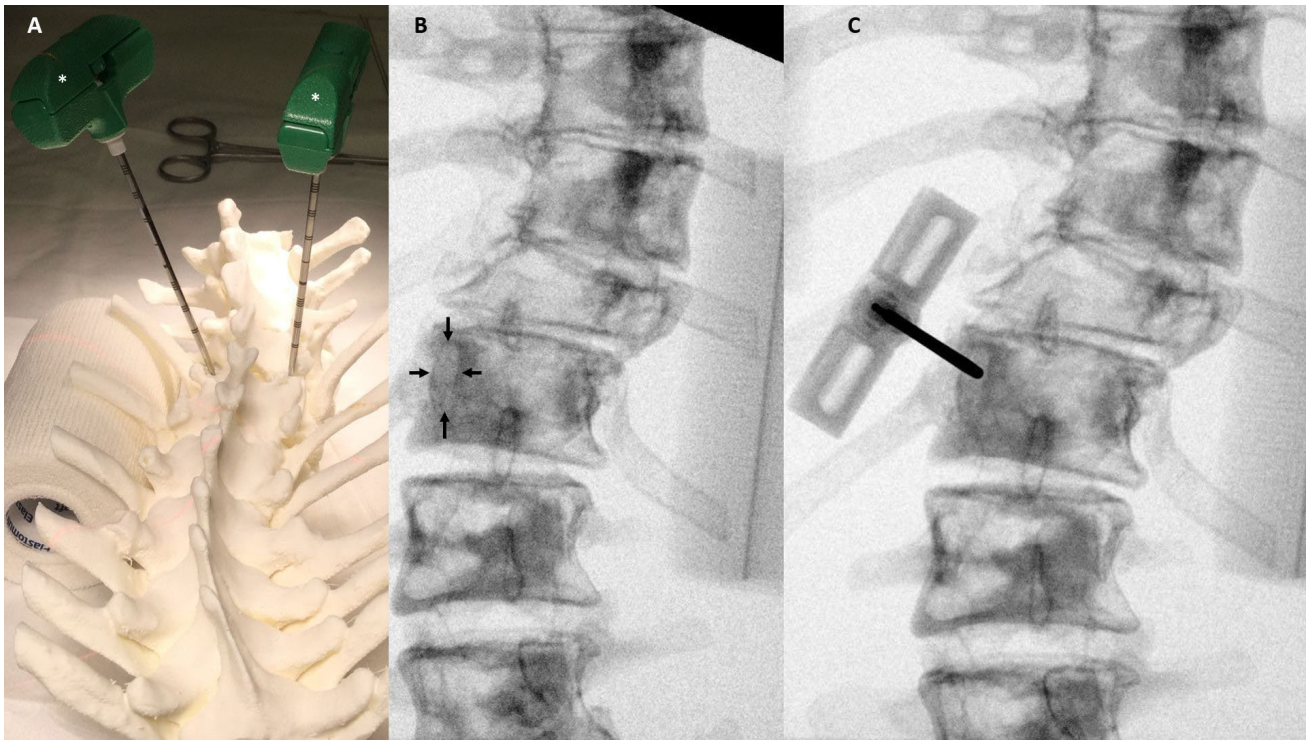

Fig. 5.- Image corresponding to the preoperative simulation of pedicle (arrows in B) cannulation in a spinal fracture in a case of severe scoliosis. **A**: Shows the 3D printed model simulating pedicle cannulation. **B** and **C**: Plain X-ray of the printed model. In C the cannula is placed with the tip over the pedicle AP projection. Asterisk in A are placed on bone access needles, used in Kyphoplasty.

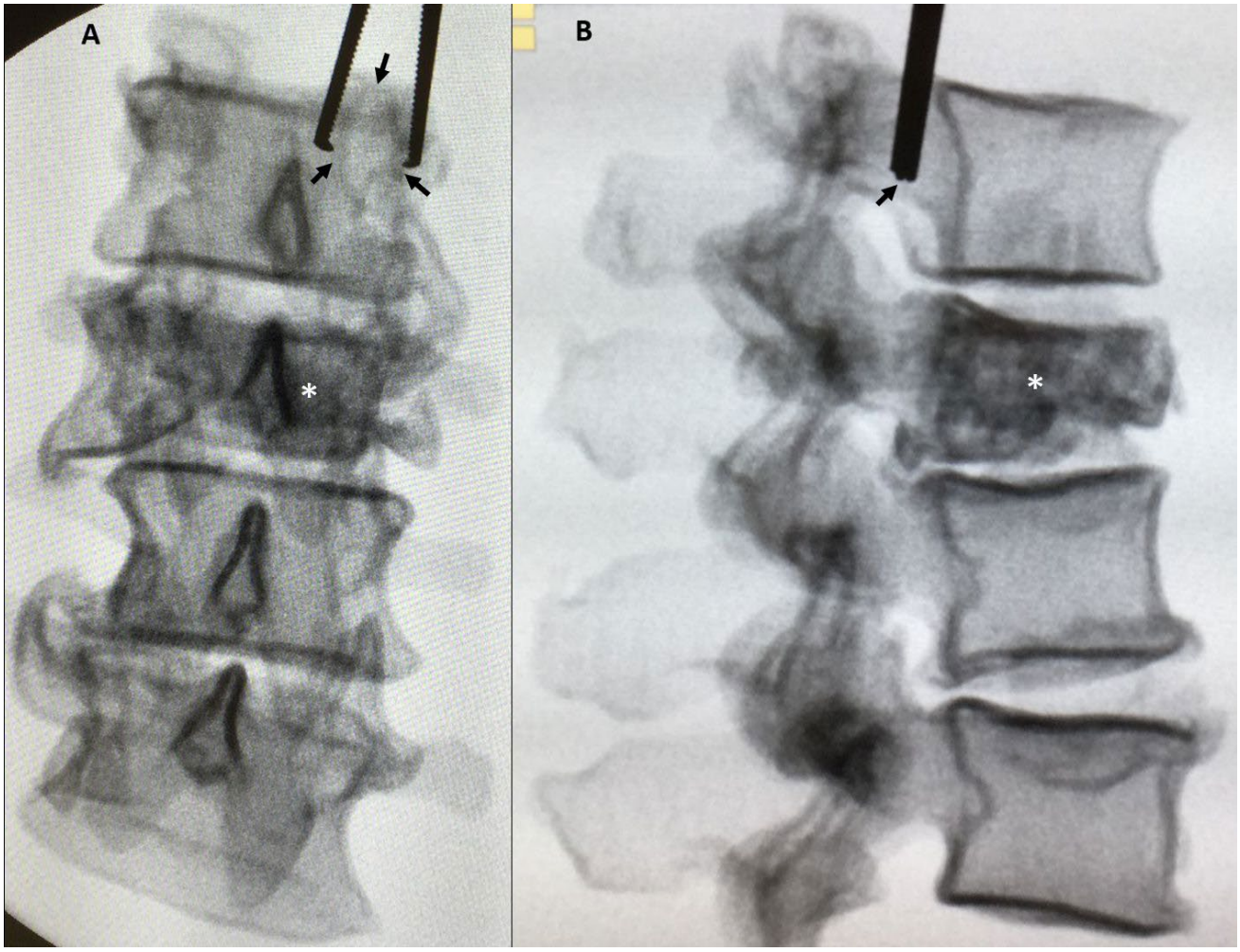

Fig. 6.- Radiological image of a 3D printed model corresponding to a crush fracture. Note the excellent quality that render almost indifferentiable the X-ray appearance of the model from an actual spine. The X-ray of the specimen is used to reproduce in the 3D printed model the same actions that would be carried-out in surgery. From the educational point of view, the image demonstrates how plain X-rays of the models can be also used to explain radiological anatomy. Arrows mark the optical cut od the pedicle in **A**, and the corresponding level in **B**. Forceps are used as a reference of pedicle position.

This allows simulating operations and interacting with implants that, in turn, can be measured and adjusted to fit the model on which it will be implanted.

Another important matter found of great usefulness is the information to the patient associated to surgical informed consent.

In all the cases, the procedures have been explained to the patients and relatives, using the 3D models, which has facilitated their understanding of the technique and significantly helped in the tasks of informed consent. The degree of satisfaction of patients with this kind of information was excellent.

Weaknesses

The first weakness of this work is the relatively small number of specimens collected to the date (due in part to the current pandemic situation). Surely, an expansion of these programs can help increase the casuistry, being desirable that it be adopted in a cooperative manner between several centers.

Another weakness, already pointed out, derives from the still scarce training in IAPT by healthcare personnel. There is still a gap between technology development and its level of use by the health professionals, which could very well be filled through teaching in morphological sciences.

The last weakness derives from the still incipient development of imaging techniques. For example, 3D printing is a procedure that requires time and that, for the moment, cannot be applied to emergency care cases. A greater introduction in the assistance and teaching of these techniques can also serve as a spur to the development of faster and more efficient technologies, not only for printing but also for the rest of the tasks inherent to image analysis and processing.

Future perspectives

It must be considered that with the technology available today a significant number of IAPT can be carried out, but that, in the future, it will be possible to extend these actions to fields currently in development (holography, study of diseases by means of CT voxel analysis or MRI, cerebral tractography, etc.). This will probably require an organization of virtual resources that can be used, so the present program and its extension to other centers could be an element of interest for the not-too-distant future.

There is a new generation of learners called "digital natives" (Prensky, 2001) and medical students are not an exception. The task of medical educators is to use the new technologies as a complementary tool in teaching, but technologies are just one tool, not a replacement of traditional face-to-face method of learning (Guze, 2015).

Under this perspective, the VBDP appears to be a promising reality to complement the traditional learning of Medicine, as well as a continuous source of material suitable to be organized and explored by the emergent and future image techniques. They can provide also a legal and ethical framework, protecting the rights of patients and allowing both the medical teaching, investigating and clinical use of the material donated by them.

CONCLUSIONS

The recently proposed virtual donation programs are an effective means of providing useful models both in medical and healthcare teaching as in research.

The experience in the use of these systems is very satisfactory and opens many possibilities for both clinicians, teachers, and researchers in anatomy, morphological or related sciences.

Patients have shown enthusiastic adhesion to the program, being the refusal an exception. Students also considered very useful the program and its implication, and the work with the virtual specimens as an excellent complementary method of learning anatomy.

The generation of virtual repositories of objects from digital acquisitions revealed to be extremely useful in healthcare (surgical planning), teaching (both undergraduate and graduate) and research. For this reason, an extension to regional centers that could favor the transversality of these systems is desirable.

Departments and chairs of morphological sciences are considered the ideal environment to take advantage of the implementation and growth of virtual donation programs, either by means of the use of specimens generated by other institutions in teaching and investigation, creating Medical Digital image teaching programs, or implementing virtual donation programs themselves as a complement to the human body donation of corpses.

REFERENCES

AFFOLTE R, EGGERT S, SIEBERTH T, THALI M, CHRISTIAN EBERT L (2019) Applying augmented reality during a forensic autopsy—Microsoft HoloLens as a DICOM viewer. *J Forensic Radiol,* 16: 5-8.

AMORIM P, MORAES T, SILVA J, PEDRINI H (2015) Invesalius: an interactive rendering framework for health care support. *Lect Notes Comput Sci,* 9474: 45-54. Software available in: https://invesalius.github.io/download.html. Consulted the: 15/11/2021.

ASO ESCARIO J, GIL-BEGUÉ M, SEBASTIÁN-SEBASTIÁN C, ASO-VIZÁN A, MARTÍNEZ-QUIÑONES JV, CONSOLINI F, ARREGUI R, NUEZ A (2019) Primer programa español de donación corporal virtual. Aspectos medicolegales e interés en docencia, asistencia e investigación. *Rev Esp Med Leg*, 45(4): 147-154.

ASO ESCARIO J, SEBASTIÁN-SEBASTIÁN C, ASO-VIZAN A, MARTÍNEZ-QUIÑONES JV, CONSOLINI ROSSI F, ARREGUI CALVO R (2018) Body mass index and sagittal lumbar balance. A geometric morphometrics approach. *Eur J Anat*, 22 (1): 37-49.

AUTODESK 3DS MAX (2018). Available in: http://usa.autodesk.com/adsk/servlet/index?id=5659302&siteID=123112. Consulted the 14-11-2019.

BANKMAN IN, Editor (2000) *Handbook of Medical Imaging: Processing and Analysis*. Academic Press Inc, Cambridge, Massachusetts.

BOLLIGER SA, THALI MJ (2015) Imaging and virtual autopsy: looking back and forward. *Philos Trans R Soc Lond B Biol Sci,* 370(1674): 20140253. 1-7.

CIGNONI P, CALLIERI M, CORSINI M, DELLEPIANE M, GANOVELLI F, RANZUGLIA G (2008) MeshLab: An Open-Source Mesh Processing Tool. *Sixth Eurographics Italian Chapter Conference*, page 129-136. Salerno, Italy, July 2nd - 4th , 2008. Software available in: http://www.meshlab.net/. Consulted the: 15/11/2021.

DAPPA E, HIGASHIGAITO K, FORNARO J, LESCHKA S, WILDERMUTH S, ALKADHI H (2016) Cinematic rendering – an alternative to volume rendering for 3D computed tomography imaging. *Insights Imaging*, 7: 849-856.

FOGAL T, KRÜUGER J, TUVOK (2010) An architecture for large scale volume rendering. *Proceedings of the 15th International Workshop on Vision, Modeling, and Visualization*. Available in: http://www.sci.utah.edu/~tfogal/academic/tuvok/Fogal-Tuvok.pdf. Software available in: http://www.sci.utah.edu/software/imagevis3d.html. Consulted the 15/11/2021.

GUZE PA (2015) Using technology to meet the challenges of medical education. *Trans Am Clin Climatol Assoc*, 126: 260-270.

HECKEL F, SCHWIER M, PEITGEN HO (2009) Object oriented application development with MeVisLab and Python. *Lecture Notes in Informatics. Informatik 2009: Im Focus das Leben*, 154: 1338-1351. 02/10/2009. Lübeck. Software available in: https://www.mevislab.de/. Consulted the 15/11/2021.

INRIA TEAMS MEDINRIA. Medinria. Platform for the diffusion of research software in medical imaging. Accessible in: http://med.inria.fr/. Consulted the 15/11/2021.

JAVAN R, RAO A, JEUN BS, HERUR-RAMAN A, SINGH N, HEIDARI P (2020) From CT to 3D printed models, serious gaming, and virtual reality: framework for educational 3D visualization of complex anatomical spaces from within-the pterygopalatine fossa. *J Digit Imaging*, 33(3): 776-791.

KIKINIS R, PIEPER SD, VOSBURGH K (2014) 3D Slicer: a platform for subject-specific image analysis, visualization, and clinical support. In: Ferenc A, Jolesz (eds.). *Intraoperative Imaging Image-Guided Therapy*, 3(19): 277-289. Software available in: https://www.slicer.org/. Consulted the 15/11/2021.

LEY 30/1979, de 27 de octubre, sobre extracción y trasplante de órganos (1979) Boletín oficial del Estado, 6 de noviembre de 1979, núm. 266, pp 25742-25743. Available in: https://www.boe.es/buscar/doc.php?id=BOE-A-1979-26445.

MATESANZ R (2004) Factors that influence the development of an organ donation program. *Transplantation Proceedings*, 36: 739-741.

McHANWELL S, BRENNER E, CHIRCULESCU ARM, DRUKKER J, VAN MAMEREN H, MAZZOTTI G, PAIS D, PAULSEN F, PLAISANT O, CAILLAUD MM, LAFORÊT E, RIEDERER BM, SAÑUDO JR, BUENO-LÓPEZ JL, DOÑATE-OLIVER F, SPRUMONT P, TEOFILOVSKI-PARAPID G, MOXHAM BJ (2008) The legal and ethical framework governing Body Donation in Europe – A review of current practice and recommendations for good practice. *Eur J Anat*, 12(1): 1-24.

NAPOLI M, NANNI M, CIMARRA S, CRISAFULLI L, CAMPIONI P, MARANO P (2003) Picture archiving and communication in radiology. *RAYS,* 28(1): 73-81.

NEMA (2001) Digital imaging and communications in medicine (DICOM). *Tech Rep. National Electrical Manufacturers Association*. Available in: http://medical.nema.org/dicom/2000.html. Consulted the 23/05/2018.

PRENSKY M (2001) Digital natives, digital immigrants. On the horizon. *MCB University Press,* 9(5): 1-6.

REAL DECRETO 1723/2012, de 28 de diciembre, por el que se regulan las actividades de obtención, utilización clínica y coordinación territorial de los órganos humanos destinados al trasplante y se establecen requisitos de calidad y seguridad. Available in: BOE núm. 313, de 29 de diciembre de 2012, pp 89315- 89348. https://www.boe.es/buscar/doc.php?id=BOE-A-2012-15715.

REGLAMENTO UE 2016/679 del Parlamento Europeo y del Consejo de 27 de abril de https://www.boe.es/doue/2016/119/L00001-00088.pdf, relativo a la protección de las personas físicas en lo que respecta al tratamiento de datos personales y a la libre circulación de estos datos y por el que se deroga la Directiva 95/46/CE (Reglamento General de Protección de Datos) así como a las disposiciones legales nacionales vigentes en materia de protección de datos de carácter personal, (2016). Available in: https://www.boe.es/doue/2016/119/L00001-00088.pdf.

RORDEN C (2018) The DICOM standard. Available in: https://people.cas.sc.edu/rorden/dicom/index.html. Consulted the 08/02/2022.

ROSSET A, SPADOLA L, RATIB O (2004) OsiriX: An open-source software for navigating in multidimensional DICOM Images. *J Digit Imaging,* 17: 205-216. Software available in: https://www.osirix-viewer.com/. Consulted the 15/11/2021.

SCHINDELIN J, ARGANDA-CARRERAS I, FRISE E, KAYNIG V, LONGAIR M, PIETZSCH T, CARDONA A (2012) Fiji: an open-source platform for biological-image analysis. *Nat Methods*, 9(7): 676-682. Software available in: https://imagej.net/Fiji. Consulted the 15/11/2021.

VÁZQUEZ R, RIESCO JM, JUANES JA, BLANCO E, RUBIO M, CARRETERO J (2007) Educational strategies applied to the teaching of anatomy. The evolution of resources. *Eur J Anat*, 11 (Suppl 1): 31-43.

YUSHKEVICH PA, PIVEN J, CODY HAZLETT H, GIMPEL SMITH R, HO S, GEE JC, GERIG G (2006) User-guided 3D active contour segmentation of anatomical structures: significantly improved efficiency and reliability. *Neuroimage,* 31(3): 1116-1128. Software available in: http://www.itksnap.org/pmwiki/pmwiki.php. Consulted the 15/11/2021.

Isolation of adult rat kidney derived stem cells and differentiation into podocyte-like cells

Esrafil Mansouri[1], Armita Valizadeh Gorji[2], Forouzan Absalan[3]

[1] Cellular and molecular research center, Medical Basic Sciences Research Institute, Department of Anatomical Sciences, School of Medicine, Ahvaz Jundishapur University of Medical Sciences, Ahvaz, Iran

[2] Department of Anatomical Sciences, Iran University of Medical Sciences, Tehran, Iran

[3] Department of Anatomical Sciences, Abadan University of Medical Sciences, Abadan, Iran

SUMMARY

Studies have shown that adult stem cells can be isolated from different organs. However, no agreement has yet been reached on the identification of adult kidney stem cells. In this study, we have shown that the adult rat kidney contains a population of stem cells that are isolatable and, under suitable culture conditions, these stem cells can differentiate into podocyte. Six adult Wistar rats were used in the present study. Their kidneys were chopped and exposed to collagenase I. Then, with passing through 100 µm mesh, single cells in filtered fraction were cultured in a proliferation medium. After 4 passages, the cells were analyzed by flow cytometry, differentiation and gene expression. Morphological analyses revealed that isolated cells are spindle-shaped, and can differentiate into osteocytes and adipocytes. Flow cytometry demonstrated that these cells expressed cell surface markers CD44, CD90, CD133, c-kit, Pax-2, Oct4, sca-1 and vimentin significantly. Also, the high expression of Wt-1 and Wnt-4 genes was seen in these cells. Moreover, expression of synaptopodin and podocalyxin genes showed differentiation of stem cells into podocyte cells. Our findings demonstrate that isolated cells from the kidney of adult rats are mesenchymal stem cells or progenitor cells and can differentiate to podocyte-like cells.

Key words: Stem cell – Kidney – Adult rat – Differentiation – Podocyte

INTRODUCTION

The detection of specific stem cells of different tissues is a main target of recent investigations and can provide a route to remedy of various diseases such as cardiac diseases and neurodegenerative disorders. Moreover, stem cells probably play a key role in regenerative medicine (Bonaventura et al., 2021; Liu et al., 2016). Several studies have shown that stem cells progeny divide rapidly; however, the turnover term of these cells in the skin and bone marrow is relatively slow (Liu et al., 2016). Also, evidence suggests that stem cells are involved in repairing organs and tissues following injury (Trovato et al., 2020; Nourian Dehkordi et al., 2019). Research has characterized adult stem cells and their niches in different organs such as the bone marrow, skin, liver, intestine, gastrointestinal mucosa, brain and prostate, and

Corresponding author:
Esrafil Mansouri. Department of Anatomical sciences, Faculty of Medicine, Ahvaz Jundishapur University of Medical Sciences, 61335 Ahvaz, Iran. Fax: +98-6133332036. E-mail: esrafilmansori@yahoo.com

Submitted: February 21, 2022. **Accepted:** March 2, 2022

https://doi.org/10.52083/LCXR8059

there is reliable evidence of the presence of such cells in the kidney (Liu et al., 2016; Liu et al., 2020). These cells play a role in normal turnover of the noted organs and can be considered a potential source of cells following organ damage. Renal stem cells (RSCs) are found in the adult kidneys of some organisms like the freshwater teleost and the skate. The renal stem cells can play a role in the formation of new nephron following partial nephrectomy (Gupta et al., 2006; Ahmadi et al., 2020). One of the characteristics of renal stem cells is that these cells can differentiate into different renal and non-renal cells. However, it is important to note that all of these cells are not yet able to differentiate into podocytes. This is a key target, because podocyte damage is one of the main causes of kidney disease (Mora et al., 2012).

Studies have used a variety of detection techniques to find stem cells in the adult mammalian kidney (Kitamura et al., 2005). Due to slow cycling feature of stem cells, researchers have used a bromodeoxyuridine-retaining technique to demonstrate that adult kidneys have progenitor cells (Maeshima et al., 2003), and the renal papilla was introduced as a niche for these cells (Oliver et al., 2004). The RSCs can be the major source of healing following injuries (Lin et al., 2005; Andrianova et al., 2019). Thus, they can be the target for designing new therapeutic approaches (Chen et al., 2008). Although studies have shown the presence of stem cells in adult kidneys, the main methods of isolating these cells and studying their features need more development. The present study attempts to test the hypothesis of existence of RSCs in the kidneys of adult rats and their potential for generating podocyte.

MATERIALS AND METHODS

Subjects and ethics statement

Six adult female Wistar rats weighting 190-220 g were used in the present study. The rats were maintained in controlled temperature (22 ± 2°C) with humidity 50-55% and under a 12-h light/dark cycle, with ad libitum access to food and water. All procedures performed in this study were approved by the Ethics Committee of Ahvaz Jundishapur University of Medical Sciences (AJUMS). Animal care and handling were done in accordance with National Institutes of Health guidelines.

Isolation of renal stem cells

Rats were anesthetized with intraperitoneal injection of Ketamin (75 mg/kg) and Xylazine (10 mg/kg). Kidneys were harvested under standard aseptic technique. Then the kidneys were washed in PBS containing 1% penicillin/streptomycin (Gibco, USA) and removed perirenal fat and renal capsule. The kidneys were cut into very small pieces and were re-suspended in 0.3% collagenase type I (Sigma, USA) for 20 minutes at 37°C in shaking water bath. After passing through 100 µm mesh to remove undigested chunks, the filtered fraction containing mainly single cells was centrifuged at 1500 rpm for 5 minutes and re-suspended in proliferation medium that consisted of Dulbecco's modified eagle medium: nutrient mixture F-12 (DMEM/F12, Gibco, USA) with 15% fetal bovine serum (FBS, Gibco, USA), 1% penicillin/streptomycin (P/S) and cultured at 37°C in the presence of 5% CO2. The medium was replaced every three days by fresh medium. The cells were detached using trypsin (0.25%)/EDTA (0.1%) solution (Sigma, USA) and passaged when they reached 70-80% confluence. During isolation and cultivation period, the morphology of cells was monitored by light inverted microscope. After 4 passages, the cells were characterized by flow cytometry, and differentiate into adipogenic and osteogenic lineages.

Flow cytometry evaluations

Flow cytometry evaluations for surface markers of RSCs were performed. Briefly, the cells were incubated with anti-rat antibodies in a dilution of (1:100) against CD44, CD133, CD90, vimentin, c-kit, Oct4, sca-1, Pax_2 (as positive markers) and CD45 (as a negative marker) overnight at 4°C in the dark condition. All antibodies were purchased from Abcam (Cambridge, UK). Negative and isotype controls were performed. After cell staining, for each reaction 5000 events were counted by a Dako Galaxy flow cytometer and data were analyzed using FlowJo version 8.8.7 software (Treestar, OR).

Table 1. Primer sequences for real-time PCR.

Gene name	Forward sequence	Reverse sequence
Wnt-4	TTGGTCAGAGGGTGAGAGGGA	AGTCCAGGTGTGGTGGTTAGGG
WT-1	GTGACTTCAAGGACTGCGAGAGA	TTCTCTGGTGCATGTTGTGATGG
Synaptopodin	CCACAGAGGCACATAATG	GGATACAGAGTAGAATAAGAGG
Podocalyxin	ACC GGT CCT TAA TTG GTT CC	CCT TTG GCA GTT AGG AGC TG
GAPDH	GGATAGTGAGAGCAAGAGAGAGG	ATGGTATTGGAGAGAAGGGAGGG

Gene Expression Analysis

To identify isolated stem cells as peronephrogenic cells, the mRNA expression levels of Wnt4, Wt1 as pronephrogenic markers were analyzed by real-time polymerase chain reaction. Bone marrow-derived stem cells were used as control (BMSCs) because these cells do not express peronephrogenic markers.

Differentiation of RSCs into adipogenic and osteogenic lineage

Renal stem cells at Passage 4 were evaluated for adipogenic, and osteogenic differentiation potential. Cells were plated at 1×10^6 cells / ml in 6 well plates under proliferation medium (DMEM/F12 and 15% FBS). After reaching ~80% confluency, medium was replaced with appropriate differentiation medium, either adipogenic or osteogenic medium (2 ml / well). The mediums were replaced with fresh medium every 2 days until 21 days. Adipogenic differentiation medium contained DMEM, FBS (10%), 0.5 µM isobutyl-methylxanthine, 1 µM dexamethasone, 10 µM insulin, and 200 µM indomethacin. Osteogenic differentiation medium contained DMEM, FBS (10%), 0.1 µM dexamethasone, 10 µM β-glycerophosphate, and 50 µM ascorbate phosphate. To assess differentiation, cells were fixed with paraformaldehyde (4%) for 30 mins at room temperature and stained with oil red-O for 15-30 mins at room temperature to detect the production of lipid droplets for adipogenesis or alizarin red for 1 h at room temperature in the dark to detect the presence of a calcium deposition for osteogenesis.

Differentiation of RSCs to podocyte-like cells

For differentiation of RSCs toward podocyte-like cells, cells were grown to confluence in four-well chamber slides and incubated with a podocyte differentiation medium (PDM) that contained DMEM-F12 with 2.5% FBS, 100 mM nonessential amino acids, 100 mM beta mercaptoethanol with the addition of 10 ng/ml of activin A, 15 ng/ml of BMP7, and 0.1 mM retinoic acid. At 10 days of differentiation, cells were assessed by the specific morphology and the gene expression of synaptopodin and podocalyxin by real-time PCR.

Real-time reverse transcriptase-polymerase chain reaction analysis

Total RNA was isolated from the cultured stem cells using an RNeasy Mini Kit (Qiagen, Gaithersburg, MD, USA) based on the manufacturer's protocol and quantitated with a Nanodrop (Nanodrop Thermo Scientific S.N:D015). cDNA was synthesized by a QuantiTect Reverse Transcription Kit (Qiagen, Gaithersburg, MD, USA). Real-Time PCR was performed using 2X Master Mix including Syber Green (Biofact, South Korea). The forward and reverse primers used are listed in Table 1. GAPDH was used as an internal standard to normalize gene expression levels.

Statistical analysis

All experiments were performed in triplicate. Statistical analysis of viability data was performed using SPSS software (version 21.0, SPSS Inc., Chicago, IL, USA). One-way ANOVA was used to analyze the mean values statistically at a statistical significance of $P<0.05$.

RESULTS

Cell isolation and their morphology

As a source of renal mesenchymal stem cell, after processing of adult rat kidney, primary cells were cultured in vitro condition from kidney as mentioned above. Briefly, after 6 days of culture,

adherent cells were observed, and their number increased rapidly after 15 days by displaying a spindle shape and process resembling fibroblasts and formed a monolayer of about 80% confluence (Fig. 1).

Flow cytometry analysis

The immunophenotypes of RSCs were analyzed by flowcytometry. Flow cytometric analysis at passage 4 showed that the expression patterns by immunophenotyping undifferentiated renal stem cells revealed cells positive for CD44, CD90, CD133, c-kit, Pax-2, Oct4, sca-1 and vimentin RSCs markers and CD45 was expressed in a small number of cells (Fig. 2, A and B). CD45 is considered hematopoietic surface markers that were not expected to be expressed much in RSCs as confirmed in the present study**.**

Characterization of RSCs by Real-time-PCR

The results of real time-PCR analyses showed an increase in mRNA expression of Wt-1 and Wnt-4 in RSCs ($P < 0.05$) when compared with bone-marrow-derived stem cells (Fig. 3).

Differentiation potential into adipogenic and osteogenic

The certain affirmation of multipotency for each cell is the potency to differentiate into more than one cell type. Cells isolated from all kidneys of adult rats displayed the potential to differentiate into varying degrees, as demonstrated by positive adipogenic and osteogenic staining. Adipogenesis was observed with positive oil red-O staining (Fig. 4A) and osteogenic differentiation was showed with alizarin red staining (Fig. 4B).

Podocyte Differentiation

By day 10, the cells adopted morphological features characteristic of podocyte. We observed large and arborized cells with cytoplasmic processes (Fig. 5A). Moreover, gene expression for podocyte-specific genes such as synaptopodin and podocalyxin was analyzed by qRT-PCR, and the expression of podocyte markers was detected during differentiation (Fig. 5B). Undifferentiated RSCs did not express detectable levels of synaptopodin and podocalyxin that had been observed in RT-PCR analysis.

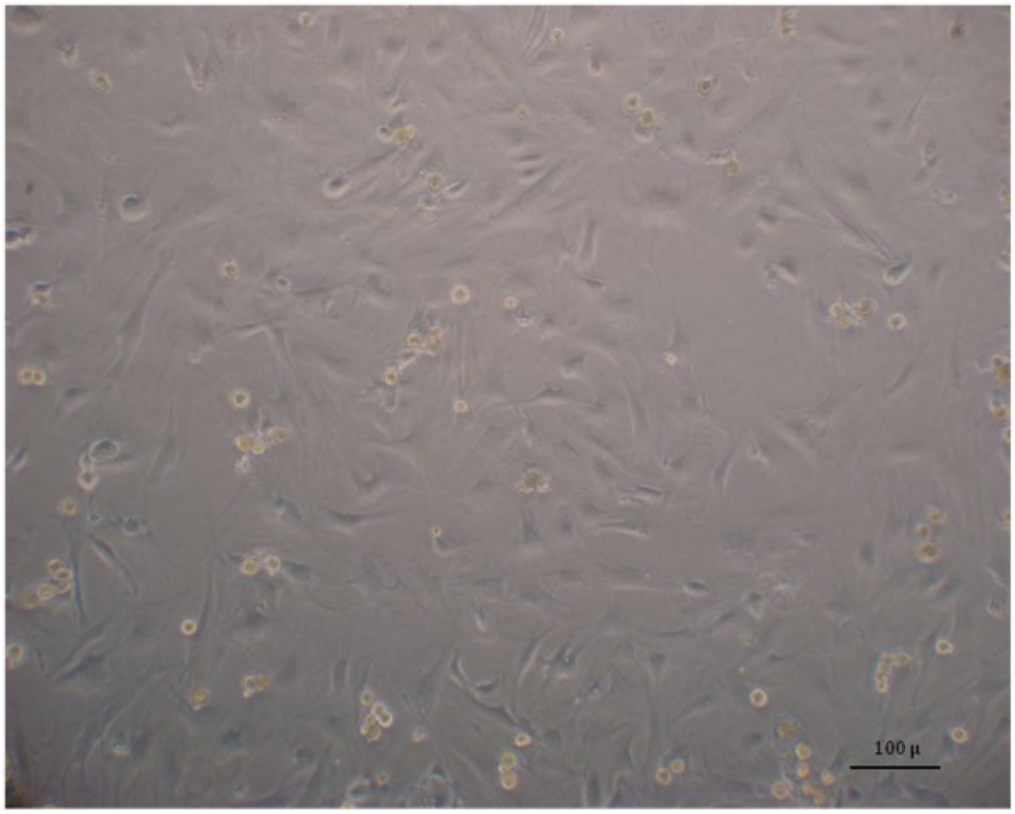

Fig. 1.- Characteristics of renal stem cells at passage 4. The cells are monomorphic with a spindle-shaped morphology and slightly similar to fibroblast cells. Scale bar: 100 µm.

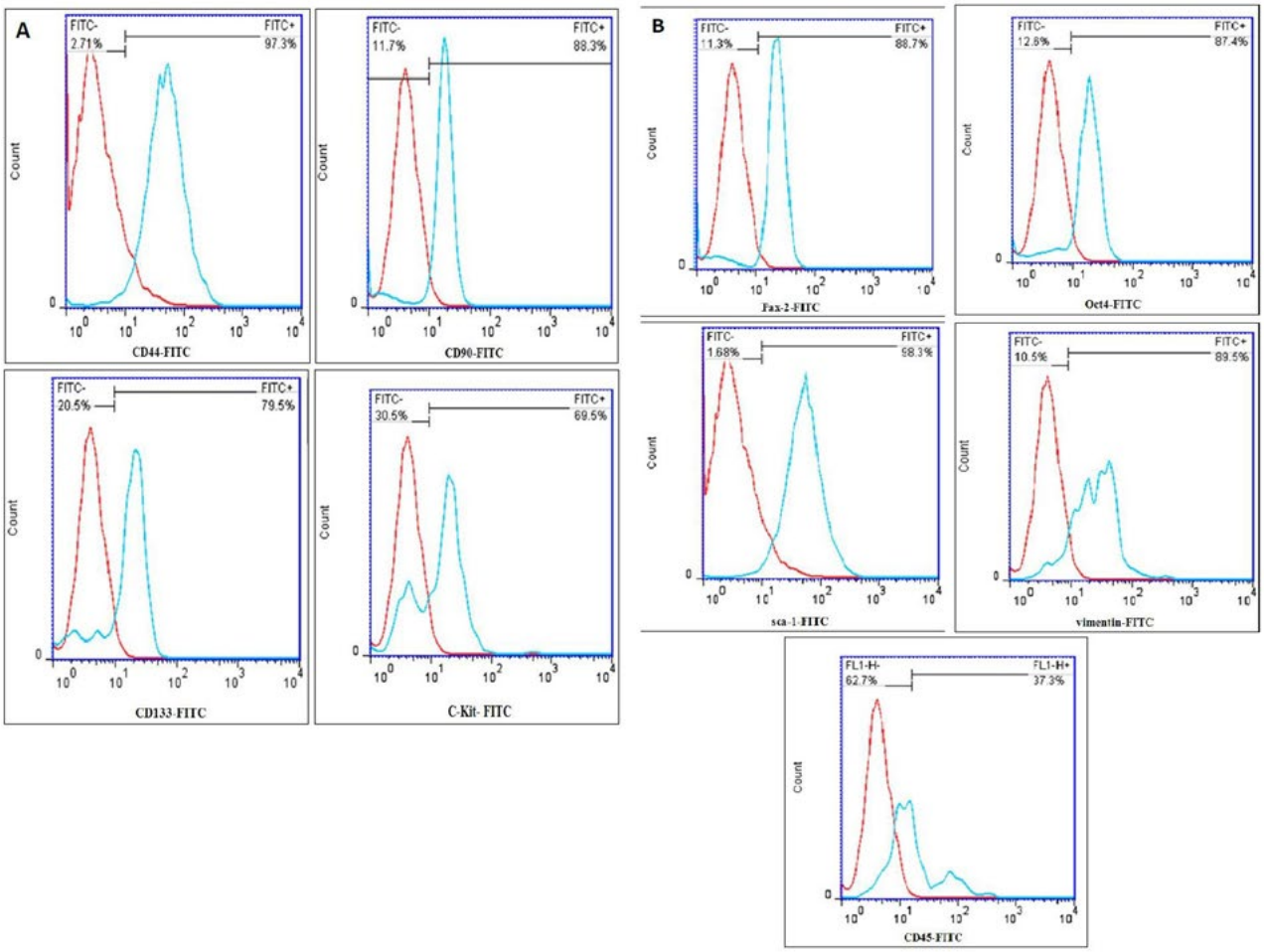

Fig. 2.- A and B: Flow cytometry analysis of cell surface markers present on renal stem cells (RSCs).

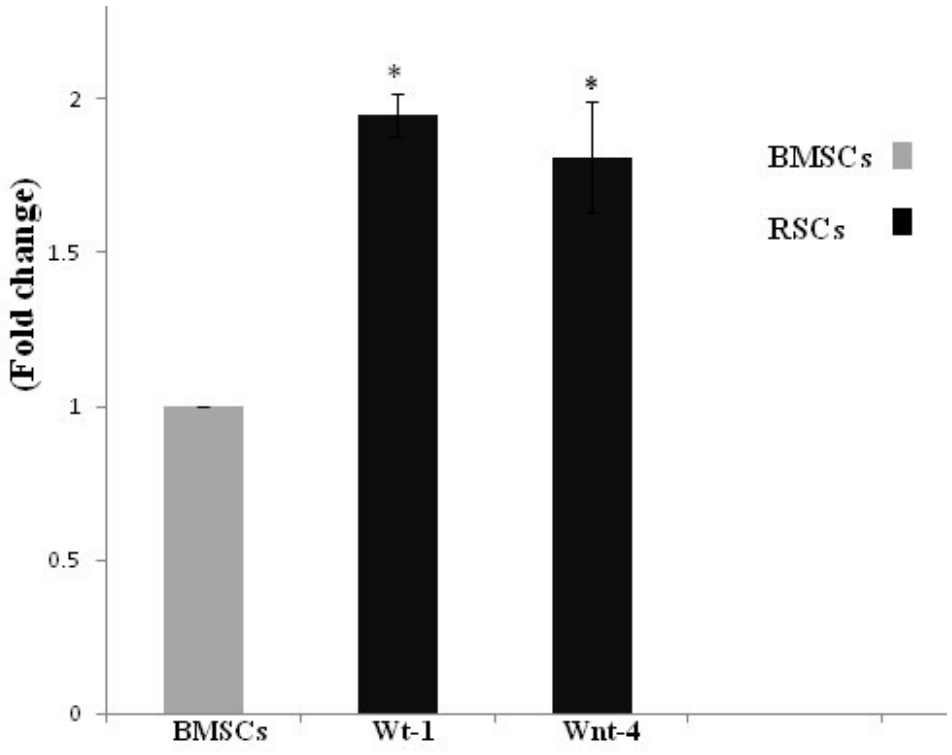

Fig. 3.- Real-time PCR analysis for mRNA expression of Wt-1 and Wnt-4 in RSCs (renal stem cells) and BMSMCs (bone marrow stem cells). *$p < 0.05$ compared with BMSCs.

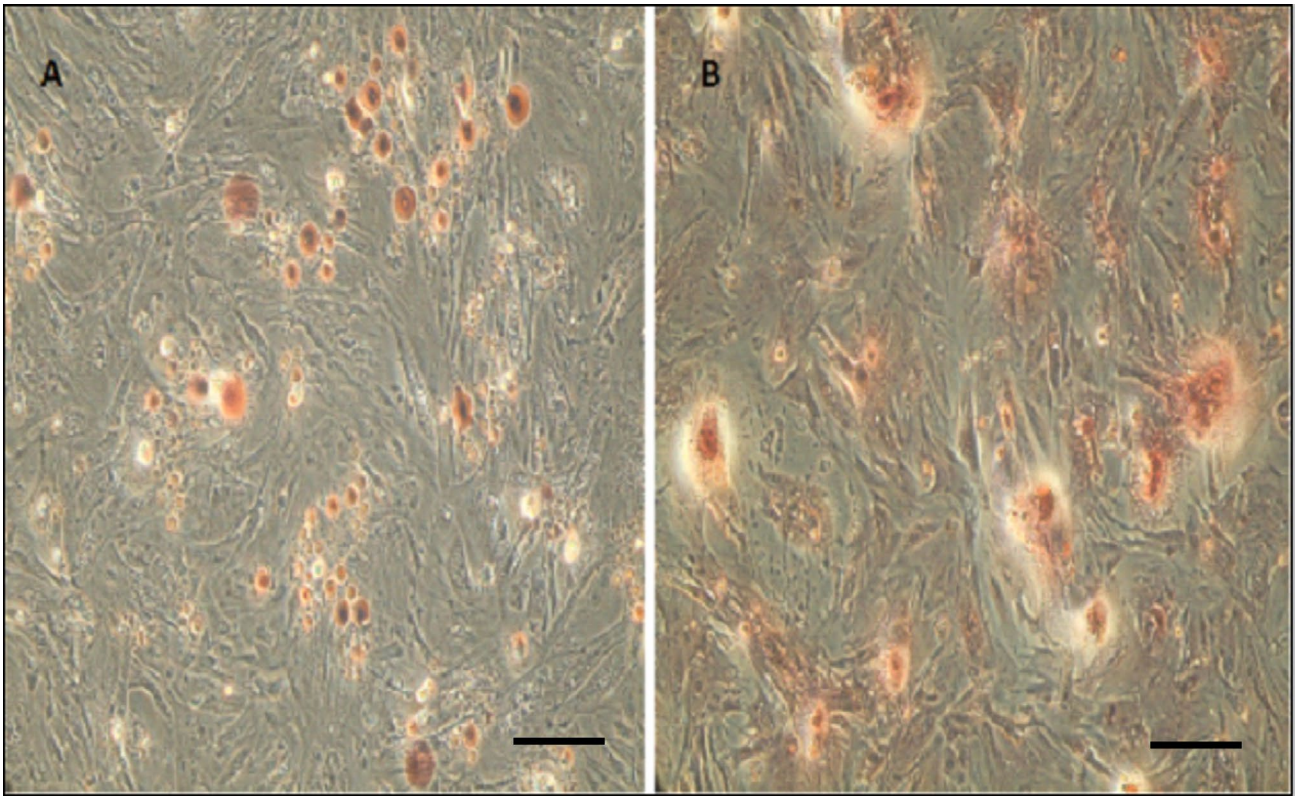

Fig. 4.- Photomicrographs representative of the morphological appearance of adipogenic and osteogenic differentiation of RSCs. **A:** adipogenic differentiation after 21 days showing lipid droplets stained with Oil Red; **B:** presence of calcium mineralization after 20 days of induction Alizarin Red staining. Scale bar: 100 µm.

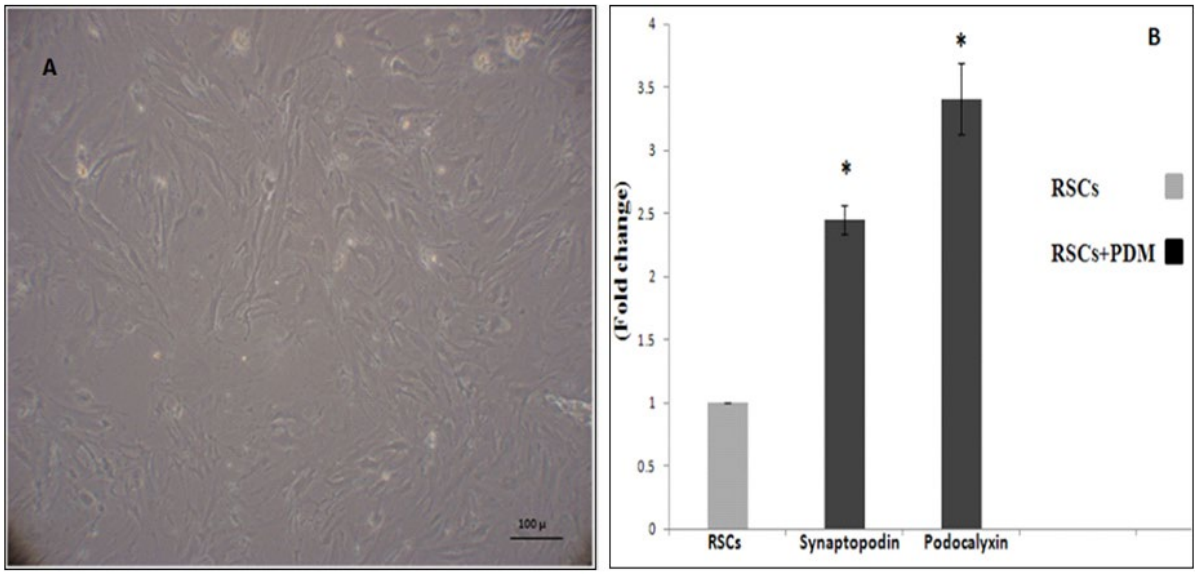

Fig. 5.- A: Morphological alterations of RSCs after treatment with podocyte differentiation medium (PDM). At day 10 cells had cytoplasmic extensions with an arborized appearance like podocytes. Scale bar: 100 µm. **B:** Real-Time PCR analysis of podocyte specific genes in cells cultured PDM for 10 days. *$p < 0.05$ compared with RSCs.

DISCUSSION

One of the most complicated and vital organs in the human body is the kidneys, so that despite notable redundancy built in, the gradual deterioration of the renal tissue might induce life threats. In spite of some species,the adult human body cannot generate new nephrons, but it is able to replace individual lost cells (Diep et al., 2011; Little and Kairath, 2016). However, the regenerative capability is limited, and by aging

or developing disease renal function might drop below critical levels (Huling and Yoo, 2017) . Available treatment choices for chronic kidney disease are limited. Some of the lost functions can be restored through dialysis; still, the underlying problem remains effective. Also, whole organ transplants are very effective; however, there is a low supply of organs and the long-term survival rate is blow 40% (Huling and Yoo, 2017; Levey and Coresh, 2012). Regenerative medicine and tissue engineering try to find more efficient treatment choices through using adult renal stem cells. Stem cells obtained from the adult kidney can improve renal engraftment and differentiation so that they can be used for autologous therapies. Several studies have been conducted to find renal stem cells, yet there is no consensus in this field (Huling and Yoo, 2017). In this study, unique cells were isolated from adult rat kidneys that behave consistently with a renal stem cell. These cells are featured with spindle-shaped morphology and self-renewal. The RSCs demonstrate plasticity through the ability of cells to differentiate into cells of adipocytes and osteocytes. These findings are consistent with other works in this field (Gheisari et al., 2009).

In the present study, we isolated the cells that expressed CD133 and Vimentin significantly. Lindgren et al. noted that CD133-positive cells exist in proximal tubule (Lindgren et al., 2011); and, in a recent study, Sagrinati et al. (2006) mentioned that these cells (CD133-positive) in parietal layer of bowman's capsule are adult kidney stem cells. They utilized Vimentin and CD133 as markers of possible kidney adult stem cells.

Here, RSCs were studied using the stem cell markers Pax-2 and Oct-4, so that the both of them were expressed in these cells significantly. Pax-2 is determined as a main regulator in the development of the kidney (Tayyeb et al., 2017) and a transcription factor expressed by stem cells that are found in the metanephric mesenchyme and other stem cells isolated from adult kidneys (Yamamura et al., 2021; Oliver et al., 2002). The Oct-4 as a transcription factor is found in embryonic stem cells and primordial germ cells in adult gonads. It has a vital role in keeping pluripotency of embryonic stem cells and the viability of primordial germ cells. Recent studies have shown that the cells that express Oct-4 are found in adult organs such as kidneys, and they are potential in vivo markers of adult stem cells (Zhong et al., 2022; Rosenberg and Gupta, 2007).

Studies have shown that expression of c-kit and Sca-1 in cells isolated from adult kidneys might have the potential to serve as renal progenitor or stem cells (Kitamura et al., 2005). Our results also showed that RSCs significantly express markers of c-kit and Sca-1.

The CD44 and CD90 are usual markers of mesenchymal stem cells (L.Ramos et al., 2016). We found that cells isolated from adult rats' kidneys had a notable volume of these markers. According to the study by Gupta et al. (2006), RSCs can be considered mesenchymal-like cells, since they express CD44 and CD90. Our results are consistent with these findings.

Moreover, RSCs expressed CD45 at a lower level, and this marker is one of the markers of endothelial progenitor or hematogenous cells (lee et al., 2010), which reject the chance of extrarenal origin of stem cells isolated in the present study.

Real-time PCR analysis showed that stem cells isolated from adult rats' kidneys expressed mRNA Wt-1 and Wnt-4. Based on the molecular events mediating nephrogenesis hierarchy, Wnt-4 is a key autoregulator of the mesenchymal-epithelial transformation that supports tubulogenesis (Tayyeb et al., 2017; Gallegos et al., 2012; Vainio, 2003). In addition, Wnt-4 mediates tubulogensis in the kidney by nancanonical calcium-Wnt pathway (Tanigawa et al., 2011). The Wt-1 is a key marker of early nephrogenesis (Kreidberg, 2010). According to other study, Wnt-4 and Wt-1 are renal epithelial and mesenchymal markers. A metanephric mesenchyme cell line including embryonic renal stem cells demonstrated expression of epithelial and mesenchymal markers (Kitamura et al., 2005).

In this study, a suitable and specific culture medium (PDM) was used to differentiate stem cells into podocytes. The findings demonstrated that under differentiating conditions, the stem cell isolated from the kidney was able to generate

podocytes. The previous results suggested that, with the appropriate culture medium, stem cells can differentiate into some of renal cells, such as proximal tubule- and podocyte-like cells, as well as non-renal cells, such as osteocytes and adipocytes (Mora et al., 2012). Till now, a number of researches have demonstrated which renal-derived stem cells in vitro can differentiate into podocytes. These reports are usually due to the expression of one or two podocyte markers (Bruno et al., 2009: Ronconi et al., 2009). In appearance, these cells are slightly similar to primary podocytes. Recently, it has been suggested that in order to identify true podocytes in vitro, in addition to expressing specific markers, these cells should show the usual specific appearance characteristics of the podocyte, such as appearance of arborized, high ratio of cytoplasm to nucleus, and obvious cell processes (Shankland et al., 2007). Therefore, according to the contents, the present study results are consistent with previous studies.

CONCLUSION

This study provides a simplified isolation and characterization procedure for SCs from the adult rat's kidney. Expression of markers in these cells indicated that these cells can be mesenchymal stem cells or progenitor cells that are able to spontaneously differentiate in vitro to cells that have the typical characteristics podocytes. Although the physiological roles of such cells are currently unclear, these cells have the potential to be a valuable resource for the regeneration of kidneys.

ACKNOWLEDGEMENTS

This work was supported by the Vice Chancellor of Research Affairs of Ahvaz Jundishapur University of Medical Sciences (grant number CMRC-9404), Ahvaz, Iran.

REFERENCES

AHMADI A, RAD NK, EZZATIZADEH V, MOGHADASALI R (2020) Kidney regeneration: stem cells as a new trend. *Curr Stem Cell Res Ther*, 15(3): 263-283.

ANDRIANOVA N, BUYAN IM, ZOROVA DL, PEVZNER BI, POPKOV AV, BABENKO AV, SILACHEV ND, PLOTNIKOV YE, ZOROV BD (2019) Kidney cells regeneration: dedifferentiation of tubular epithelium, resident stem cells and possible niches for renal progenitors. *Int J Mol Sci,* 20: 6326.

BONAVENTURA G, MUNAFÒ A, BELLANCA CM, LA COGNATA V, IEMMOLO R, ATTAGUILE GA, DI MAURO R, DI BENEDETTO G, CANTARELLA G, BARCELLONA ML, SEBASTIANO CAVALLARO S, BERNARDINI R (2021) Stem cells: innovative therapeutic options for neurodegenerative diseases? *Cell,* 10(8): 1992.

BRUNO S, BUSSOLATI B, GRANGE C, COLLINO F, DI CANTOGNO LV, HERRERA MB, BIANCONE L, TETTA C, SEGOLONI G, CAMUSSI G (2009) Isolation and characterization of resident mesenchymal stem cells in human glomeruli. *Stem Cells Dev,* 18: 867-879.

CHEN J, PARK H-C, ADDABBO F, NI J, PELGER E, LI H, PLOTKIN M, GOLIGORSKY MS (2008) Kidney-derived mesenchymal stem cells contribute to vasculogenesis, angiogenesis and endothelial repair. *Kidney Int,* 74(7): 879-889.

DIEP CQ, MA D, DEO RC, HOLM TM, NAYLOR RW, ARORA N, WINGERT RA, BOLLIG F, DJORDJEVIC G, LICHMAN B, ZHU H, IKENAGA T, ONO F, ENGLERT C, COWAN CA, HUKRIEDE NA, HANDIN RI, DAVIDSON AJ (2011) Identification of adult nephron progenitors capable of kidney regeneration in zebrafish. *Nature,* 470: 95-100.

GALLEGOS TF, KOUZNETSOVA V, KUDLICKA K, SWEENEY DE, BUSH KT, WILLERT K, FARQUHAR MG, NIGAM SK (2012) A protein kinase A and Wnt-dependent network regulating an intermediate stage in epithelial tubulogenesis during kidney development. *Dev Biol,* 364: 11-21.

GHEISARI Y, SOLEIMANI M, ZEINALI S, AREFIAN E, ATASHI A, ZARIF MN (2009) Isolation of stem cells from adult rat kidneys. *Biocell,* 33(1): 33-38.

GUPTA S, VERFAILLIE C, CHMIELEWSKI D, KREN S, EIDMAN K, CONNAIRE J, HEREMANS Y, LUND T, BLACKSTAD M, JIANG Y, LUTTUN A, ROSENBERG ME (2006) Isolation and characterization of kidney-derived stem cells. *J Am Soc Nephrol,* 17(11): 3028-3040.

HULING J, YOO JJ (2017) Comparing adult renal stem cell identification, characterization and applications. *J Biomed Sci,* 24(1): 32.

KITAMURA S, YAMASAKI Y, KINOMURA M, SUGAYA T, SUGIYAMA H, MAESHIMA Y, MAKINO H (2005) Establishment and characterization of renal progenitor like cells from S3 segment of nephron in rat adult kidney. *FASEB J,* 19(13): 1789-1797.

KREIDBERG JA (2010) WT1 and kidney progenitor cells. *Organogenesis*, 6: 61-70.

LEE PT, LIN HH, JIANG ST, LU PJ, CHOU KJ, FANG HC, CHIOU YY, TANG MJ (2010) Mouse kidney progenitor cells accelerate renal regeneration and prolong survival after ischemic injury. *Stem Cells,* 28(3): 573-584.

LEVEY AS, CORESH J (2012) Chronic kidney disease. *Lancet*, 379: 165-180.

LIN F, MORAN A, IGARASHI P (2005) Intrarenal cells, not bone marrow–derived cells, are the major source for regeneration in postischemic kidney. *J Clin Invest,* 115(7): 1756-1764.

LINDGREN D, BOSTRÖM AK, NILSSON K, HANSSON J, SJÖLUND J (2011) Isolation and characterization of progenitor-like cells from human renal proximal tubules. *Am J Pathol,* 178(2): 828-837.

LITTLE MH, KAIRATH P (2016) Regenerative medicine in kidney disease. *Kidney Int,* 90(2): 289-299.

LIU D, CHENG F, PAN S, LIU Z (2020) Stem cells: a potential treatment option for kidney diseases. *Stem Cell Res Ther*, 11: 249.

LIU QZ, CHEN XD, LIU G, GUAN GJ (2016) Identification and isolation of kidney-derived stem cells from transgenic rats with diphtheria toxin-induced kidney damage. *Exp Ther Med,* 12(3): 1651-1656.

MAESHIMA A, YAMASHITA S, NOJIMA Y (2003) Identification of renal progenitor-like tubular cells that participate in the regeneration processes of the kidney. *J Am Soc Nephrol,* 14(12): 3138-3146.

MORA CF, RANGHINI E, BRUNO S, BUSSOLATI B, CAMUSSI G, WILM B, EDGAR D, KENNY SE, MURRAY P (2012) Differentiation of podocyte and proximal tubule-like cells from a mouse kidney derived stem cell line. *Stem Cells Dev,* 21(2): 296-307.

NOURIAN DEHKORDI A, MIRAHMADI BABAHEYDARI F, CHEHELGERDI M, RAEISI DEHKORDI S (2019) Skin tissue engineering: wound healing based on stem-cell-based therapeutic strategies. *Stem Cell Res Ther*, 10: 111.

OLIVER JA, BARASCH J, YANG J, HERZLINGER D, AL-AWQATI Q (2002) Metanephric mesenchyme contains embryonic renal stemcells. *Am J Physiol Renal Physiol,* 283: F799-809.

OLIVER JA, MAAROUF O, CHEEMA FH, MARTENS TP, AL-AWQATI Q (2004) The renal papilla is a niche for adult kidney stem cells. *Am J Physiol Renal Physiol,* 114(6): 795-804.

RAMOS T, SÁNCHEZ-ABARCA LI, MUNTIÓN S, PRECIADO S, PUIG N, LÓPEZ-RUANO G, HERNÁNDEZ-HERNÁNDEZ A, REDONDO A, ORTEGA R, RODRÍGUEZ C, SÁNCHEZ-GUIJO F, DEL CAÑIZO C (2016) MSC surface markers (CD44, CD73, and CD90) can identify human MSC-derived extracellular vesicles by conventional flow cytometry. *Cell Commun Signal,* 14: 2.

RONCONI E, SAGRINATI C, ANGELOTTI ML, LAZZERI E, MAZZINGHI B, BALLERINI L, PARENTE E, BECHERUCCI F, GACCI M, CARINI M, MAGGI E, SERIO M, VANNELLI GB, LASAGNI L, ROMAGNANI S, ROMAGNANI P (2009) Regeneration of glomerular podocytes by human renal progenitors. *J Am Soc Nephrol,* 20: 322-332.

ROSENBERG ME, GUPTA S (2007) Stem cells and the kidney: where do we go from here? *J Am Soc Nephrol,* 18: 3018-3020.

SAGRINATI C, NETTI GS, MAZZINGHI B, LAZZERI E, LIOTTA F, FROSALI F, RONCONI E, MEINI C, GACCI M, SQUECCO R, CARINI M, GESUALDO L, FRANCINI F, MAGGI E, ANNUNZIATO F, LASAGNI L, SERIO M, ROMAGNANI S, ROMAGNANI P (2006) Isolation and characterization of multipotent progenitor cells from the Bowman's capsule of adult human kidneys. *J Am Soc Nephrol,* 17: 2443-2456.

SHANKLAND SJ, PIPPIN JW, REISER J, MUNDEL P (2007) Podocytes in culture: past, present, and future. *Kidney Int,* 72: 26-36.

TANIGAWA S, WANG H, YANG Y, SHARMA N, TARASOVA N, AJIMA R, YAMAGUCHI TP, RODRIGUEZ LG, PERANTONI AO (2011) Wnt4 induces nephronic tubules in metanephric mesenchyme by a non-canonical mechanism. *Dev Biol,* 352: 58-69.

TAYYEB A, SHAHZAD N, ALI G (2017) Differentiation of mesenchymal stem cells towards nephrogenic lineage and their enhanced resistance to oxygen peroxide-induced oxidative stress. *Iran J Kidney Dis,* 11(4): 271-279.

TROVATO L, NARO F, D'AIUTO F, MORENO F (2020) Promoting tissue repair by micrograft stem cells delivery. *Stem Cells Int*, 2020: 2195318.

VAINIO SJ (2003) Nephrogenesis regulated by Wnt signaling. *J Nephrol,* 16: 279-285.

YAMAMURA Y, FURUICHI K, MURAKAWA Y, HIRABAYASHI S, YOSHIHARA M, SAKO K, KITAJIMA S, TOYAMA T, IWATA Y, SAKAI N, HOSOMICHI K, MURPHY P, TAJIMA A, OKITA K, OSAFUNE K, KANEKO S, WADA T (2021) Identification of candidate PAX2-regulated genes implicated in human kidney development. *Sci Rep*, 11: 9123.

ZHONG C, LIU M, TAO Y, WU X, YANG Y, WANG T, MENG Z, XU H, LIU X (2022) Pou5f1 and nanog are reliable germ cell-specific genes in gonad of a protogynous hermaphroditic fish, orange-spotted grouper (*Epinephelus coioides*). *Genes,*13: 79.

Sella turcica anomalies and their association with malocclusion – a lateral cephalometric study

Karthikeya Patil, Prasanna S. Deshpande, V.G. Mahima, Romali Panda, C.J. Sanjay, D. Nagabhushana

Department of Oral Medicine and Radiology, JSS Dental College and Hospital, JSS Academy of Higher Education and Research, Mysore - 570 015, India

SUMMARY

The aim of the study is to estimate the prevalence of sella turcica anomalies on lateral cephalograms of individuals with malocclusion, so as to utilize it as a predictive indicator of malocclusion in adolescents. Lateral cephalograms of 224 subjects aged between 8-18 years with good visibility of cephalometric structures including sella turcica were assessed for the variants of malocclusion. The study group consisted of 133 cephalograms with abnormal sella turcica, while the control group consisted of 91 cephalograms without any abnormality. Cramer's V test was applied to find out association of classes of malocclusion and Sellar anomalies, and chi-square test was applied to know the frequency of each sellar anomaly among the class-wise distribution within the subjects.

Males were more associated with sellar anomalies as compared to females. A significant association between skeletal classes of malocclusion and sella turcica with Cramer's V value of 0.365 and significance of 0.001 was observed; so, it is clear that Class I malocclusion is associated with normal anatomy, while individuals with Class II and III are associated with sellar anomalies. An early predictive sign for prompt orthodontic intervention and correlating it with skeletal malocclusion can benefit both patients, as well as clinicians for interventional treatment.

Key words: Malocclusion – Sella túrcica – Radiology – Adolescent – Esthetics

INTRODUCTION

In orthodontics, the aberrant state is called a malocclusion, and it is frequently associated with facial disharmony. Although malocclusion is not a disease, it has both aesthetic and functional implications. There are psychological interferences associated to social acceptance and success from an aesthetic perspective, as well as interference with mastication, speech, and protection of the structures in the whole stomatognathic system from the functional standpoint. In this regard, one or more treatment plans can be identified, which essentially aid in organising the sequence of treatments necessary to achieve the desired goals. The main rationale is to accurately determine the time period during

Corresponding author:
Dr Prasanna Srinivas Deshpande. Department of Oral Medicine and Radiology, JSS Dental College and Hospital, JSS Academy of Higher Education and Research, Mysore - 570 015, India. Mob: +91 98864 73872. E-mail: drprasanna_deshpande@yahoo.com

Submitted: November 10, 2021. **Accepted:** March 4, 2022

https://doi.org/10.52083/QNQO7715

which orthodontic treatment would be most beneficial. (Różyło et al., 2010).

Individuals, on the other hand, differ in the timing, extent, and rate of growth. Not only does patient age impacts the circumpubertal growth spurt, but so do gender, genetics, ethnicity, diet, and socioeconomic situation. As a result, before developing a successful orthodontic treatment plan, it is critical to examine each patient's skeletal age and associate it with the patient's dental and chronological ages (Petrovic et al., 1990; Hägg et al., 1980; Coutinho et al., 1993; Hassel et al., 1995). Chronological age, dental development, and eruption sequence are not reliable predictors of skeletal maturation. Menarche (in females), voice changes (in males), hand-wrist ossification sequence, cervical vertebrae morphology, and statural growth curves have all been used to assess overall skeletal craniofacial maturity (Bhalajhi, 2018). Currently there are no methods that can accurately predict the craniofacial size that a patient will achieve at the end of active growth. This predictive inability becomes a problem in young patients with moderate maxillomandibular discrepancies (Thevissen et al., 2012). It is well known that the malocclusion is often multifactorial. Knowing the etiology of malocclusion is of prime importance for the effective treatment. In general, these factors can be categorized into genetic factors, environmental factors, or combination of both. The genetic factors relate to abnormalities in tooth development and its morphology, such as canine impaction, congenitally missing teeth, and abnormalities in shape of tooth (Bhalajhi, 2018). Sella turcica is an important structure in radiographic analysis of the neurocranial and craniofacial complex. In orthodontics, sella point which is located at the center of sella turcica is one of the most commonly used landmarks in Cephalometric Analysis. Such landmarks located within the craniofacial region are used to measure the positions of maxilla and mandible in relation to the cranium and to themselves (Hinck et al., 2012). The benefits gained from studying these structures range from assisting the orthodontist during diagnosis, as a tool to understand the growth in an individual through superimposition of structures on a longitudinal basis followed by evaluation of results. The knowledge about sound structure of the sella turcica is not only beneficial in evaluating cranial morphology, but also aids in assessing later growth changes and its treatment results. Few studies have shown that, at age of 5 years, the anterior sella turcica wall becomes stable and the morphology of the sella turcica does not change significantly after 12 years (Hinck et al., 2012; Sathyanarayana et al., 2015).

During embryological development, the sella turcica area is a key point for the migration of the neural crest cells to the frontonasal and maxillary developmental fields (Bjork, 1965); also, formation and development of the sella turcica and teeth share, in common, the involvement of neural crest cells. In fact, the anterior part of the sella turcica is believed to develop mainly from neural crest cells, and dental epithelial progenitor cells differentiate through sequential and reciprocal interaction with neural crest-derived mesenchyme. In the embryological development of the sella turcica, neural crest cells and mesodermal cells are involved (Miletich et al., 2004) Besides this developmental relationship, no systematic study has been undertaken to examine the presence of any association between sella turcica anomalies and dental malocclusion. Thus, shape anomalies of sella turcica may both be because of functional disorders in the pituitary gland and by morphological abnormalities of the facial bones (Sharpe, 2001). Recent studies indicate that localized dental anomalies such as hypodontia and palatal displacement of the maxillary canine are associated with calcification of the interclinoid ligament (ICL) or sella turcica bridging (most common type of sella turcica 5 abnormality); moreover, it has been concluded that the morphological appearance is established early in embryonic development (Kantor et al., 1987). Additionally, bridging of the sella turcica, or the union of the anterior and posterior clinoid processes, is another anatomical defect that has been associated with various syndromes and skeletal and dental deformities (Becktor et al., 2000). In orthodontics, diagnosis of facial skeletal type is essential for effective treatment planning. Until date, there have been no studies on the prevalence of sella turcica anomalies in a

homogenous groups of patients defined by both age and skeletal class of malocclusion. Therefore, this study was planned and designed to establish associations between the prevalence of Sella turcica anomalies on lateral cephalometric radiographs and skeletal malocclusion.

MATERIALS AND METHODS

The study group comprised of 250 subjects, aged between 8-18 years of age visiting the Department of Oral Medicine and Radiology, Jagadguru Sri Shivarathreeshwara Dental College and Hospital, Jagadguru Sri Shivarathreeshwara University, Mysore with malocclusion and enrolled for interventional orthodontic treatment in the Department of Orthodontics. An ethical clearance was taken from the Institutional Ethics Committee (No: JSS/DCH/MD-31/2015- 16(2)), with an informed consent taken from study subjects in accordance with the Declaration of Helsinki.

Sampling method

This prospective observational study comprised 250 subjects in the age group 8-18 years who were selected by simple random sampling technique having both maxillary and mandibular central incisors and all permanent first molars with integrated dentition and good occlusion. The sampling formula employed was:

n (sample size) = z2 pq/d2
= (1.96)2 (0.11) (0.89) / (0.05)2
= 150

(Where n=sample size, Z=1.96 (95% confidence interval), p= proportion of prevalence, q= (1-P), d=margin of error in decimal points)

Exclusion and inclusion criteria

The study did not include subjects with history of facial trauma and/or the presence of a cleft lip and palate and craniofacial syndromes. Lateral cephalographs obtained were assessed for good visibility of cephalometric structures, including the Sella turcica, and the absence of craniofacial congenital deformities and central pathologies. All cephalographs were analyzed as monitor-displayed images according to Segner and Hasund (1994), using a computer program. Subsequently, anomalies of the Sella turcica according to Axelsson et al. (2003) were identified on lateral cephalographs. In order to analyze bridging of Sella turcica as bridge Type A ribbon-like fusion Sella anomalies and bridge Type B- Sella turcica extension of the clinoid process, the classification of Becktor et al. (2000) was used, which also employed lateral cephalographs. Moreover, a classification of the patients in either of the groups based on malocclusion was done. Skeletal malocclusion analysis was done with ANB angle and Wits appraisal. Patients with an ANB angle less than −1 degree and a Wits appraisal less than −2 mm were categorized as skeletal Class III, and patients with ANB 3-5 degree and a wWits appraisal of 2-9 mm were classified as Class II, whereas those with an ANB angle 0–4 degree and a Wits appraisal ±1 mm were categorized as skeletal Class I (Fig. 1 showing Planmeca Romexis software for cephalometry for measurement of ANB angle and the form of sella turcica). The obtained data were analyzed using SPSS software version 22 for the correlation of sella turcica abnormalities and skeletal/dental malocclusions

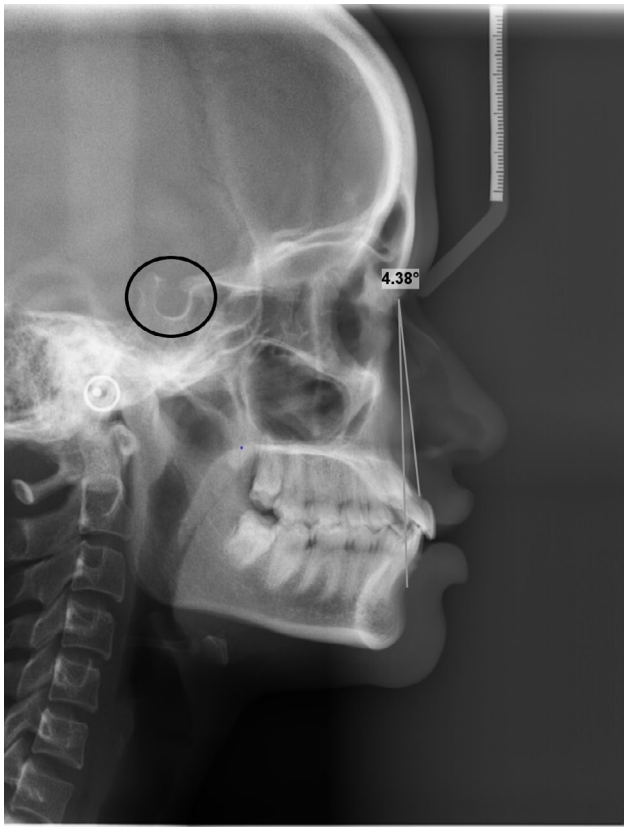

Fig. 1.- Planmeca Romexis software for cephalometry for measurement of ANB angle and the form of sella turcica.

by descriptive statistics, Cramer's V test and chi-square test for determining the frequency among different sella turcica anomalies and skeletal malocclusion.

RESULTS

A total of 250 subjects were included in the study. After scrutiny, 26 of them were excluded because of poor diagnostic criteria of lateral cephalograms. Out of 224 radiographs (Males-112, Females-112) evaluated for the sella anomalies, 91 radiographs had normal sella (control group) whereas 133 radiographs displayed sellar anomalies (study group). Study group comprised subjects in the age range of 8-18 years, with a mean age of 13.99 ± 3.65 years in subjects with sellar anomalies and the mean age range of subjects with normal sella was 14.5 ± 3.12 years (Graph 1 shows the mean age of the study population).

In normal sella, 47 (51.64 %) radiographs were of female subjects and 44 (48.35%) were of male subjects, whereas, in abnormal sella, 65 radiographs were of females (48.8%) and 68 radiographs were of males (51.12%) (Graph 2 shows the gender distribution of the study population).

Subjects were classified on the basis of skeletal malocclusion. Normal sella was seen in 45 (68.2%) in skeletal class I, 25 (31.2%) in skeletal class II and 21 (26.9%) in skeletal class III. The

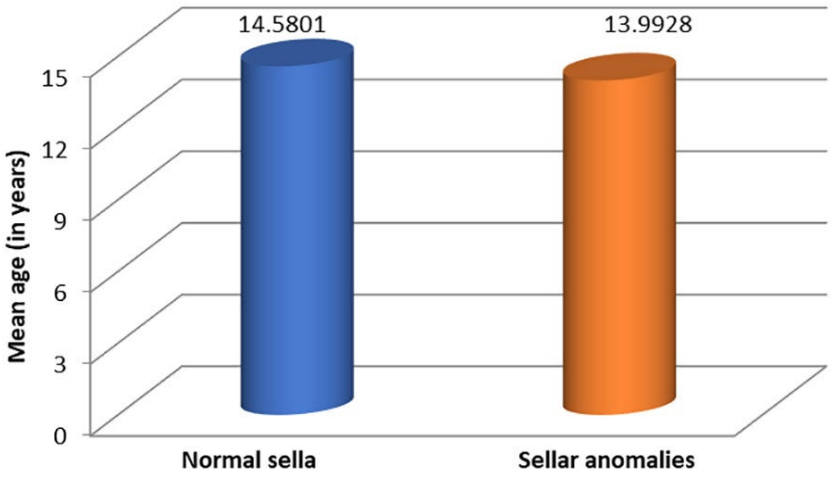

Graph 1. Mean age of the study population.

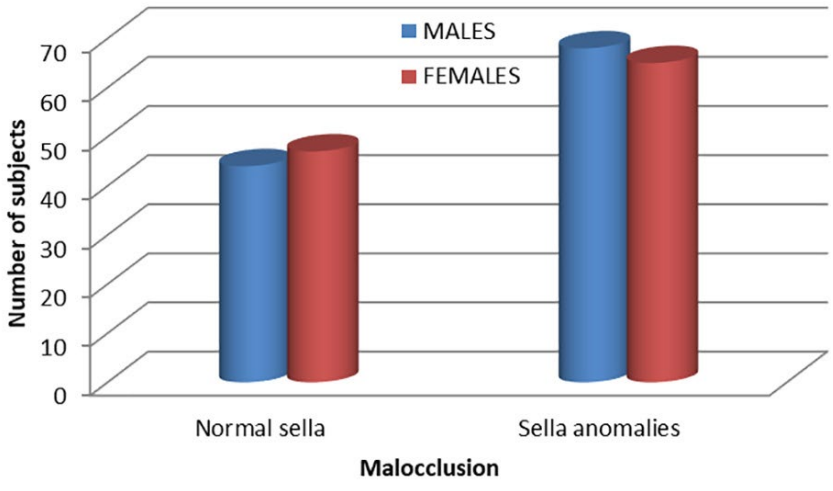

Graph 2. Gender distribution of the study population.

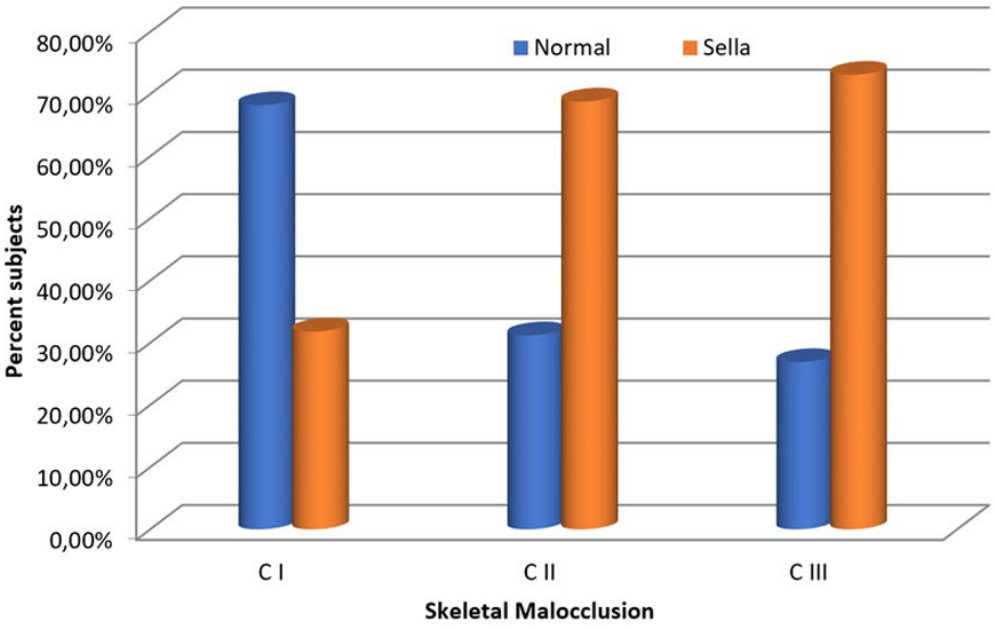

Graph 3. Distribution of skeletal malocclusion among study subjects.

sellar anomalies were seen in 21 (31.8%) in skeletal class I, 55 (68.8%) in skeletal class II and 57 (73.1%) in skeletal class III (Graph 3 shows the distribution of skeletal malocclusion among study subjects).

Application of Cramer's V test between the groups showed a statistical significance of 0.365 and p value of 0.001, which shows that a significant association was found between classes of skeletal malocclusion and Sella turcica anomalies. Thus it is clear that Class I malocclusion occurs with normal anatomy, and class II and III were associated with sellar anomalies.

Among the sella anomalies observed, maximum prevalence was detected in class III cases (57 subjects) with highest frequency of incomplete bridging (20 subjects; chi-square value=10.32), followed by hypertrophic posterior clinoid process (10 subjects; chi-square value= 4.75) (Table 1 shows the frequency of sella turcica

Table 1. Frequency of sella tursica anomalies among the skeletal malocclusion classes.

Sella Anomalies	Skeletal Class I	Skeletal Class II	Skeletal Class III	Total	Chi Square	P value
Sella turcica Bridge Type A Ribbon-like fusion	1	1	2	4	-	-
Sella Turcica bridge Type B - extension of the clinoid process	2	5	2	9	2.0	.368
Incomplete Bridge	4	14	20	38	10.32	.006
Hypertrophic posterior clinoid process	3	11	10	24	4.75	.093
Hypotrophic posterior clinoid process	3	6	3	12	1.50	.472
Irregularity (notching) in the posterior part of the sella turcica	1	3	2	6	-	-
Pyramidal shape of the dorsum sellae	1	1	2	4	-	-
Double contour of the floor	1	2	3	6	-	-
Oblique anterior wall	1	3	5	9		
Oblique contour of the floor	4	9	8	21	2.00	.368
Total study group	**66**	**80**	**78**	**224**		
	100%	**100%**	**100%**	**100%**		

anomalies among the skeletal malocclusion classes). For very low frequencies, statistics cannot be applied. In Table 1, p value of less than 0.05 (typically ≤ 0.05) is statistically significant; so, p value of 0.006 is highly significant in the present study: i.e., incomplete bridging followed by p value of 0.093, i.e., hypertrophic posterior clinoid process. Moderate significance with p value of 0.368 was found in sella turcica bridge Type B- extension of clinoid process and oblique contour of floor (Fig. 2 shows the different forms of sella turcica anomalies as they appear in lateral cephalograms).

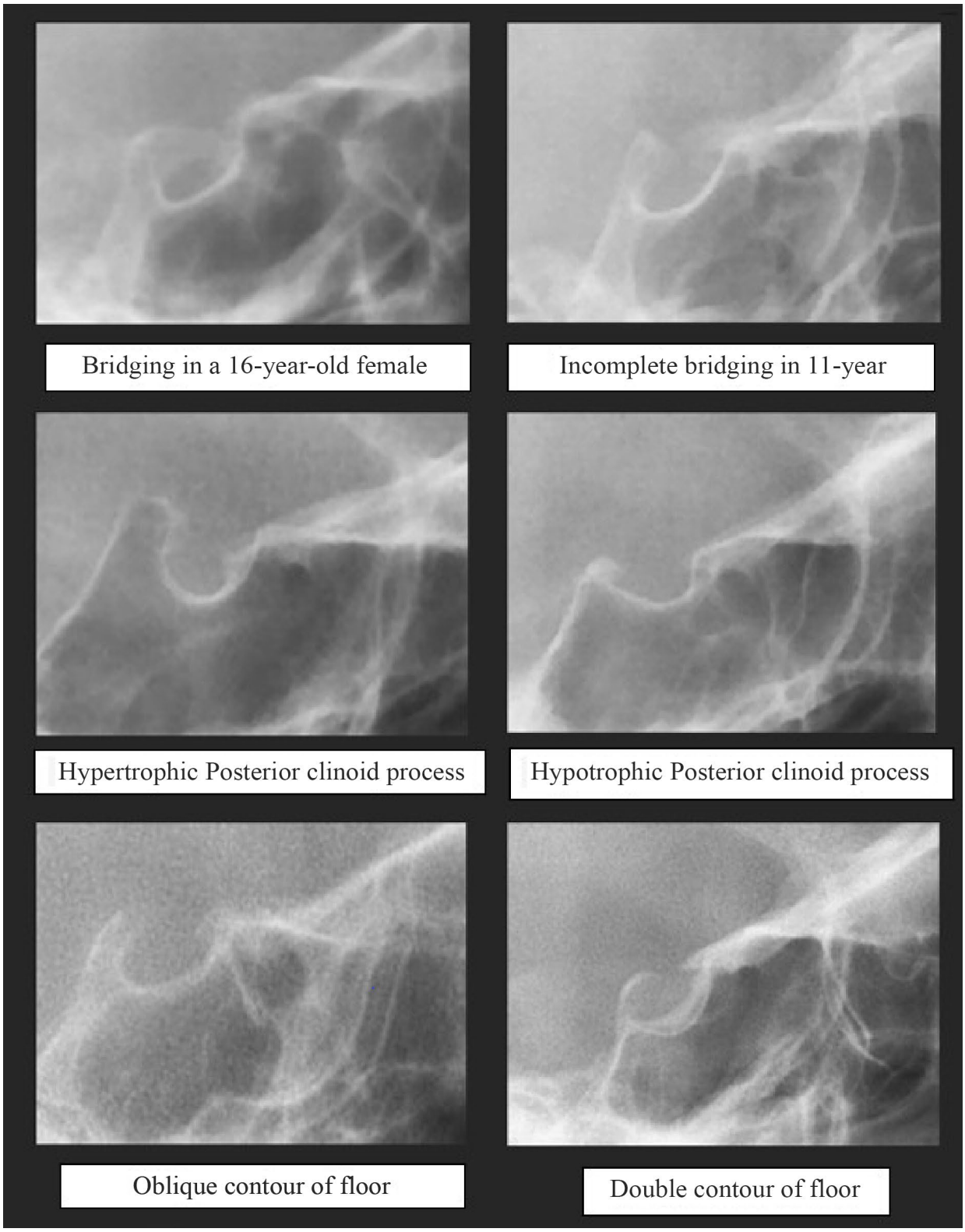

Fig. 2.- Different forms of sella turcica anomalies as they appear in lateral cephalograms.

DISCUSSION

A prompt and early diagnosis of any skeletal condition needs to be assessed in the patient by utilizing all the information available to us with the least amount of radiological intervention. In 1931, Broadbent pioneered a precise technique for taking standardized head radiographs, thus providing a valuable means for the investigation of facial and cranial growth. In the present study, an attempt was made to analyze and differentiate various types of sellar anomalies and their relationship with classes of malocclusion, so as to utilize this as an adjunct to diagnostic armamentarium (Broadbent et al., 1934; Hans et al., 2015). Sella turcica is a readily recognized structure on lateral cephalometric radiographs, and routinely traced in cephalometric analysis.

Calcification of interclinoid ligament, also known as sella turcica bridging, is found to be more prevalent in patients with severe craniofacial deviations and tooth anomalies, and is positively associated with complex craniofacial malformations that require combined surgical and orthodontic treatment protocols (Leonardi et al., 2006). This includes naevoid basal cell carcinoma syndrome, along with calcification of the falx cerebri and vertebral anomalies. This might be attributed to the shared embryogenic origin of sella turcica, many midfaces skeletal fields, and progenitor cells of the dental epithelium (neural crest cells), as well as shared genes involved in their development (e.g., HOX or sonic hedgehog genes) (Miletich et al., 2004). The mean diameter of sella turcica at the age of 8 years is 10 mm, and at the age of 16 years is 11 mm. It is stringently dependent on hypophyseal morphology, and thus the size alterations may be the signs of glandular pathology, which suggests that the individual should undergo further evaluation. (Neha et al., 2016). Axelsson et al. (2003) classified the sella turcica shapes into normal sella turcica, oblique anterior wall, double contoured sella, sella turcica bridge, irregularity (notching) in the posterior part of the sella, oblique contour of the floor, and pyramidal shape of the dorsum sellae. However, it should be kept in mind that two-dimensional representation of a three-dimensional structure using conventional radiography has its limitation in identifying these sellar anomalies.

A recent study conducted among Japanese female patients undergoing orthodontic treatment (Kashio et al., 2017) found that interclinoid distance decreased with advancing age. The combination of increase in sella turcica dimension and a slight decrease in interclinoid distance results in greater degree of interclinoid ligament calcification in the subjects over 19 years of age than in the subjects between 7-12 years of age.

A similar observation was also made in our study, with only 38.45% individuals presenting with sella turcica bridging and incomplete bridging in the study group accounting to a mean age of 13.99 ± 3.65 yrs., which was lesser than the average age of the overall study population being 14 years. The reported prevalence of bridging is highly variable: 4 % - 8.68% on dry skulls, 1.54 % - 6% in autopsy specimens and 3.74% - 11.1% on cephalograms (Axelsson et al., 2003; Camp, 1924; Kjær, 2015). In this study, sella turcica bridge was found in 13 subjects and seems to be “5.80%” (13 out of 224 subjects of the study sample). This is in accordance with the previous studies and research data (Axelsson et al., 2003; Camp, 1924; Kjær, 2015).

Becktor et al (2000) reported that one third of the sella bridges were Type A in Caucasians, and the rest were Type B. In our present prospective observational study, the sex difference among the study population is not significant. However, it was found from our study that there was strong association of male subjects and sellar anomalies as compared with females. The strong association of the male subjects and sella tursica anomalies could be attributed to the homogenous group of study population belonging to same ethnicity, race and nationality.

According to our findings, normal sella was found in 68.2 % of skeletal class I individuals,31.2% of skeletal class II respondents, and 26.9% of skeletal class III subjects. Sellar abnormalities were seen in 31.8 percent of skeletal class I patients, 68.8% of skeletal class II patients, and 73.1 percent of skeletal class III patients. As a

result, a substantial link was discovered between skeletal malocclusion classes and sella turcica abnormalities, indicating that class I malocclusion is related with normal anatomy while class II and III malocclusion are connected with sellar anomalies. As a consequence, this study serves as a foundation for future research, indicating that the presence of a sellar abnormality is a predictor of skeletal malocclusion.

Ghadimi et al. (2017), while observing cephalographs of 35 orthodontic patients with palatally displaced canines (PDC) and 75 patients without them, found that the presence of ponticulus posticus and sella turcica bridging (STB) might be associated with increased odds of PDC occurrence. They found correlation between degree of calcification of ICL and skeletal growth in patients has not been established, but it can be used as a guide for detection of craniofacial deviations ranging from palatally displaced canine to atlas posterior arch deficiency.

Busch et al. (1951) had assessed 343 skulls of deceased individuals with a slightly higher (2.1%) prevalence for incomplete bridging than complete bridging (1.2%). Kucia et al. (2014) and Abdel-Kader (2007), while observing cephalograms of patients for orthodontic treatment, had noted a frequency of only 2.5-3.5% for bridging in the study population. Details regarding incomplete bridging or any other signs of calcification of interclinoid ligament were not studied by Abdel-Kader (2007), but a higher prevalence of incomplete bridging (6.8%) was observed by Kucia et al. (2014).

Also, the age group of the study was 9-16 years, so it can be attributed to the slower progress happening in the sellar region for calcification.

Kashio et al. (2017), in the observation of 232 Japanese female orthodontic subjects in the age group of 7-35, had observed the highest frequency of 65.1% (150 Individuals) for incomplete bridging. They were further classified into Type II A (half calcified) based on the extent of bridging. It was found that subjects >19years had a larger extent of these calcification than those in 7-12 years age group. They had observed that sella turcica morphology and bridging were associated with tooth impaction, but not with maxillofacial skeletal deviation.

Limitations and future study prospects

In the present study, there was a higher association of sellar anomalies with skeletal malocclusion, class II and III. Hence, sella anomalies were taken as an indication for the predisposition of skeletal malocclusion, and all patients were advised for interventional orthodontic treatment. The morphology of sella is also determined genetically at an early period of time; any evidence of increased calcification of interclinoid ligament should alert the diagnostician for further follow up and recall. In the present study, all patients desiring orthodontic correction for malalignment of teeth were randomly selected, and no specific attempt to segregate them based on skeletal malocclusion was done employing random sampling. Hence, a small discrepancy was seen among the distribution pattern of the sample.

This can also be attributed to facts like population included were residents of single city- Mysuru in South India. Race and ethnicity of the populace included in the study should also be considered. Our study forms the basis on which further studies could be conducted on larger samples for better understanding of the relationship of skeletal malocclusions and sella turcica prevalence. This study has extended the scope for analyzing different types of sella anomalies and its correlation with malocclusion, as studies on similar grounds have not been performed.

CONCLUSION

In the current orthodontic scenario, many people seek orthodontic treatment for betterment of occlusion, improved oral function and harmonized facial appearance. To recapitulate, we conclude by stating that any evidence of Sella turcica anomaly should be considered as evidence for impending craniofacial malformations. Diagnosing any disease at the earliest stages has been a perpetual attempt by researchers all over the world. In this study, an attempt was made to predict malocclusions before they actually

manifest clinically. A positive association of malocclusion in young male population aged between 8-18 years with sella turcica anomalies was observed.

REFERENCES

ABDEL-KADER HM (2007) Sella turcica bridges in orthodontic and orthognathic surgery 14 patients. A retrospective cephalometric study. *Austral Orthod J*, 23(1): 30.

AXELSSON S, STORHAUG K, KJÆR I (2003) Post-natal size and morphology of the sella turcica. Longitudinal cephalometric standards for Norwegians between 6 and 21years of age. *Eur J Orthod*, 26(6): 597-604.

BECKTOR JP, EINERSEN S, KJAER I (2000) A sella turcica bridge in subjects with severe craniofacial deviations. *Eur J Orthod*, 22: 69-74.

BHALAJHI SI (2018) Orthodontics the art and science, 7th edition. Arya MEDI Publishing House, pp 10-31.

BJORK A (1963) Variations in the growth pattern of the human mandible: longitudinal radiographic study by the implant method. Pt 2. *J Dent Res*, 42(1): 400-411.

BROADBENT BH (1931) A new X-ray technique and its application to orthodontia. *Angle Orthod*, 1: 45-66.

BUSCH W (1951) Die Morphologie der Sella turcica und ihre Beziehungen zur Hypophyse. [In German]. *Virchows Arch*, 320: 437-458.

CAMP JD II (1924) The normal and pathological anatomy of the sella turcica as revealed by roentgenograms. *Am J Roentgenol*, 12: 143-156.

COUTINHO S, BUSCHANG PH, MIRANDA F (1993) Relationships between mandibular canine calcification stages and skeletal maturity. *Am J Orthod Dentofacial Orthop*, 104: 262-268.

GHADIMI MH, AMINI F, HAMEDI S, RAKHSHAN V (2017) Associations among sella turcica bridging, atlas arcuate foramen (ponticulus posticus) development, atlas posterior arch deficiency, and the occurrence of palatally displaced canine impaction. *Am J Orthod Dentofacial Orthop*, 151(3): 513-520.

HÄGG U, TARANGER J (1980) Menarche and voice change as indicators of the pubertal growth spurt. *Acta Odontol Scand*, 38: 179-186.

HANS MG, PALOMO JM, VALIATHAN M (2015) History of imaging in orthodontics from 15 Broadbent to cone-beam computed tomography. *Am J Orthod Dentofacial Orthop*. 148(6): 914-921.

HASSEL B, FARMAN AG (1995) Skeletal maturation evaluation using cervical vertebrae. *Am J Orthod Dentofacial Orthop*, 107: 58-66.

HINCK VC, HOPKINS CE (1965) Concerning growth of sphenoid sinus. *Arch Otolaryngol*, 82: 62-66.

KANTOR ML, NORTON LA (1987) Normal radiographic anatomy and common anomalies seen in cephalometric films. *Am J Orthod Dentofacial Orthop*, 91: 414-426.

KASHIO H, TORIYA N, OSANAI S, OKA Y, KONNO-NAGASAKA M, YAMAZAKI A, MUGURUMA T, NAKAO Y, SHIBATA T, MIZOGUCHI I (2017) Prevalence and dimensions of sella turcica bridging in Japanese female orthodontic patients. *Orthodontic Waves*, Jun 9.

KJÆR I (2015) Sella turcica morphology and the pituitary gland — a new contribution to craniofacial diagnostics based on histology and neuroradiology. *Eur J Orthod*, 37(1): 28-36.

KUCIA A, JANKOWSKI T, SIEWNIAK M, JANISZEWSKA-OLSZOWSKA J, GROCHOLEWICZ K, SZYCH Z, WILK G (2014) Sella turcica anomalies on lateral cephalometric radiographs of Polish children. *Dentomaxillofacial Radiol*, 43(8): 20140165.

LEONARDI R, BARBATO E, VICHI M, CALTABIANO M (2006) A sella turcica bridge in subjects with dental anomalies. *Eur J Orthod*, 28(6): 580-585.

MILETICH I, SHARPE PT (2004) Neural crest contribution to mammalian tooth formation. 16 Birth Defects. *Res C Embryo Today*, 72: 200-212.

NEHA SM, SHETTY VS, SHETTY S (2016) Sella size and jaw bases – Is there a correlation? *Contemp Clin Dent*, 7: 61-66.

PETROVIC A, STUTZMANN J, LAVERGNE J (1990) Mechanism of craniofacial growth and modus operandi of functional appliances: A cell-level and cybernetic approach to orthodontic decision making. In: Carlson DS (ed). *Craniofacial Growth Theory and Orthodontic Treatment*. Monograph 23. Ann Arbor: Center for Human Growth and Development, University of Michigan.

RÓŻYŁO-KALINOWSKA I, KOLASA-RĄCZKA A, KALINOWSKI P (2010) Relationship between dental age according to Demirjian and cervical vertebrae maturity in Polish children. *Eur J Orthod*, 33(1): 75-83.

SATHYANARAYANA HP, KAILASAM V, CHITHARANJAN AB (2013) Sella turcica. Its importance in orthodontics and craniofacial morphology. *Dental Res J*, 10(5): 571.

SEGNER D, HASUND A (1994) Individualisierte Kephalometrie. Aufl Hamburg, Germany: Franklin Printing and Publishing House Ltd.

SHARPE PT (2001) Neural crest and tooth morphogenesis. *Adv Dent Res*, 15: 4-7.

THEVISSEN PW, KAUR J, WILLEMS G (2012) Human age estimation combining third molar and skeletal development. Int J Legal Med, 126(2): 285-292.

An unusual accessory soleus muscle with its clinical implications

Y. Lakshmisha Rao, Padma Priyadarshini, Mangala M. Pai, Prameela M. Dass

Department of Anatomy, Kasturba Medical College, Mangalore, Manipal Academy of Higher Education, Manipal, India

SUMMARY

Anomalous, supernumerary or accessory muscles in the flexor compartment of the leg are reported in the medical literature. The accessory soleus muscle is one of the variations found in this region, with the incidence ranging from 0.7-5.5%. The presence of an accessory muscle in the posterior compartment is of clinical significance, as it can be mistaken for a tumor during the clinical examination, or it can lead to the compression of surrounding neurovascular structures. During routine dissection of a cadaver, an accessory muscle was found in the medial aspect of the middle portion of the posterior compartment of the left leg. It originated with two heads from the middle portion of the soleus muscle and got inserted onto the medial surface of the calcaneum. The muscle was unilateral and was supplied by the tibial nerve. Evidence about these accessory muscles and their location and attachments are useful in making a proper diagnosis and management.

Key words: Anatomic variation – Soleus muscle – Nerve entrapment – Tarsal tunnel syndrome – Soft tissue tumor

INTRODUCTION

The flexor or posterior compartment of the leg consists of superficial and deep layers of muscles. They are supplied by the tibial nerve and they act as plantar flexors of foot at ankle, invertor of the foot and plantar flexors of toes. The superficial layer is formed by two heads of the gastrocnemius, plantaris and soleus muscle. All three superficial muscles get inserted into the calcaneum bone and they help in the plantar flexion of the foot at the ankle joint. The underlying deep layer of muscles includes popliteus, flexor digitorum longus (FDL), flexor hallucis longus (FHL) and tibialis posterior (TP). The FDL, FHL and TP form long cord-like tendons inferiorly and are arranged from medial to lateral as TP, FDL and FHL under the flexor retinaculum (Standring, 2008). Supernumerary or accessory muscles in the flexor compartment of the leg are reported in the medical literature (Paul et al., 2008). Accessory soleus muscle (ASM) is one such variation, which was first reported by Cruveilhier in 1843. The incidence of ASM ranges from 0.7-5.5% (Mihovil et al., 2020). We present an unusual muscle in the posterior compartment of the leg supplied by the tibial nerve.

Corresponding author:
Dr Prameela M. Dass. Department of Anatomy, Kasturba Medical College, Mangalore, Manipal Academy of Higher Education, Manipal, Karnataka, India 575004. Phone: +91 9945935680. E-mail: prameela.md@manipal.edu

Submitted: November 8, 2021. **Accepted:** February 16, 2022

https://doi.org/10.52083/RBBB4530

CASE REPORT

During routine dissection of a formalin fixed, 81-year-old female cadaver, an accessory muscle was found unilaterally in the medial and middle portion of the posterior compartment of the left leg. It had tendinous origin with two heads from the middle portion of the anterior surface of the soleus muscle, and got inserted onto the medial surface of the calcaneus as a tendon. The lateral slip of origin was measuring 5.2 cm long and the medial slip was 4.9 cm long; the length of the muscle belly was 9.2 cm, the length of the tendon of insertion was 3.8 cm, width and thickness at the bulkiest part of the muscle belly was 3.6 cm and 0.9 cm respectively. The muscle was supplied by a branch of the tibial nerve (Fig. 1 and Fig. 2). The surrounding neuro-vascular structures appeared to be normal. Origin and insertion of the soleus muscle was found to be normal.

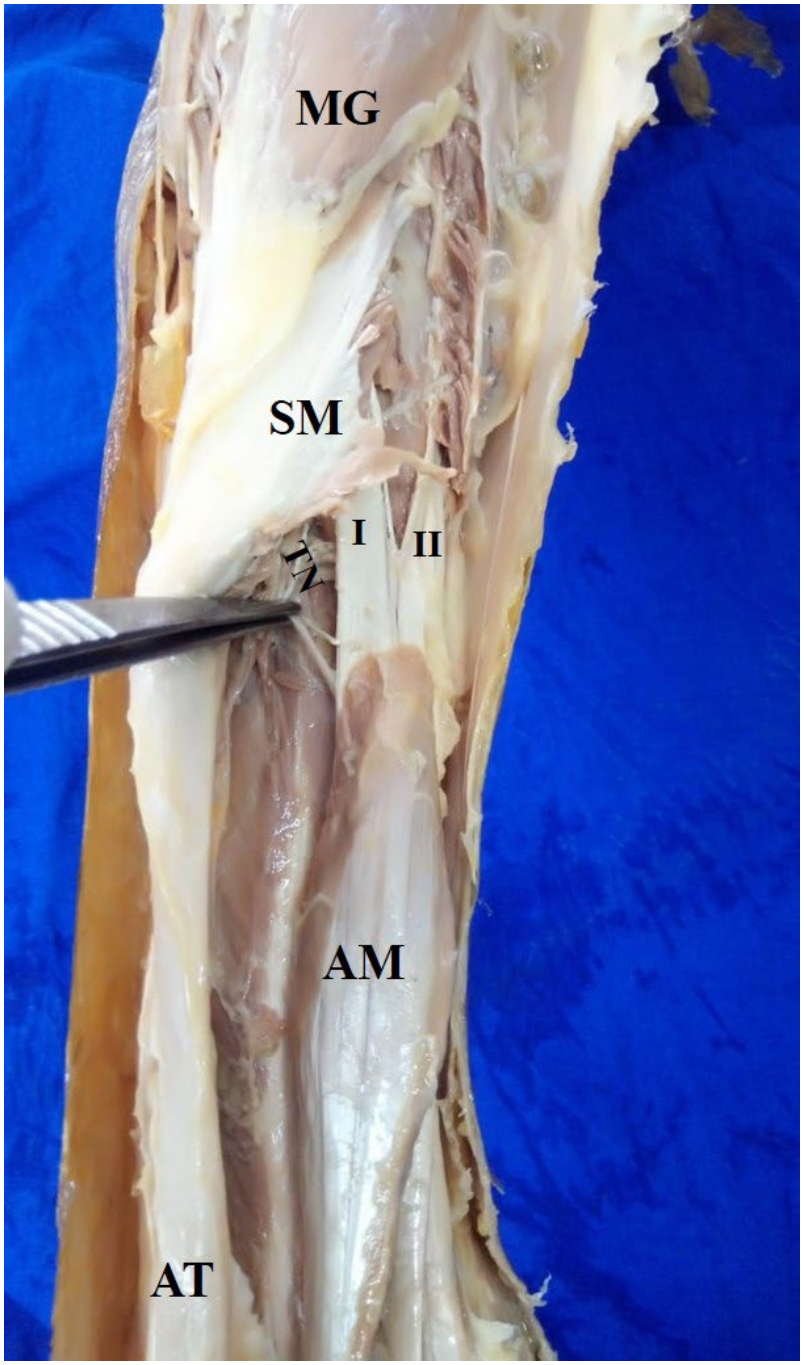

Fig. 1.- Right lower limb of a cadaver showing accessory muscle. (Origin of Soleus is partially divided to show the two heads of origin of AM). AM- Accessory muscle, AT- Achilles tendon, SM- Soleus muscle, MG- Medial head of Gastrocnemius, I- Lateral head of accessory soleus, II- Medial head of accessory soleus taking origin from anterior surface of soleus, TN- Branch of tibial nerve.

DISCUSSION

The presence of anatomical variation in the posterior compartment muscles is of clinical significance, as it may be mistaken for a soft tissue tumor during the clinical examination, or it may lead to the compression of surrounding neurovascular structures and cause painful syndromes like tarsal tunnel syndrome (Carrington et al., 2016). The ASM is one such muscle, which was first described by Cruveilhier in 1843. Its incidence ranges from 0.7% to 5.5%. It may be present bilaterally in 15% of cases, and it is twice as common in men compared to women (Brodie et al., 1997). The ASM may arise from the anterior surface of the soleus or from the fibula and soleal line of the tibia (Brodie et al., 1997; Lorentzon and Wirell, 1987). On the basis of the insertion of ASM, it can be classified into 5 types. It may get inserted to the Achilles tendon, to the upper surface of the calcaneus by fleshy muscle fibres, upper surface of the calcaneus by a tendon,

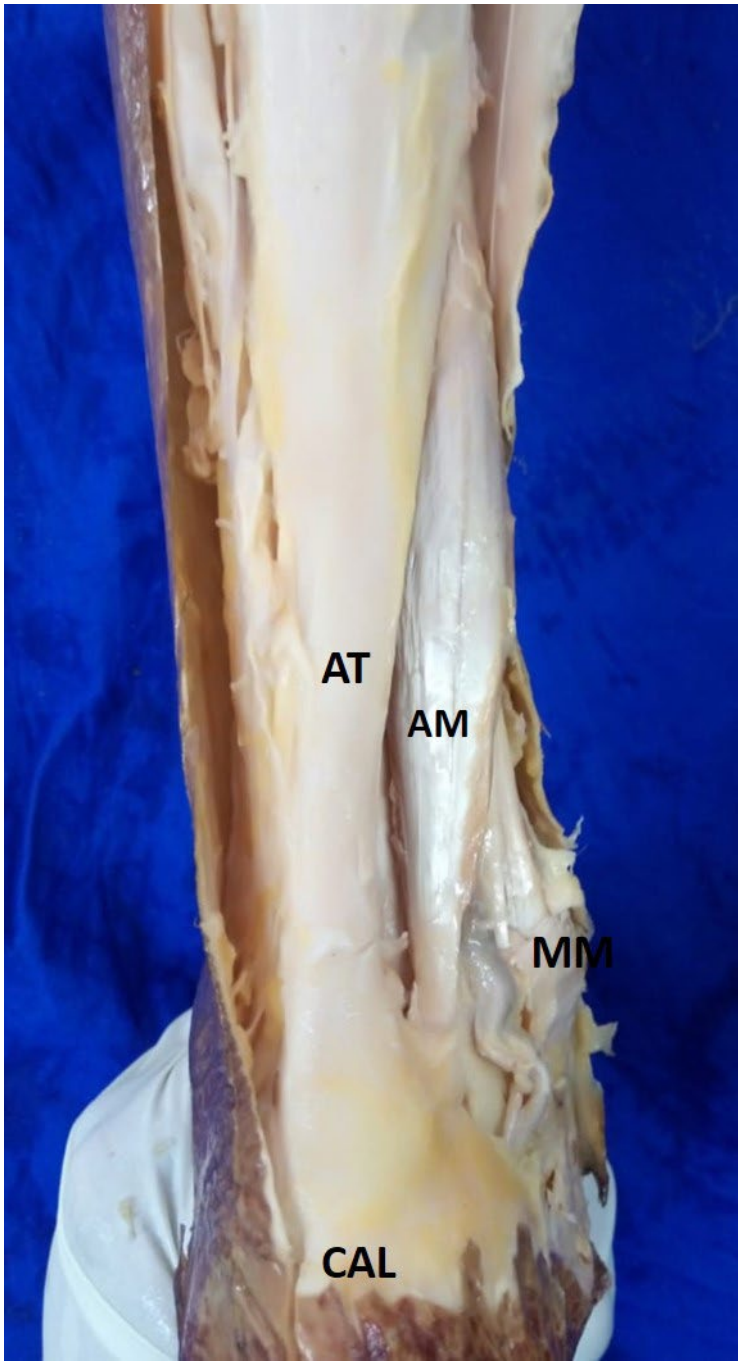

Fig. 2.- Right lower limb of a cadaver showing insertion of accessory muscle. AM- Accessory muscle, AT- Achilles tendon, SM- Soleus muscle, MM- Medial malleolus, CAL- Calcaneus.

medial surface of the calcaneus by fleshy muscle fibre or medial surface of calcaneus by a tendon (Lorentzon and Wirell, 1987; Yu et al., 1994). Like any other accessory muscles, they are also usually asymptomatic and can be identified incidentally during radiological investigations. Identifying these accessory muscles and defining their position, attachment and neuro-vascular supply is useful for making an appropriate diagnosis, as well as planning the surgical approach and procedures (Dunn, 1965). The authors describe an accessory muscle, with the origin from the anterior surface of the soleus with two fascicles and with insertion in the posterior tuberosity of the calcaneus, medial to the Achilles tendon, which we consider as ASM. This variation corresponds to type 5 of ASM by Yu et al. (1994). A branch of the tibial nerve was supplying the ASM in our case, which is similar to the report by Sekiya et al. (1994), Christodoulou et al. (2004) and Yildirim et al. (2011). Some researchers have described this variant muscle as accessory plantaris muscle. This muscle takes origin from the fascia of the soleus, due to its caudal migration from the femoral origin (Mayer et al., 2013). Embryological aspects state that lower limbs develop from the mesoderm at the end of fourth week of development as outpocketings from the ventrolateral body wall, which corresponds to stage 13 of Carneggie (O'Rahilly et al., 1981). Abnormal migration and rearrangement of muscles may lead to variations (Hamilton et al., 1978).

Olewnik et al. (2021) have classified the soleus muscle according to its fiber morphology into four types. Type 1- Bipennate muscle, with the fascicles attached to both sides of central tendon, Type 2- Unnipennate, with fascicles running at an acute angle from one side of the tendon, Type 3- Multipennate, in which fascicles are attached to many tendons within the muscle and Type 4- Non pennate lacking any central tendon. The muscle we found was similar to type 4 of Olewnik et al. (2021).

Common presentation of ASM is posteromedial ankle swelling which may become painful during physical activity (Kendi et al., 2004). Sometimes it may present as painless swelling and rarely it may be associated with club foot deformity (Brodie et al., 1997). Even though ASM is congenital, the symptoms are usually seen in 2nd or 3rd decade of life. Increasing muscle mass and more physical activity during this age may be the reason for symptoms (Mayer et al., 2013). Mihovil et al. (2020) have reported a rare case of ASM with symptom of pain at the ankle without swelling.

Nayak and Shetty (2019) have noticed an anatomical variation of two accessory muscle bellies in the flexor compartment of the leg. One belly was connected between FHL and TP whereas another belly was taking origin from the connective tissue around the posterior tibial artery and was inserted into the lateral border of the tibia. The muscles were crossing the posterior tibial artery. They have also opined that these muscles can compress the posterior tibial vessels. The ASM can cause nerve entrapment at the tarsal tunnel leading to many conditions like painful legs, moving toes syndrome (Pla et al., 1996). Accessory soleus in athletes with ankle pain may confuse the orthopedicians to differentiate from the exertion pain (Randell et al., 2019).

According to Cheung (2017), identifying such accessory muscles can be difficult for radiologists during the evaluation as they follow the path of other normal flexor muscles. As suggested by Kendi et al. (2004), absence of Kager's fat in the plain radiograph may be highly suggestive of ASM. Even though ultrasound and CT scan may be useful in the diagnosis, definitive diagnosis can be done only with magnetic resonance imaging (Mihovil et al., 2020).

In patients with chronic Achilles tendon rupture, treatment is challenging for surgeons. Usually, semitendinosus and gracilis will be used to graft the tendon (Bakowski et al., 2020). Pre-operative evaluation for any accessory muscles in the lower limb may be beneficial in such patients, as these accessory muscle tendons can be used as a graft material for the repair of the injured tendon.

CONCLUSION

We present an accessory muscle in the posterior compartment of the leg supplied by the tibial nerve. Many times, accessory muscles will be unnoticed when they are asymptomatic. Evidence

about these accessory muscles and their location and attachments is useful in making a clinical and radiological diagnosis. Sometimes the presence of this type of anatomical variation is of clinical significance, as it may be mistaken for a soft tissue tumor during the clinical examination, or it may lead to the compression of surrounding neurovascular structures.

ACKNOWLEDGEMENTS

The authors sincerely thank those who donated their bodies to science so that anatomical research and teaching could be performed. Results from such research can potentially increase scientific knowledge and can improve patient care. Therefore, these donors and their families deserve our highest respect.

REFERENCES

BĄKOWSKI P, CIEMNIEWSKA-GORZELA K, TALAŚKA K, GÓRECKI J, WOJTKOWIAK D, KERKHOFFS GMMJ, PIONTEK T (2020) Minimally invasive reconstruction technique for chronic Achilles tendon tears allows rapid return to walking and leads to good functional recovery. *Knee Surg Sports Traumatol Arthrosc*, 28(1): 305-311.

BRODIE JT, DORMANS JP, GREGG JR, DAVIDSON RS (1997) Accessory soleus muscle. A report of 4 cases and review of literature. *Clin. Orthop Relat. Res,* 337: 180-186.

CARRINGTON SC, STONE P, KRUSE D (2016) Accessory soleus: a case report of exertional compartment and tarsal tunnel syndrome associated with an accessory soleus muscle. *J Foot Ankle Surg*, 55(5): 1076-1078.

CHEUNG Y (2017) Normal variants: accessory muscles about the ankle. *Magn Reson Imaging Clin N Am*, 25(1): 11-26.

CHRISTODOULOU A, TERZIDIS I, NATSIS K, GIGIS I, POURNARAS J (2004). Soleus accessorius, an anomalous muscle in a young athlete: case report and analysis of the literature. *Br J Sports Med,* 38(6): e38.

DUNN AW (1965) Anomalous muscles simulating soft-tissue tumors in the lower extremities: report of three cases. *J Bone Joint Surg Am*, 47: 1397-1400.

HAMILTON WJ, BOYD JD, MOSSMAN HW (1978) Cardiovascular system. In: Hamilton WJ, Mossman HW (eds). *Human Embryology*, 4th ed. Williams Wilkins, Philadelphia, pp 271-290.

KENDI TK, ERAKAR A, OKTAY O, YILDIZ HY, SAGLIK Y (2004) Accessory soleus muscle. *J Am Podiatr Med Assoc,* 94: 587-589.

LORENTZON R, WIRELL S (1987) Anatomic variations of the accessory soleus muscle. *Acta Radiol*, 28: 627-629.

MAYER WP, BAPTISTA JDS, AZEREDO RA, MUSSO F (2013) Accessory soleus muscle: a case report and clinical applicability. *Autops Case Rep*, 3(3): 5-9.

MIHOVIL P, IGOR K, DAMJAN D, MARIO J, IVAN B (2020) Accessory soleus muscle: Two case reports with a completely different presentation caused by the same entity. *Case reports in Orthopaedics*, Article ID 8851920. 1-7. https://doi.org/10.1155/2020/8851920

NAYAK SB, SHETTY SD (2019) Two accessory muscles of leg: potential source of entrapment of posterior tibial vessels. *Surg Radiol Anat,* 41(1): 97-99.

OLEWNIK L, ZIELINSKA N, PAULSEN F, PODGORSKI M, HALADAJ R, KARAUDA P, POLGUJ M (2020) A proposal for a new classification of soleus muscle morphology. *Ann Anat,* 232: 151584.

O'RAHILLY R, BOSSY J, MÜLLER F (1981) Introduction to the study of embryonic stages in man. *Bull Assoc Anat (Nancy)*, 65(189): 141-236.

PAUL AS, ALI MN, ROBERT RB, ROSY J, OTTO C, LAWRENCE MW (2008) Accessory muscles: anatomy, symptoms and radiological evaluation. *RadioGraphics*, 28(2): 481-499.

PLA ME, DILLINGHAM TR, SPELLMAN NT, COLON E, JABBARI B (1996) Painful legs and moving toes associates with tarsal tunnel syndrome and accessory soleus muscle. *Mov Disord,* 11(1): 82-86.

RANDELL M, MARSLAND D, JENKINS O, FORSTER B (2019) Minimally invasive tendon release for symptomatic accessory soleus muscle in an athlete: a case report. *J Foot Ankle Surg*, 58(4): 644-646.

SEKIYA S, KUMAKI K, YAMADA TK, HORIGUCHI M (1994) Nerve supply to the accessory soleus muscle. *Acta Anat (Basel),* 149(2): 121-127.

STANDRING S (2008) *Gray's Anatomy. The Anatomical Basis of Clinical Practice*. 40th ed. Churchill-Livingstone, London, pp 1420-1424.

YILDIRIM FB, SARIKCIOGLU L, NAKAJIMA K (2011) The co-existence of the gastrocnemius tertius and accessory soleus muscles. *J Korean Med Sci*, 26(10): 1378-1381.

YU JS, RESNICK D (1994) MR imaging of the accessory soleus muscle appearance in six patients and a review of the literature. *Skeletal Radiol*, 23: 525-528.

Poland syndrome

Zehra Seznur Kasar[1], Ersen Ertekin[2]

[1] *Adnan Menderes University, Faculty of Medicine, Department of Anatomy, Aydın, Türkiye*
[2] *Adnan Menderes University, Faculty of Medicine, Department of Radiology, Aydın, Türkiye*

SUMMARY

Poland syndrome is a congenital anomaly with unilateral agenesis or hypoplasia of the pectoral muscles, deformity of the anterior chest wall and upper extremity anomalies. In patients with Poland syndrome, varying rates of breast asymmetry, from hypomastia to amastia, accompany. It is observed that the incidence of dextrocardia is increased in patients with left-sided Poland syndrome. Vital lung capacity may be reduced due to anterior chest wall deformity. This syndrome is thought to be due to a temporary impairment of circulation in the arteria subclavia or any of its branches or hypoplasia of these vessels during the development of the upper extremities in the intrauterine period. We aimed to emphasize the characteristics of Poland syndrome in a 26-year-old female case. On physical examination, pectus excavatum deformity was observed besides the absence of left pectoralis major and minor muscles with plica axillaris anterior. In terms of congenital or acquired pathologies that may accompany, the cases should be evaluated clinically in detail and followed up.

Key words: Poland syndrome – Pectus excavatum – Dextrocardia – Computed tomography – Poland sequence

INTRODUCTION

Poland syndrome is an anomaly characterized by hypoplasia or agenesis of the anterior chest wall muscles. It can be observed sporadically or congenitally. The most commonly affected muscle is the sternocostal part of the major pectoral muscle, followed by the minor pectoral muscle (Ergüven et al., 2011). In Poland syndrome, the agenesis of pectorals muscles may be accompanied by hypoplasia of the nipple, breast and subcutaneous adipose tissue, aplasia of costal cartilages or ribs (II-IV or III-V), alopecia of axilla and chest region, and ipsilateral upper extremity deformities (Ergüven et al., 2011; Fokin and Robicsek, 2002).

This syndrome was first described in 1841, when Sir Alfred Poland was a student at Guy's Hospital in London. He performed an autopsy on the cadaver of a 27-year-old prisoner named George Elt, and reported the case with left-sided complete absence of the major and minor pectoral muscles, as well as ipsilateral partial absence of the serratus anterior muscle and symbrachydactyly (Poland, 1841). In 1962, Patrick Clarkson, a hand surgeon, operated on a type of patient with similar features to those in Alfred Poland's case, and made the definition of "Poland syndactyly" in refrence to to that case (Clarkson, 1962). This syndrome affects men more often than women, and occurs usually on the right side (Yiğit et al.,

Corresponding author:
Zehra Seznur Kasar, PhD Student. Department of Anatomy, Aydın Adnan Menderes University, Faculty of Medicine, 09010 Aydın, Türkiye. Phone: +90 533 6130381. E-mail: zehra.kasar@adu.edu.tr Orcid number: 0000-0001-9226-0659

Submitted: June 1, 2021. **Accepted:** February 19, 2022

https://doi.org/10.52083/PKVU6349

2015). Poland's syndrome is mostly unilateral, but a few bilateral cases have been reported (Fokin and Robicsek, 2002; Yiğit et al., 2016).

Although the etiology is not known precisely, genetic factors, vascular causes, viral infections and teratogenic agents are thought to be effective (Yiğit et al., 2016). One of the generally accepted theories in its etiopathogenesis is insufficient blood flow in the intrauterine period (6-8 weeks). It is thought to be due to a temporary impairment of circulation in the arteria subclavia, or any of its branches or hypoplasia of these vessels during the developmentof the upper extremities. The degree of deterioration of arterial circulation determines the severity of this syndrome (Lasko et al., 2008). This syndrome may accompany Sprengel deformity, Klippel-Feil syndrome and Möbius syndrome (Van der Feen et al., 2006). In addition, case reports have been reported in the literature in which it is seen with various cardiac anomalies and organ malignancies (Ergüven et al., 2011). However, cases involving all the abnormalities associated with this syndrome are extremely rare.

CASE REPORT

A 26-year-old female patient was admitted to the clinic of chest diseases with complaint of shortness of breath. On physical examination, pectus excavatum deformity, agenesia of the left pectoral minor muscle, hypoplasia of the

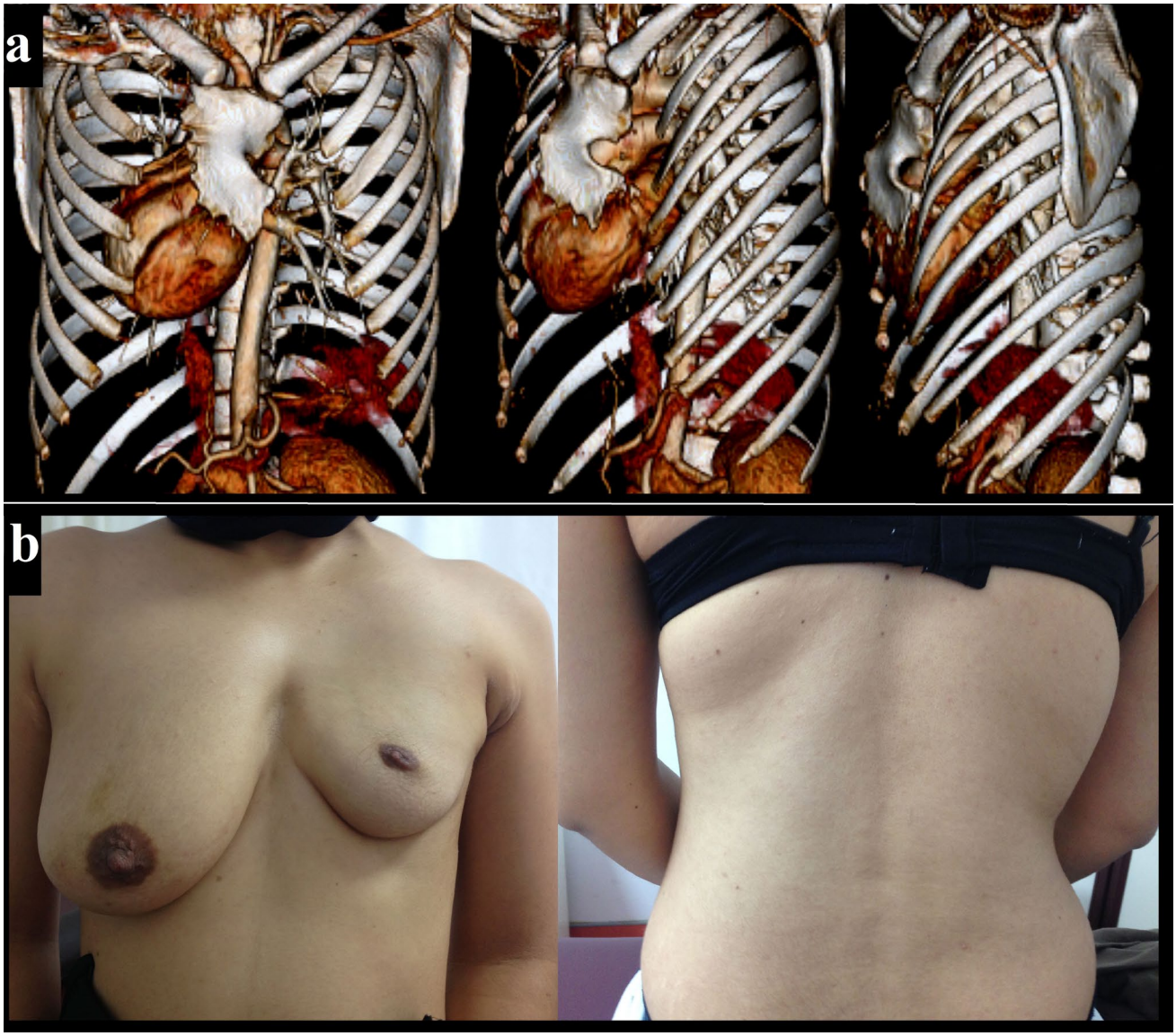

Fig. 1.- a) 3D-volume-rendered computed tomography images demonstrating pectus excavatum deformity and dextrocardia due to malformation of the sternum and costal cartilage on the left chest wall. **b)** Photos of the case show hypoplasia of the left breast and absence of the plica axillaris anterior, due to hypoplasia of pectoralis major muscle and hypoplasia of subcutaneous adipose tissue. The papillae mammaria and areola mammae are hypoplastic and superiorly sited.

pectoralis major muscle and breast asymmetry were observed (Fig. 1a). Furthermore, plica axillaris anterior was absent, but plica axillaris posterior was complete (Fig. 1b). In the left breast, glandular tissue, papillae mammaria, areola mammae, and subcutaneous adipose tissue were hypoplasic (Fig. 1b). Left axilla alopecia and axilla sweating disorder accompanied in the case. The patient's respiratory sounds were normal, and there were no additional pulmonary symptoms. There was no history of illness in his medical history. There were no any additional deformities in the left upper extremity, and the patient had full range of motion and muscle strength. The patient's liver and kidney function tests and complete hemogram tests were normal. Spirometric measurement results were borderline in terms of mild restrictive pathology [predicted VC max: 3.95 VC max: 3.08 L (%78), predicted FVC:3.90 FVC: 3.08 L (%79), predicted FEV1 %M: 84.35 FEV1 %M: 86.17 L].

Intravenous contrast-enhanced thorax CT was performed on 160-slice computed tomography (CT) device. Multiplanar reformed images (axial, sagittal and coronal planes) with a slice thickness of 3 mm were obtained from volumetric data (0.5 mm in the axial plane). CT images indicated that the pectoralis minor muscle is agenesic, and that the pectoralis major muscle is hypoplasic (Fig. 2). However, the costae, intercostales, serratus anterior, latissimus dorsi, external oblique and shoulder muscles were normal. CT confirmed that the left ribs were deformed and the volume in the left hemithorax was reduced. The patient had dextrocardia, because left hemithorax volume was reduced, but the heart structure was normal. The trachea was in the midline. The calibration and lumen of the main vascular

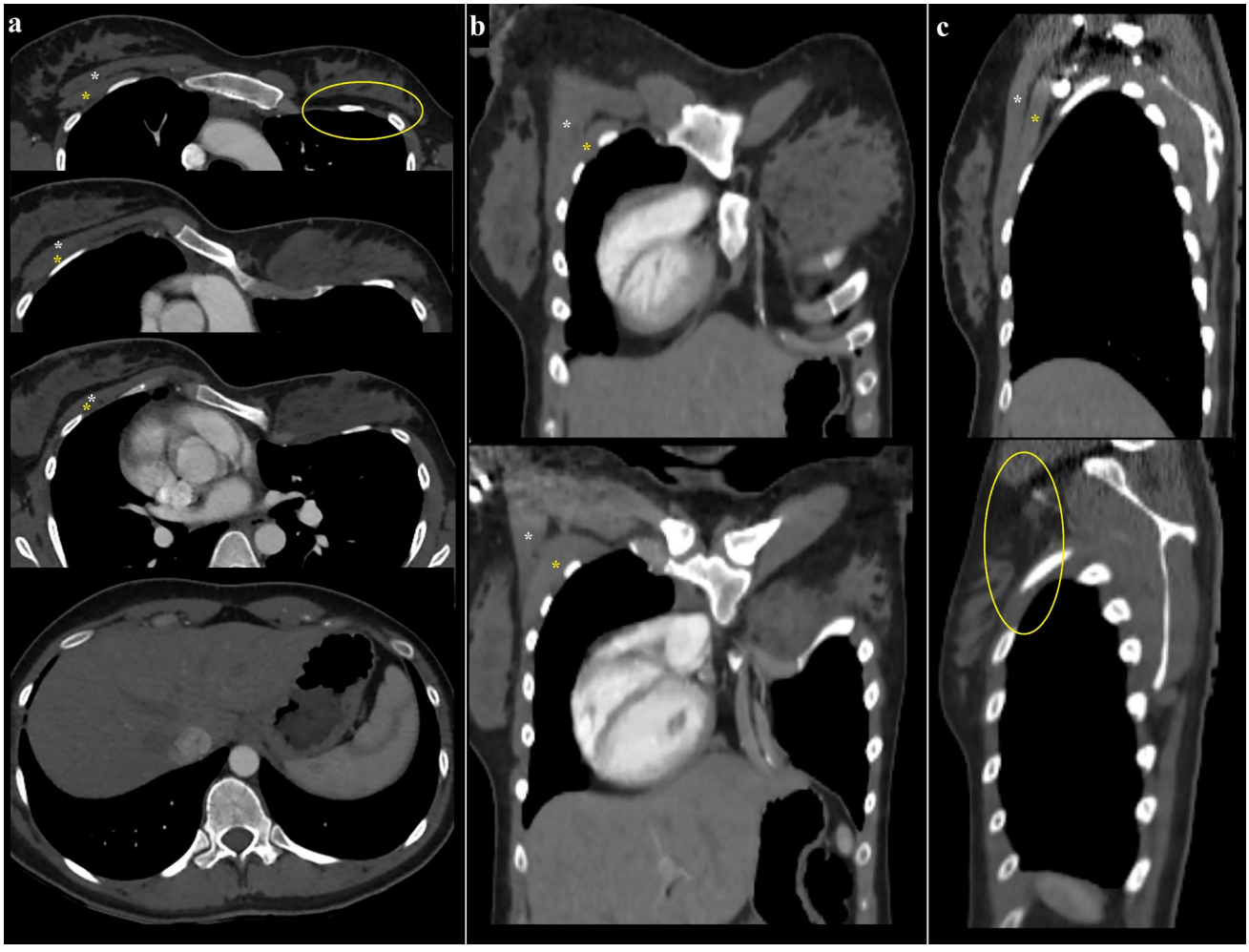

Fig. 2.- Chest computed tomography images obtained in axial (**a**), coronal (**b**) and sagittal (**c**) planes; It is noteworthy that the pectoral muscles are seen normally on the right side (white asterisk: pectoralis major; yellow asterisk: pectoralis minor) but the pectoralis major muscle is hypoplasic and the pectoralis minor muscle is agenesic on the left side. In addition, due to malformation in the sternum and left rib cartilages, pectus excavatum deformity and secondarily dextrocardia are observed.

structures in the mediastinum were normal. Both lung parenchymas were normal and the bronchovascular distribution was symmetrical and natural.

COMMENTS

Poland syndrome is a congenital or sporadic anomaly with agenesis or hypoplasia of major and minor pectoral muscles, hypoplasia of breast or nipple and of subcutaneous tissue, chest wall deformity, pectoral alopecia, and hand anomalies (Bıçakçı, 2010; Yiğit et al., 2015). The case had the agenesia of the left pectoral minor muscle and hypoplasia of the left pectoral major muscle, left breast, glandular tissue, papillae mammaria, areola mammae, and subcutaneous adipose tissue similar to the literature. Poland syndrome is a rare congenital anomaly. Its prevalence ranges from 1/7.000 to 1/100.000 live births. This syndrome is more common in men than in women, and the right side, more than the left side, is affected in males. However, left- and right-side is affected almost equal in females (Fokin and Robicsek, 2002). Our case was a woman with no family history of heredity, with left-sided involvement. Left axilla alopecia and axilla sweating disorder accompanied in the case. In Poland syndrome, ipsilateral syndactyly defects such as hypo / aplasia in the 3rd and 4th fingers of the upper extremity can be seen. Furthermore, serratus anterior, latissimus dorsi, and other shoulder muscles can be added to the agenesics of pectoral muscles (Torre et al., 2010). However, in our case, there was no other muscle affected except the pectoral muscles, and there was no deformity in the ipsilateral (left) upper extremity. Additionally, intercostales, serratus anterior, latissimus dorsi and shoulder muscles were complete.

In addition, it was noticeable that the heart and mediastinum were located in the right hemithorax in our case. Secondary dextrocardia cases associated with Poland syndrome have been reported in the literature, and this condition is called the 'Poland sequence' (Fraser et al., 1997). Torre et al. (2010) determined dextrocardia anomaly in 20 (14%) of 122 patients with Poland syndrome. This situation is explained as the heart displacement to the right side due to the narrowing of the left thoracic cavity during the intrauterine period. Due to the narrowing of the chest cavity, restrictive pulmonary symptoms can be observed and detected by spirometric measurements. In our case, spirometric measurements were borderline in terms of mildly restrictive pulmonary pathology (Deniz et al., 2005).

There are also publications reporting malignancy in patients with Poland syndrome in theliterature. In some cases, especially carcinomas in the hypoplasic breast, gastric carcinoma, lung tumors and intracranial solid tumors have been reported (Elli et al., 2009; Kurt et al., 2006; Ahn et al., 2000; Ji et al., 2008). However, there is no evidence that there is a genetic predisposition for cancer formation. For all that, cases of Poland syndrome should be followed up in terms of possible malignancy risk. We did not find any malignancy findings in our 26-year-old case.

CONCLUSION

Poland syndrome is a congenital or sporadic syndrome characterized by the absence of pectoral muscles. In terms of congenital or acquired pathologies that may accompany, the cases should be evaluated clinically in detail and followed up. Written informed consent was obtained from the patient for publication of this case report and accompanying images.

REFERENCES

AHN MI, PARK SH, PARK YH (2000) Poland's syndrome with lung cancer. A case report. *Acta Radiol,* 41(5): 432-434.

BIÇAKÇI Z (2010) Hafif Form Bir Poland Sendromu Olgusu. *ADÜ Tıp FakültesiDergisi,* 11: 39-42.

CLARKSON P (1962) Poland's syndactyly. *Guys Hosp Rep,* 111: 335-346.

DENİZ O, TOZKOPARAN E, GUMUŞ S, YILDIZ Y, SAVCI S, BILGIÇ H, EKIZ K, DEMIRCI N (2005) Poland Sendromu Olgu Sunumu. *Tüberk Toraks Dergisi,* 53: 275-279.

ELLI M, OĞUR G, DAĞDEMIR A, PINARLI G, CEYHAN M, DAĞÇINAR A (2009) Poland syndrome with intracranial germ cell tumor in a child. *Pediatr Hematol Oncol*, 26: 150-156.

ERGUVEN M, MALÇOK M, ÇELENK N (2011) Poland sendromu. *Göztepe Tıp Dergisi,* 26: 133-136.

FOKIN AA, ROBICSEK F (2002) Poland's syndrome revisited. *Ann Thorac Surg,* 74: 2218-2225.

FRASER FC, TEEBI AS, WALSH S, PINKY L (1997) Poland sequence with dextrocardia: Which comes first? *Am J Med Genet,* 73: 194-196.

JI J, ZHANG S, SHAO C, XU M, CHEN S, LU C, WANG Z, ZHAO Z, FAN X, TU J (2008) Poland's syndrome complicated with breast cancer:

mammographic, ultrasonographic, and computed tomographic findings. *Acta Radiol,* 49(4): 387-390.

KURT Y, DEMİRBAS S, ULUUTKU AH, AKIN ML, CELENK T (2006) Poland's syndrome and gastric cancer: report of a case. *Eur J Cancer Prev,* 15: 480-482.

LASKO D, THOMPSON WR, BUCKNER DM, SOLA JE (2008) Titanium mesh prosthesis repair of symptomatic Poland syndrome in a premature infant. *J Pediatr Surg,* 43: 234-237.

POLAND A (1841) Deficiency of the pectoral muscles. *Guys Hosp Rep*, 6: 191-193.

TORRE M, BABAN A, BULUGGIU A, COSTANZO S, BRICCO L, LERONE M, BIANCA S, GATTI GL, SÉNÈS FM, VALLE M, CALEVO MG (2010) Dextrocardia in patients with Poland syndrome: phenotypic characterization provides insight into the pathogenesis. *J Thorac Cardiovasc Surg,* 139(5): 1177-1182.

VAN DER FEEN C, VAN OORT AM, PELLEBOER RA (2006) A neonate with the heart in the right hemithorax. *Ned Tijdschr Geneeskd,* 150: 2681-2685.

YIĞIT N, IŞITMANGIL T, OKSUZ S (2015) Clinical analysis of 113 patients with Poland syndrome. *Ann Thorac Surg,* 99(3): 999-1004.

YIĞIT N, CANDAŞ FH, YILDIZHAN A, GORUR R, IŞITMANGIL T (2016) Bilateral Poland's syndrome. *J Clin Anal Med,* 7(3): 393-395.

Palmaris profundus and carpal tunnel syndrome: is it really a palmaris muscle?

Alejandro Ortiz[1], Eduvigis Aranda[1], José R. Sanudo[2], Paloma Aragonés[1,2]

[1] Hospital Universitario Santa Cristina, Madrid, Spain

[2] Department of Human Anatomy and Embryology, Universidad Complutense, Madrid, Spain

SUMMARY

The palmaris profundus (PP) is a variable muscle present in the flexor muscle region of the forearms. Its implication in the etiopathogenesis of carpal tunnel syndrome has been discussed in the literature.

We present a case of a PP with a characteristic morphology, associated with a bifid median nerve (MN), found during surgery for a recurrence of carpal tunnel syndrome in a 51-year-old female patient.

The PP muscle was first described with this morphology by Frohse in 1908. Initially, this muscle was considered an anatomical variation of the palmaris longus, but since 1984 the existence of both muscles has been observed in the same forearm, so the PP is considered an accessory muscle.

Some authors associate the existence of a PP with compression of the median nerve in the carpal tunnel. Others, however, argue that it may be an aggravating factor but not the primary cause, or simply a casual finding during surgery. We believe that this tendon is not the primary cause of compression of the MN, but it can aggravate the situation in case of a reduced canal due to any other cause, so we recommend surgeons to resect it if it is found.

Furthermore, based on the embryological origin of the forearm muscles, we believe that this PP could actually be the radio-carpal, radio-palmar or short radial forearm muscle described as early as the 19th century.

Key words: Palmaris profundus – Median nerve – Carpal tunel – Palmaris longus – Radio-carpian muscle

INTRODUCTION

The palmaris profundus (PP) is a variable muscle present in the flexor muscle region of the forearms. It has been reported as originating from the lateral aspect of the middle third of the radius, deep to the pronator teres muscle and lateral to the flexor digitorum superficialis muscle. The distal tendon of this muscle passes through the carpal tunnel, deep to the flexor retinaculum and lateral to the median nerve (MN), and reaches the palm of the hand to insert into the deep aspect of the palmar aponeurosis (Tountas and Bergman, 1993).

This muscle was first described with this morphology by Frohse and Frankel (1908). It has subsequently been cited in the literature as a casual finding in cadaveric hands (Razik et al., 2012; Reimann et al., 1944), and in hands undergoing carpal tunnel surgery (Afshar, 2009;

Corresponding author:
Paloma Aragonés, MD, PhD. Department of Orthopedics, Hospital Universitario Santa Cristina, C/Amadeo Vives, s/n. 28009 Madrid, Spain. Phone: +34625081082. E-mail: palo_82@hotmail.com - Orcid no.: 0000-0002-4067-3950

Submitted: January 31, 2022. **Accepted:** February 25, 2022

https://doi.org/10.52083/KYEN4006

Afshar, 2014; Brones and Wilgis, 1978; Browne et al., 2015; Carstam, 1984; Chou et al., 2001; Dyreby and Engber, 1982; Fatah, 1984; Floyd et al., 1990; Gwynne-Jones, 2006; Kostoris et al., 2019; Mc Clelland and Means, 2012; Pezas and Jose, 2021; Pirola et al., 2021; Razik et al., 2012; Sahinoglu et al., 1994; Server et al., 1995; Van Denmar et al., 2018).

This variable muscle has been associated with compressive neuropathy of the anterior interosseous nerve and the MN, in the distal forearm and the wrist (Brones and Wilgis, 1978; Dyreby and Engber, 1982; Fatah, 1984; Kostoris et al., 2019; Spinner, 1978).

We describe a case of a PP with a characteristic morphology, associated with a bifid MN. We will also discuss the clinical relevance of this finding and its association with the compressive pathology of the MN at the carpal tunnel.

CASE REPORT

We present the case of an aberrant muscle found during a left-hand carpal tunnel recurrence surgery in a woman of 51 years old. The muscle found partially coincides with the description of the PP found in the literature.

The patient had undergone open carpal tunnel release surgery in another hospital, with favorable evolution. Four years after the intervention, the symptoms reappeared and the electromyographic study showed a severe subacute entrapment of the MN at the carpal tunnel level, so we proposed a new surgical intervention.

During surgery, an incision was made over the previous scar, with proximal and distal extension until healthy non-scar tissue was visualized. Longitudinal section of the transverse ligament of the carpus was performed, which was fibrosed, and when exposing the carpal canal, a bifid MN was visualized (Fig. 1) and a tendinous structure that ran longitudinally through the space between both median nerves was identified (Fig. 2). This tendon had a length of 5 cm and ended up inserting into the deep aspect of the palmar aponeurosis, distal to the flexor retinaculum.

Proximally, this tendon continued with an elongated muscle belly, located lateral to the MN, which originated from fascia of the distal third of the flexor digitorum superficialis belly.

The tendon of this muscle was removed. Microsurgical neurolysis and a fatty flap was performed to cover the MN. At the 4-week review the symptoms had disappeared.

COMMENTS

We present an unusual case of a palmaris profundus muscle with the distal portion of its belly located into the carpal tunnel, coexisting with a bifid median nerve, in a patient with compressive carpal tunnel symptomatology despite having already undergone surgery for this cause.

The PP is a variable muscle first described in 1908 (Fröhse and Fränkel, 1908). Years later Reimann found it in 2 forearms belonging to the same subject in a very huge sample of 1600 human cadavers, which would represent an incidence of 0.13% (Reimann et al., 1944).

Subsequently, the PP muscle has been described in the literature on several occasions, almost always as isolated cases or series of 2 cases (Table 1). On some subjects, this muscle has been found bilaterally (Fatah, 1984; Floyd et al., 1990; Razik et al., 2012; Reimann et al., 1944).

Initially, this muscle was considered an anatomical variation of the palmaris longus (Brones and Wilgis, 1978; Carstam, 1984; Fröhse and Fränkel, 1908; Reimann et al., 1944), being described in forearms where the palmaris longus muscle was always absent.

But since 1984 the existence of both muscles has been observed in the same forearm, so the PP is considered an accessory muscle and no longer an anatomical variation of the palmaris longus muscle (Afshar, 2009; Afshar, 2014; Browne et al., 2015; Dyreby and Engber, 1982; Fatah, 1984; Floyd et al., 1990; Gwynne-Jones, 2006; Pirola et al., 1009; Sahinoglu et al., 1994; Server et al., 1995). The PP has been described only in adults, not appearing in fetal studies on the variability of the palmaris longus muscle (Olewnik, 2018), although this is probably due to its very low incidence.

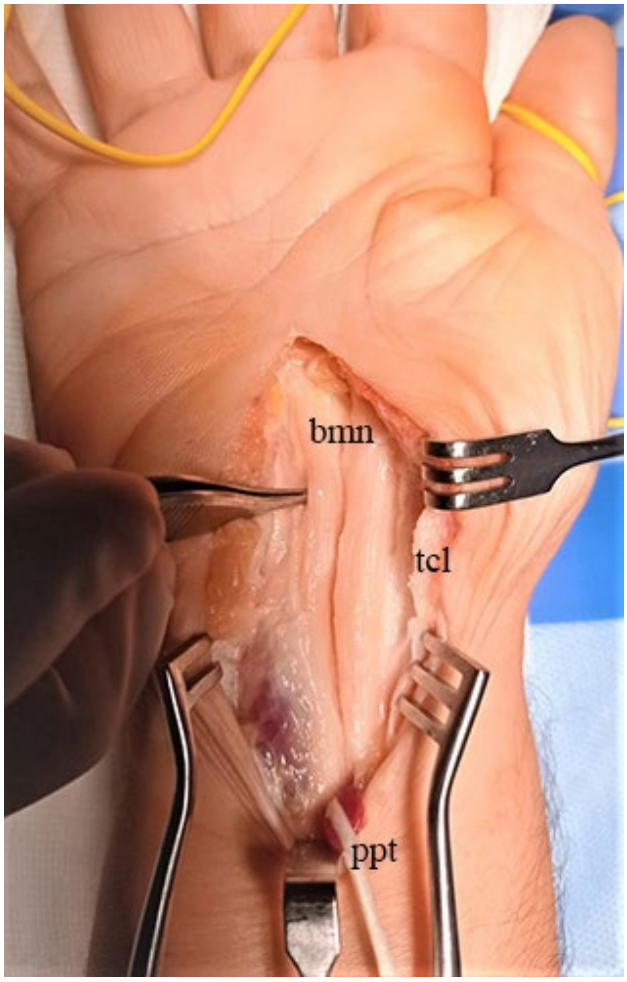

Fig. 1.- Intraoperative photograph of the patient's right hand showing a bifid median nerve (bmn) after the transverse carpal ligament (tcl) has been transected. The tendon of the palmaris profundus (pp) muscle has been disinserted and retracted proximally.

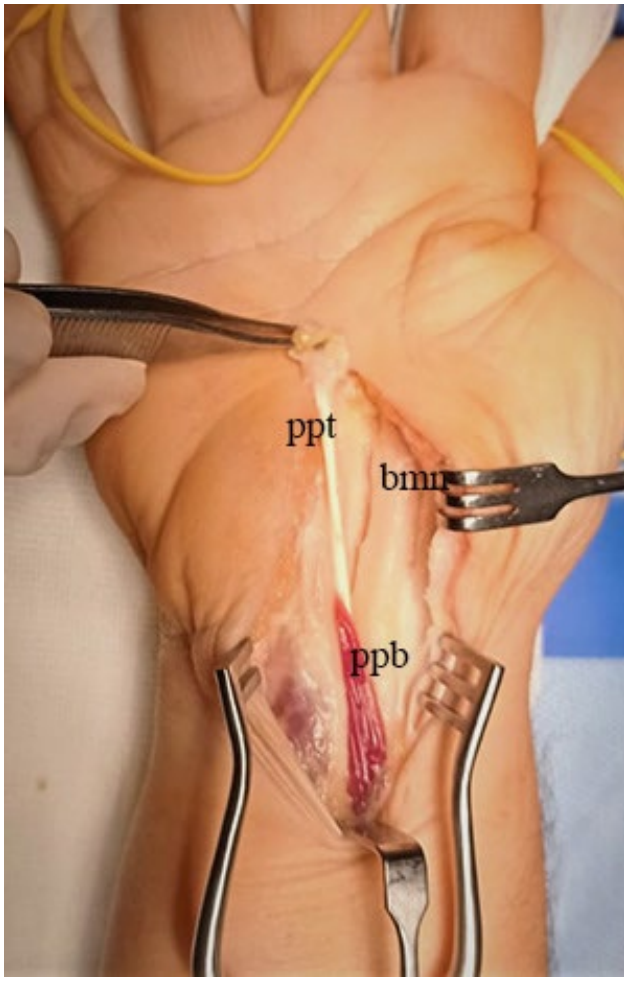

Fig. 2.- Intraoperative photograph of the patient's right hand showing a bifid median nerve (bmn) and palmaris profundus muscle in which the tendon (ppt) runs through the space between both median nerves, and the muscle belly (ppb) reaches the inside of the carpal tunnel.

The muscle has been described in cadaver forearms and in patients in whom open carpal tunnel surgery has been performed (Table 1). Only once has it been described during endoscopic carpal tunnel surgery, which had to be reconverted to open surgery, because the instruments could not be advanced through the endoscopic portal (Mc Clelland and Means, 2012). The instruments probably collided with the PP muscle, making it impossible to continue with endoscopic surgery, which therefore does not seem to be an adequate technique for treating cases with anatomical variables of any type that increase the content of the carpal tunnel.

It has been seen that this muscle also presents certain variability in its attachments, course and morphology. The proximal attachments described are: middle third of the radius, fascia of the flexor digitorum superficialis, ulna (Pirola et al., 2009), epimysium of the flexor pollicis longus (Chou et al., 2001), palmaris longus muscle (Sánchez-Lorenzo et al., 1996) and common flexor origin (Sahinoglu et al., 1994). In our case, it originated from fascia of the distal third of the flexor digitorum superficialis belly.

The belly of this anomalous muscle is located proximally and its long tendon distally, presenting variable lengths according to the cases described, although there are only 2 cases reporting the approximate length of this tendon: 10 and 15 cm (Carstam, 1984). In our case the tendon was much shorter, 5cm, with the beginning of the muscle belly inside the carpal tunnel.

Within the carpal tunnel, the tendon of the PP may appear radial (Carstam, 1984; Chou et al., 2001; Fatah, 1984; Floyd et al., 1990; Pirola et al., 2009; Reimann et al., 1944), or ulnar to the

Table 1. Cases of the palmaris profundus muscle reported in the literature. Distribution by authors, date of publication, type and size of the sample, origin and insertion, presence or absence of the palmaris longus muscle, bilaterality and concomitant findings.

AUTHOR	YEAR	SAMPLE	N	ORIGIN	INSERTION	PALMARIS LONGUS	BILATERAL	OTHERS
Fröhse	1908	Cadaveric	1	Mid third radius	Palmar aponeurosis	Absent	No	-
Reimann	1944	Cadaveric	2/1600	Mid third radius	Deep surface palmar aponeurosis	Absent	Yes	-
Brones	1978	Patients	2	-	Palmar aponeurosis	Absent	No	-
Dyreby	1982	Patient	1	-	Palmar aponeurosis	Present	No	-
Carstam	1984	Patient	2	-	Deep surface palmar aponeurosis	Absent	No	-
Fatah	1984	Patient	2	Mid third radius	Distal border of flexor retinaculum	1 absent / 1 present	Yes	-
Floyd	1990	Patient	2	-	Deep surface palmar fascia	Present	Yes	-
Stark	1992	Patient	1	-	Palmar fascia	-	No	-
Sahinoglu	1994	Patient	2	Common muscle flexor tendon	Deep surface palmar fascia / Common muscle flexor tendon	Present	No	Median artery 1 case, Bitendinous palmaris profundus
Server	1995	Patient	1	-	Palmar aponeurosis	Present	No	-
Sánchez-L	1996	Patient	1	Dorsal epimysium of palmaris longus muscle belly	Deep surface palmar aponeurosis	Present	No	Bitendinous palmaris profundus
Chou	2001	Patient	1	Epimysium of pollicis longus	Deep surface of both the flexor retinaculum and the palmar aponeurosis	-	No	Division of the median nerve by the muscle belly
Gwynne	2006	Patient	1	-	Deep surface palmar aponeurosis	Present	No	Bifid median nerve
Afshar	2009	Patient	1	-	Deep surface palmar aponeurosis	Present	No	-
Pirola	2009	Patient	2	Flexor digitorum superficialis muscle in the distal forearm	Deep surface palmar aponeurosis	Present	No	Bifid median nerve 1 case
Mc Clelland	2012	Patient	1	-	Deep surface of transverse carpal ligament	-	No	Bifid median nerve + median artery
Razik	2012	Patient	2	-	-	-	Yes	-
Afshar	2014	Patient	1	Radius	Deep surface superficial palmar fascia	Absent	No	-
Browne	2015	Patient	1	-	Palmar aponeurosis	-	No	-
Van Denmark	2018	Patient	1	-	Palmar fascia	-	No	-
Kostoris	2019	Patient	1	-	-	-	No	Bifid median nerve
Pezas	2021	Patient	1	-	Deep surface superficial palmar fascia	-	No	-
Our case	2021	Patient	1	Flexor digitorum superficialis muscle in the distal forearm	Deep surface palmar aponeurosis	Present	No	Bifid median nerve Belly inside carpal tunnel

MN (Fatah, 1984; Sánchez-Lorenzo et al., 1996; Spinner, 1978), or also lie above the nerve itself (Afshar, 2009; Afshar, 2014; Browne et al., 2015; Dyreby and Engber, 1982; Gwynne-Jones, 2006; Razik et al., 2012; Stark, 1992). In one case, the tendon crossed over the MN from radial to ulnar within the carpal tunnel (Server et al., 1995).

In our case, the tendon of this variant muscle ran through the space between the two branches of a bifid MN, a finding also described previously (Afshar, 2014; Gwynne-Jones, 2006; Kostoris et al., 2019; Pirola et al., 2009). Mc Clelland in 2012 further found, associated with these 2 variations, a persistent median artery (Mc Clelland and Means, 2012).

The presence of a bifid MN in the carpal tunnel is caused by a high division of this nerve in the forearm, classified as group 3 within the anatomical variations of this nerve (Lanz, 1977), and described with an incidence of 2.6% (Henry et al., 2015).

Some authors associate the existence of PP with compression of the MN in the carpal tunnel, suggesting that this muscle should be resected to avoid the persistence of symptoms (Brones and Wilgis, 1978; Floyd et al., 1990; Server et al., 1995). Others however advocate that it may be an aggravating factor, but not the primary cause (Fatah, 1984; Pirola et al., 2009), or simply a casual finding during surgery (Sánchez-Lorenzo et al., 1996; Stark, 1992). We believe that this tendon is not the primary cause of compression of the MN. Otherwise, the pathology would appear in very young subjects, but it can aggravate the situation in case of a reduced canal due to any other cause, as in our case, such as; a bifid median nerve, scar tissue or a distal belly located within the tunnel that might produce compression of the bifid nerve during wrist flexion, so we recommend surgeons to resect it if it is found.

The anatomy of the carpal canal is highly variable, so surgeons should be aware of possible anatomic variations and be prepared to alter their surgical plan accordingly (Mc Clelland and Means, 2012).

The flexor muscles of the forearm appear in embryos of 11mm as a small superficial layer and a voluminous deep layer. In embryos of 16 mm., the deep layer splits off the flexor carpi ulnaris and the remainder of the deep flexor mass, a superficial flexor digitorum sublimis and a deeper flexor digitorum profundus. The superficial mass lies more on the radial aspect of the volar surface; later, this mass splits into the flexor carpi radialis and pronator teres, and the remaining portion of this superficial layer develops into the palmaris longus, which extends to the volar surface of the carpus (Lewis, 1910).

Therefore, based on this classical description about the development of the forearm muscles, we can suggest that the muscle reported as PP is not originated from the superficial mass of the forearm blastema, as the palmaris longus, but from the deep mass as the flexor sublimis. Therefore, it could be more appropriate look for another name that may not create such confusion of similar history with the palmaris longus. We believe that this PP muscle is actually the radio-carpian muscle described previously by Testut and Le Double, and that this denomination would be more correct, given its embryological origin (Le Double, 1986; Tèstut, 1884).

This radio-carpian muscle has also been called radio-carpal muscle, radio-palmar, radio-metacarpal, radio-carpo-metacarpal or posterior tibial of the forearm, given the great variability in its proximal and distal attachments. It is an accessory muscle of the anterior and inferior region of the forearm. Its proximal attachment is located on the anteroexternal aspect of the distal half of the radius, but proximal insertions have also been described in the epitrochlea, the pronator teres and the flexor digitorum muscles, the interosseous membrane and antebrachial aponeurosis. It is generally continued with a tendon that can pass deep or superficial to the transverse carpal ligament. The distal attachments described are the superficial or deep transverse carpal ligament, the palmar aponeurosis, the fascia of the thenar eminence, carpal bones such as scaphoid, capitate, trapezium and trapezoid, 2nd, 3rd or 4th metacarpal bones, flexor tendon sheath and anterior aspect of the radiocarpal joint (Le Double, 1986; Tèstut, 1884).

Le Double finds this muscle in 1/20 extremities. It can coexist or replace the palmaris longus (Le

Double, 1986; Tèstut, 1884). The first description of this muscle belongs to M. Fano (Bulletins de la Societè Anatomique de Paris, 1851).

Given the great variability of this accessory muscle, Le Double proposes to include all these possibilities as a unique accessory muscle named short anterior radial muscle. We purpose that the PP described by Fröhse and Reimann (Fröhse and Fränkel, 1908; Reimann et al., 1944), and the one found in our patient, could be included in this definition given their location, attachments and embryological origin.

AUTHOR'S CONTRIBUTION

AO and EA were involved in the development of the project, photo documentation and where the surgeons of the patient. PA performed the data collection, processed the photographs for publication and edited the manuscript. JRS performed the protocol development and collaborated with manuscript editing.

ETHICAL APPROVAL

The patient underwent surgery at the hand surgery unit of the Hospital Universitario Santa Cristina (Madrid), after signing the informed consent forms for surgery, anesthesia and hospitalization during the COVID19 pandemic. She also authorized verbally and in writing that photographs could be taken during the operation

Consent to participate

Informed consent was obtained from the participant included in the study.

Consent for publication

The authors affirm that human research participants provided informed consent for publication of the images in Figures 1 and 2.

REFERENCES

AFSHAR A (2009) Palmaris profundus as the cause of carpal tunnel syndrome. *Arch Iran Med,* 12: 415-416.

AFSHAR A (2014) Carpal tunnel syndrome due to palmaris profundus tendon. *J Hand Surg (Eur),* 39E(2): 207-217.

BRONES MF, WILGIS EFS (1978) Anatomical variations of the palmaris longus, causing carpal tunnel syndrome. *Plast Reconstr Surg,* 62: 798-800.

BROWNE KM, FAUZI Z, O'SHAUGHNESSY M (2015) The palmaris profundus, a rare sight during carpal tunnel release. *Hand,* 10: 559-561.

CARSTAM N (1984) A rare anomalous muscle, palmaris profundus, found when operating at the wrist for neurological symptoms. A report of two cases. *Bull Hosp Jt Dis Orthop Instit,* 44: 163-167.

CHOU HC, JENG H, KO TL, PAI MH, CHANG CY, WU CH (2001) Variant palmaris profundus enclosed by an unusual loop of the median nerve. *J Anat*, 199: 499-500.

DYREBY JR, ENGBER WD (1982) Palmaris profundus—rare anomalous muscle. *J Hand Surg*, 7: 513-514.

FATAH MF (1984) Palmaris profundus of Frohse and Frankel in association with carpal tunnel syndrome. *J Hand Surg*, 9B: 142-144.

FLOYD T, BURGER RS, SCIARIONI CA (1990) Bilateral palmaris profundus causing bilateral carpal tunnel syndrome. *J Hand Surg,* 15A: 364-366.

FRÖHSE F, FRÄNKEL M (1908) *Die Muskeln des menschlichen Arme*. Gustav Fischer, Jena, pp 115-118.

GWYNNE-JONES DP (2006) Bilateral palmaris profundus in association with bifid median nerve release as a cause of failed carpal tunnel release. *J Hand Surg,* 31A: 741-743.

HENRY BM, ZWINCZEWSKA H, ROY J, VIK J (2015) The prevalence of anatomical variations of the median nerve in the carpal tunnel: a systematic review and meta-analysis. *PLoS One*, 25; 10(8): e0136477.

KOSTORIS F, BASSINI S, LONGO E, MURENA L (2019) Carpal tunnel syndrome associated with bifid median nerve and palmaris profundus - case report and literature review. *J Hand Surg (Asian-Pacific Volume),* 24(2): 238-242.

LANZ U (1977) Anatomical variations of the median nerve in the carpal tunnel. *J Hand Surg Am*, 2(1): 44-53.

LE DOUBLE AF (1896) *Traité des variations du système musculaire de l´homme et de leur signification au point de vue de l´anthropologie zoologique, Muscles de l´avant-bras, vol 2*. Schleicher Fréres Editeurs, París, pp 141-148.

LEWIS WH (1910) The development of the muscular system. In: Keibel F, Mall FP (eds). *Manual of Human Embryology,* vol. 1. J.B. Lippincott Co., Philadelphia, pp 454-522.

MC CLELLAND WB, MEANS KR (2012) Palmaris profundus tendon prohibiting endoscopic carpal tunnel release: case report. *J Hand Surg Am,* 37A: 695-698.

OLEWNIK L, WASNIESKA A, POLGUJ M, PODGORSKI M, LABETOVITC P, RUZIK K, TOPOL M (2018) Morphological variability of the palmaris longus muscle in human fetuses. *Surg Radiol Anat*, 40(11): 1283-1291.

PEZAS TP, JOSE R (2021) Palmaris profundus in the carpal tunnel. *BMJ Case Rep,* 14: e241328.

PIROLA E, HEBERT-BLOUIN MN, AMADOR N, AMRAMI KK, SPINNER RJ (2009) Palmaris profundus: one name, several subtypes, and a shared potential for nerve compression. *Clin Anat,* 22(6): 643-648.

RAZIK A, AVISAR E, SORENE E (2012) Bilateral carpal tunnel syndrome with anomalous palmaris profundus tendons. *J Plastic Surg Hand Surg*, 46(6): 452-453.

REIMANN AF, DASELER EH, ANSON BJ, BEATON LE (1944) The palmaris longus muscle and tendon. A study of 1,600 extremities. *Anat Rec,* 89: 495-505.

SAHINOGLU K, CASSELL MD, MIYAUCHI R, BERGMAN RA (1994) Musculus comitans nervi mediani (M. palmaris profundus). *Ann Anat,* 176: 229-232.

SÁNCHEZ-LORENZO J, CAÑADA M, DÍAZ L, SARASÚA G (1996) Compression of the median nerve by an anomalous palmaris longus tendon: a case report. *J Hand Surg Am,* 21: 858-860.

SERVER F, MIRALLES RC, GALCERA DC (1995) Carpal tunnel syndrome caused by an anomalous palmaris profundus tendon. *J Anat,* 187: 247-248.

SPINNER M (1978) *Injuries to the major branches of peripheral nerves of the forearm, ed 2*. WB Saunders Co, Philadelphia, p 192.

STARK RH (1992) Letter to editor: Bilateral palmaris profundus causing bilateral carpal tunnel syndrome. *J Hand Surg Am,* 17A: 182-183.

TÈSTUT L (1884) *Les anomalies musculaires chez l'homme, expliquées par l'anatomie comparée: leur importance en anthropologie, vol* 3. G. Masson Editeur, Paris, pp 497-508.

TOUNTAS CP, BERGMAN RA (1993) *Anatomic variations of the upper extremity*. Churchill Livingstone, New York, pp 142.

VAN DEMARK RE, ANDERSON MC, LIST JT, HAYES M, WOODARD D (2018) Discovering an anatomic variant of the palmaris profundus during open carpal tunnel release. *Plast Reconstr Surg Glob Open,* 6(8): e1867.

A systematic review on normal and abnormal anatomy of coronary arteries

Mustafa A. Hegazy[1], Kamal S. Mansour[1], Ahmed M. Alzyat[1], Mohammad A. Mohammad[1], Abdelmonem A. Hegazy[2,3]

[1] Cardiology Department, Faculty of Medicine, Zagazig University, Zagazig City 44519, Egypt

[2] College of Biotechnology, Misr University for Science and Technology (MUST), 6th October City 12566, Egypt

[3] Anatomy and Embryology Department, Faculty of Medicine, Zagazig University, Zagazig City 44519, Egypt

SUMMARY

Coronary artery (CA) disorders are among the major causes of morbidity and mortality in humans. We attempt to explain CA anatomy and its variations in a simple, concise, and understandable way to help clinicians deal with the various disorders. There are two main arteries: right coronary artery (RCA) and left CA. The left bifurcates into two terminal branches: left anterior descending artery (LAD) and left circumflex artery (LCX). The commonest anatomical variant is trifurcation of left main coronary artery (LMCA) with presence of ramus intermedius artery (RIM), abnormal origin of LCX from RCA or right sinus of Valsalva, abnormal CA origin from unusual aortic sinus in-between aorta and pulmonary trunk, myocardial bridging, CA fistula and aneurysm. The RCA may arise abnormally from the left sinus of Valsalva rather than the usual origin from the right sinus. Furthermore, most cases of abnormal CA fistulas affect the RCA where the artery opens into the right heart chambers, pulmonary trunk, or coronary sinus. Although their incidence is relatively rare, coronary abnormalities are of critical importance in medical practice. Identification of normal and abnormal anatomy of CA is essential because not knowing one of the differences can lead to loss of a person's life.

Key words: Right coronary artery – Left coronary artery – Anterior interventricular artery – Left circumflex artery – Coronary variations

ABBREVIATIONS

CA: Coronary artery; CAD: Coronary artery disease; LAD: Left anterior descending artery; LCX: Left circumflex artery; LDL: Low-density lipoproteins; LMCA: Left main coronary artery; LV: Left ventricle; MB: Myocardial bridging; PDA: Posterior descending artery; RA: Right atrium; RCA: Right coronary artery; RIM: Ramus intermedius artery; RV: Right ventricle; SA: Sinoatrial.

INTRODUCTION

Coronary artery disease (CAD) is one of the leading causes of sudden death. This has been attributed to the resulting acute coronary syndrome, or fatal arrhythmia, due to subsequent fibrosis and/or scarring of the myocardium. While CAD is more common among the elderly, it has also been identified as a cause of sudden cardiac death in younger adults (Vahatalo et al., 2021).

Corresponding author:
Abdelmonem Hegazy. Prof. and Former Chairman of Anatomy and Embryology Department, Faculty of Medicine, Zagazig University, Zagazig 44519, Egypt. Phone: +201110504321. E-mail: ahegazy@zu.edu.eg; Orcid: 0000-0002-5993-6618.

Submitted: November 10, 2021. **Accepted:** February 25, 2022

https://doi.org/10.52083/FDTA2953

Determining the normal anatomy and its variations is essential for physicians and surgeons for the accurate diagnosis and proper management of any clinical disorder (Hegazy, 2019; Hegazy and Hegazy, 2021). Due to the significant increase in interventional procedures, awareness of the normal and abnormal anatomy of the coronary arteries has become a mandatory factor for cardiologists, radiologists, and other clinicians. This is because the incorrect interpretation or misdiagnosis of such variants or anomalies might lead to technical difficulties during coronary catheterization and interventional procedures or cause major complications at coronary surgery (Cademartiri et al., 2008). Good anatomical knowledge is also important to correctly interpret coronary computed tomography (CT) and angiography images (Kini et al., 2007). Moreover, defining the normal anatomical variation facilitates stent design and selection of optimal treatment strategy (Medrano-Gracia et al., 2016).

The CA anomalies should not be considered just rare findings as they might be associated with serious clinical consequences (Becker, 1995). In a study including 16,573 patients, CA anomalies were noticed in about 0.3% of cases (Yuksel et al., 2013). Despite the relatively uncommon prevalence, CA variants and anomalies represent the second most common cause of death among young athletes. They may go unnoticed and discovered incidentally through routine investigations or in postmortem analysis of cases of sudden death. However, some patients with CA abnormalities may present with angina pectoris, syncope, myocardial infarction, and heart failure (Kastellanos et al., 2018). Therefore, clinicians must be familiar with the normal anatomy of the coronary arteries as well as anatomical differences and abnormalities in order to accurately diagnose and manage coronary lesions.

NORMAL ANATOMY OF CORONARY ARTERIES

There are two CAs; each supplies the corresponding half of the heart although there is an overlap in blood supply particularly found in the interventricular septum (Iaizzo, 2015). The two coronary arteries arise at the root of the aorta from the two of the three aortic sinuses of Valsalva following the aortic semilunar valve. The right coronary artery (RCA) originates from the right "anteriorly located" sinus, while the left coronary artery arises from the left posterior sinus (Hegazy, 2018). Hence, there is a sinus with no CA origin, and called noncoronary sinus (Iaizzo, 2015) (Figs. 1-4). The distribution of arterial blood supply to the myocardium is variable. However, the RCA mostly supply the right ventricle (RV), while the left coronary artery supplies the anterior wall of the left ventricle (LV) and anterior part of interventricular septum. The supply of the remainder of LV depends on arterial dominance of coronaries (Kini et al., 2007). Kini et al. (2007) classified the coronary arteries into 4 arteries as follows: RCA and LMCA, and they added the two terminal branches of LMCA named the anterior interventricular artery "left anterior descending artery" (LAD) and the left circumflex artery (LCX) as another two main arteries. They described the arterial supply of the heart as a ring and half-loop; the circle is formed by RCA and LCX, while LAD and PDA (posterior descending artery) form the half-loop. However, we may add the LMCA to the ring to be formed of RCA, LMCA and LCX (Fig. 3).

1. Anatomy of RCA

Its origin from the right aortic sinus lies slightly below the level of the left coronary artery (Kini et al., 2007). It passes to the right side behind the pulmonary trunk between it and the right auricle to run in the coronary sulcus (anterior atrioventricular groove) till reaching the lower part of the right margin of the heart, where it curves posteriorly (Hegazy, 2018). At the crux of the heart, it bends to form the PDA, also called posterior interventricular artery (Iaizzo, 2015). The RCA ends by anastomosing with the continuation of LCX. The crux is the point at the posterior surface of the heart where the coronary sulcus meets the line of the interatrial and interventricular groove, forming a cross (O'Brien et al., 2007).

Near its beginning, it gives off two branches. The first is the conus artery in 50% of population passing anteriorly to supply the conus arteriosus "its pulmonary outflow". In the other part of the population, the CA arises as a separate branch

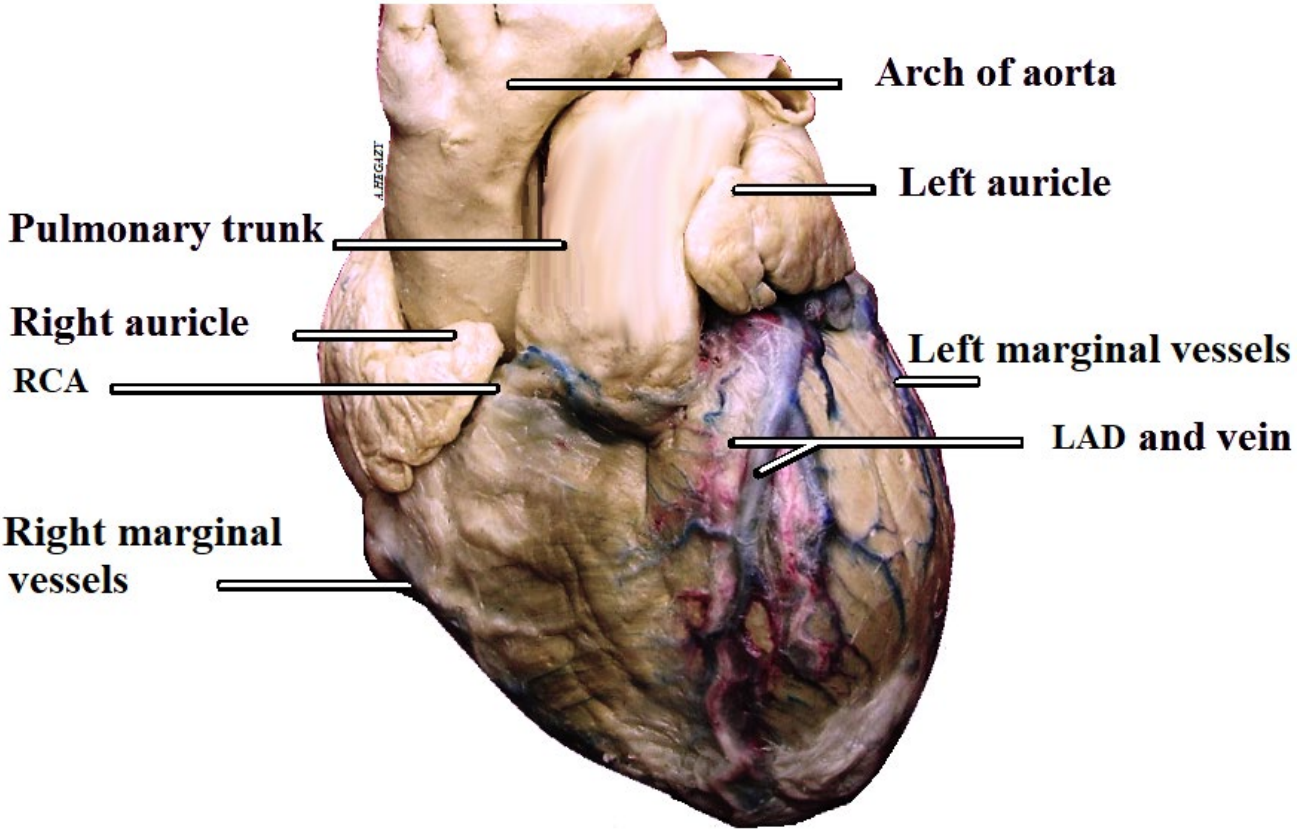

Fig. 1.- Photograph showing the sternocostal surface of heart and coronary vessels (from Hegazy, 2018).

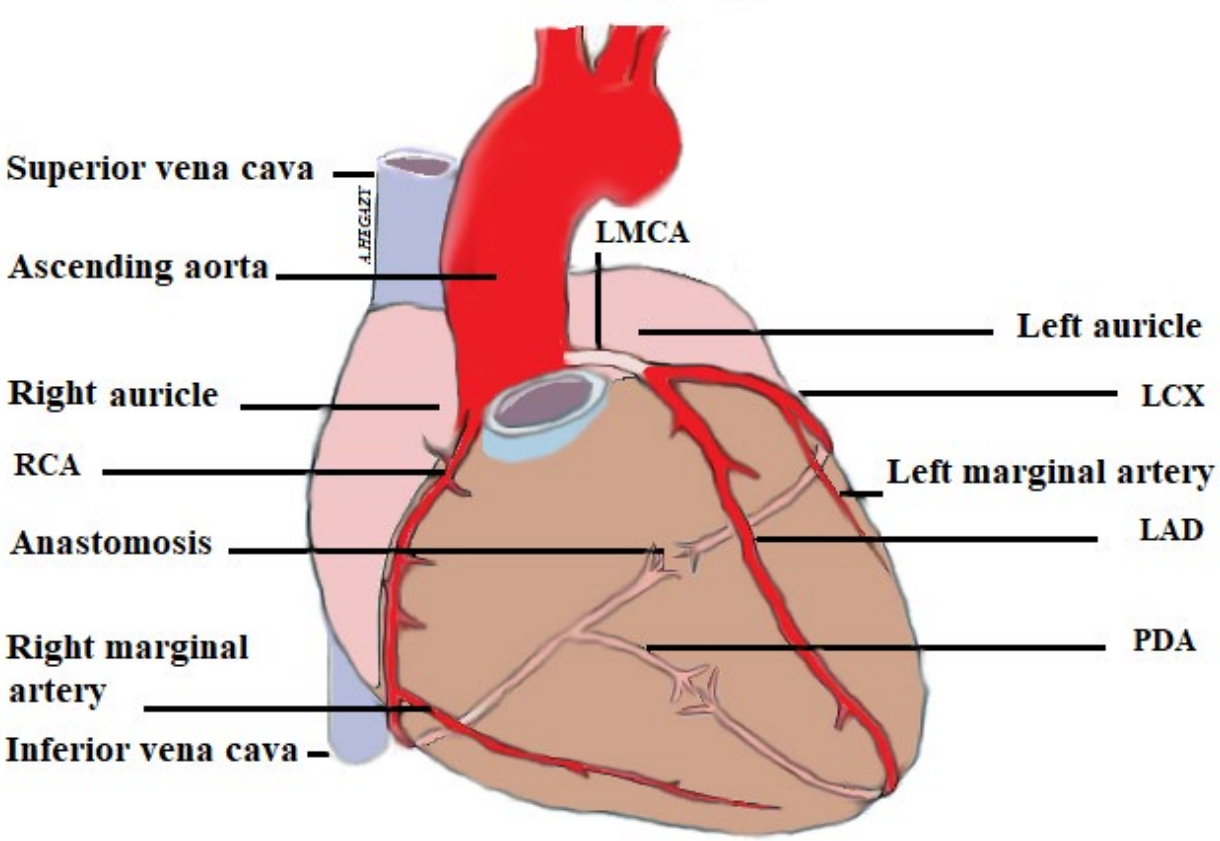

Fig. 2.- Diagram showing the arrangement of coronary arteries supplying heart.

from the aorta. The second branch is the sinoatrial (SA) nodal artery arising from RCA in 55% of cases to supply the right atrium (RA) at the inflow of the superior vena cava, and also gives SA nodal branch to SA node. In the remaining cases, this artery arises from the proximal part of left circumflex artery (Kini et al., 2007; Iaizzo, 2015). Other authors stated that conus branch arises mostly from RCA by an incidence of about 86% and from the aorta in only about 12% of cases (Cademartiri et al., 2008). They added that SA nodal originates from the RCA in about 65% and from left coronary artery in about 17%, It might arise from aorta or pulmonary trunk in rare cases (0.2%).

Before coursing to the diaphragmatic surface, the RCA gives off many small branches to supply the anterior aspect of the RA and RV; the most prominent of them is called RV marginalis or right marginal artery. Such branch supplies the part of RV coursing along it (Kini et al., 2007; Iaizzo, 2015).

At the posterior aspect of the heart, the RCA ends by giving 2 or 3 branches. The first branch is PDA passing towards the apex of the heart through the posterior interventricular sulcus. It supplies the posterior free part of RV, as well as the posterior one-third of interventricular septum in about 85% of cases (Fig. 5). The second one is the AV nodal

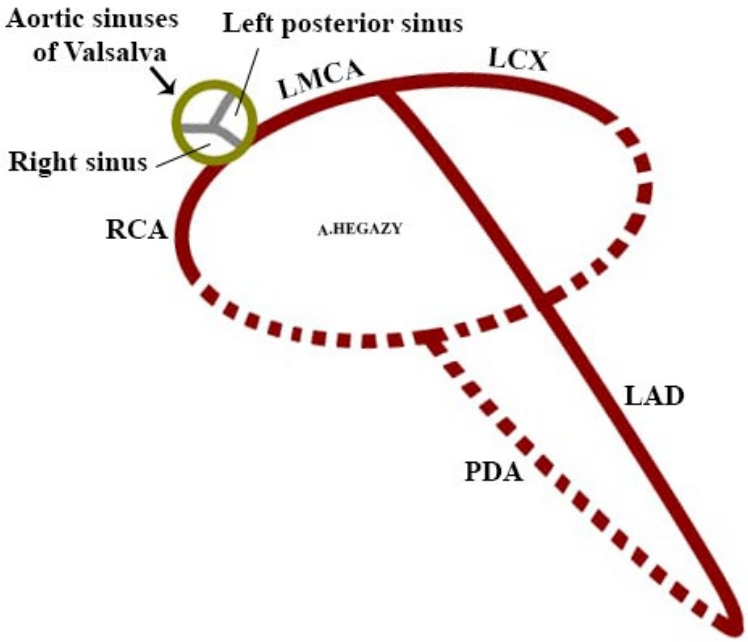

Fig. 3.- Diagram showing arrangement of the main coronary arteries.

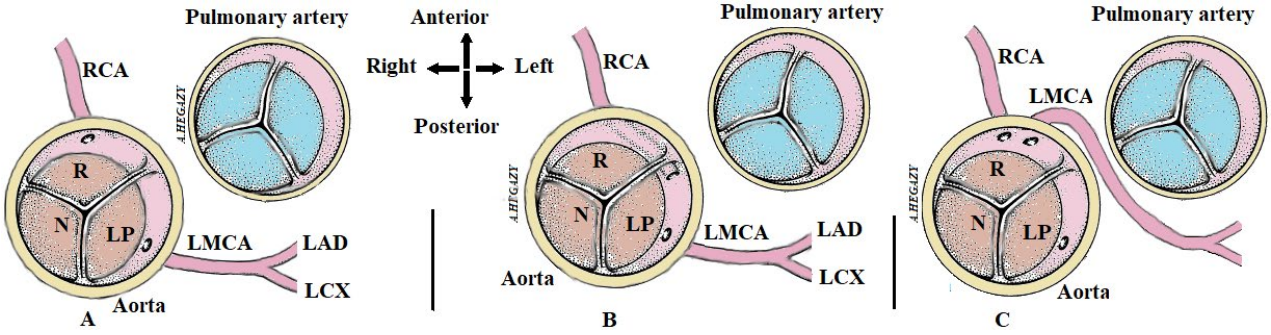

Fig. 4.- Diagrams showing origin of coronary arteries: **A)** RCA arising from right sinus of Valsalva (R), LMCA from left posterior sinus (LP) and none arising from the right posterior sinus (N). **B)** RCA arising from LP with part passing intramural "within wall of aorta". **C)** LMCA arising from R and coursing in-between aorta and pulmonary trunk.

artery. It arises from RCA at the crux of the heart, passing anteriorly along the base of interatrial septum to supply the AV node in about 55% of cases, bundle of Hiss and parts of interventricular septum surrounding it. A third artery arises from RCA at the crux of the heart, passing to the left side of AV sulcus to supply the diaphragmatic surface of LV (El-Maasarany and Aboul-Enein, 2009; Iaizzo, 2015).

Another (Kugel) artery has been described by Kugel in 1927, arising from left circumflex artery (Kugel, 1927). Other authors did not accept the presence of Kugel artery; and instead, they described small collateral connections arising from both LCX and RCA, or from one of them connecting the anterior and posterior arteries (McAlpin, 1975). However, another study found such artery in only 6% of cases originating from LCX or RCA (Nerantzis et al., 2004).

2. Anatomy of left coronary artery

The left coronary artery emerges from the posterior left the sinus of Valsalva. It passes to the left side behind the pulmonary trunk in-between it and the left auricle. It runs in the anterior part of the atrioventricular sulcus (Hegazy, 2018). This part, from its origin to bifurcation into LCX and LAD, is called the left main coronary artery (LMCA). Its length is about 5-10 mm. Sometimes the LMCA trifurcates into LCX, LAD and RIM. The presence of RIM represents the most common variation of left coronary artery; its incidence ranges from 15 to 30% of populations (O'Brien et al., 2007; Kosar et al., 2009). It is situated intermediate in a position between the two branches in case of bifurcation, namely LCX and LAD, so it is called ramus intermedius. It is also named left diagonal artery.

3. Left anterior descending artery (LAD)

It represents the largest branch arising from LMCA and carries almost 50% of blood from coronary circulation (Rehman et al., 2021). It turns around the left aspect of the pulmonary trunk to descend into the anterior interventricular sulcus towards the apex of heart. At the lower margin of the heart, it turns posteriorly to run shortly in the posterior interventricular sulcus, where it anastomoses with termination of PDA (Hegazy, 2018). Myocardium is often seen on CT to bridge over the LAD. Most cases of myocardial bridging (MB) are asymptomatic. It rarely could lead to ischemia, which might result from compression of the part of the artery by crossing myocardium at the systole (Berry et al., 2002). Branches arising from LAD include diagonals and septal perforators. Septal branches pass through the interventricular septum to supply its anterior two-thirds. On the other hand, diagonal arteries pass laterally to supply the myocardium of anterior aspect and free wall of LV (Kini et al., 2007; O'Brien et al., 2007). The

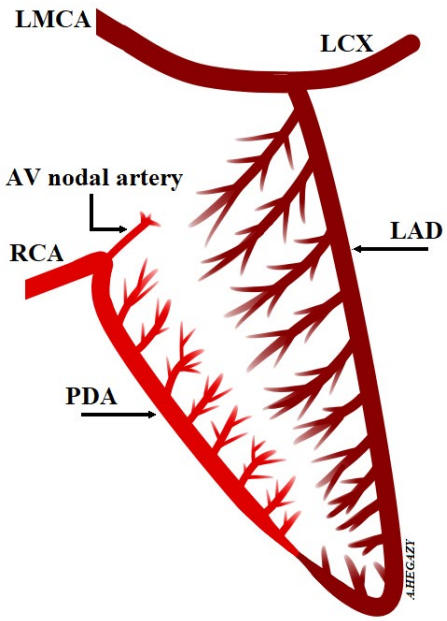

Fig. 5.- Diagram showing distribution of arterial blood supply of interventricular septum in most of cases.

first diagonal branch arising from LAD represents the main diagonal artery and is mainly responsible for supplying arterial blood to the anterolateral aspect of LV. The diagonal arteries vary in number ranging from 2-9 (Medrano-Gracia et al., 2016). The term "diagonal" is given to these arteries, because they arise from their parent artery at an acute angle. The acute angle take-off of the branches makes them more prone to possible occlusion and subsequent of sudden death (Yuan, 2014). Loss of diagonal blood flow in patients with anterior ST-segment elevation myocardial infarction is independently associated with higher incidence of major adverse cardiac events, and all-cause death (Zhang et al., 2020). In addition to origin of CA with acute angle, the anatomic features that could be associated with sudden cardiac death might also include the slit-like orifice and intramural course (Agarwal et al., 2017).

The LAD is divided for description into 3 parts: proximal, middle and distal parts. There is more than one definition to describe LAD parts. The first is based on septal branches. The proximal part extends from its origin to the origin of its first main branch (the significant diagonal or first septal perforator) (Kini et al., 2007; Zhang et al., 2020). The middle portion is extending from origin of its first branch to the point where the artery forms an acute angle coinciding with the origin of the second septal branch. If such acute angle is not marked, the middle and distal portions are marked from each other by a point mid-way between the first septal artery and apex of heart. The distal portion is the segment distal to the apex of the heart (Kini et al., 2007; O'Brien et al., 2007). Another possibility of defining parts of LAD is depending on diagonal branches: Proximal LAD is before 1st diagonal, Mid LAD between 1st and 2nd diagonals and distal LAD after the 2nd diagonal branch (Sundaram et al., 2009).

4. Left circumflex artery (LCX)

It is the smallest branch of LMCA, but appears as the direct continuation of left CA. It continues in the coronary sulcus to pass in its posterior, where its terminal branches might form an anastomosis with the RCA coming from the opposite side (Hegazy, 2018). It gives the left marginal artery, passing on the left side of the heart to supply myocardium of LV. It also gives small branches to supply the anterior and inferior aspects of LV. The LCX could be divided for description into two: "proximal and distal" parts. The parts are marked by the common branch arising from LCX, called left marginal artery (O'Brien et al., 2007).

5. Ramus intermedius artery (RIM)

It represents the most common variation in the anatomy of the left coronary artery, where it terminates by trifurcation instead of the common bifurcation. It arises and passes in-between the LAD and LCX. When present, it usually passes towards the LV free margin; and it might replace some branches of these two arteries in supplying the anterolateral aspect of LV (O'Brien et al., 2007; Kultida et al., 2018). Its course might be similar to that of the diagonal branches of LAD (O'Brien et al., 2007).

DOMINANCE OF CORONARY ARTERIES

Although each CA supplies the corresponding side of the myocardium, there is some overlap between the Cas, especially in the interventricular septum (Pappano and Wier, 2013). This could be represented as a CA dominance. This dominance depends on the supply of the posterior "inferior" one third of the interventricular septum. As previously mentioned, this part is supplied by the RCA in most (about 85%) hearts. In this case, the RCA is the dominant artery, a condition called right dominance. In the less common cases, the posterior part of the septum is supplied by branches of left CA, where the LCX crosses to the posterior interventricular groove, supplying the posterior part of interventricular septum in about 7.5% of cases, a condition named left dominance. In the remaining 7.5% of cases, the posterior "inferior" interventricular septum is perfused by branches from both RCA and LCX: this case is called codominance (Reagan et al., 1994; Kim et al., 2006). In other reports, the range of dominance were as follows: RCA: 50% - 91.4%; left CA: 7.2% - 20% and codominance: 1.4% - 30% (Table 1). However, all of them agreed regarding the dominance of RCA.

Table 1. Incidence of CA dominance.

Study	RCA dominance %	Left CA dominance %	Codominance %
Angelini et al., 2002	89.1	8.4	2.5
Pappano and Wier, 2013	50	20	30
Michalowska et al., 2016	84.1%	11.9%	4%
Kultida et al., 2018	91.4	7.2	1.4
Rafiq et al., 2020	75.8	19.8	4.8

Although considered part of normal contrast, determination of coronary dominance is very important for diagnostic imaging, prognosis, and planning for surgical treatment of myocardial ischemia or infarction (Waziri et al., 2016; Selcuk et al., 2020). It has been shown that left CA is frequently associated with poor prognosis in patients with CAD and percutaneous interventions; therefore, its evaluation should be an integral part of outpatient follow-up after elective coronary artery bypass grafting (Selcuk et al., 2020).

CORONARY ANASTOMOSES

The small terminal branches of the coronary arteries anastomose together, but the anastomosis is insufficient to give an adequate arterial blood supply if one of them is occluded. This case is called functional end-arteries (Wineski, 2019). Such anastomosis is present in fetal life and diminishes postnatally. However, it could be re-established if the atheroma development is a gradual event giving a chance for the anastomosis to proliferate. Development of atheromatous is initiated by the presence of low-density lipoproteins (LDL) carrying cholesterol in blood. Other factors that can be risk factors include smoking, hypertension, diabetes mellitus, inflammation and clonal hematopoiesis (Libby et al., 2019; Hegazy et al., 2022). Type 2 diabetes is not only a risk factor for the development of atheroma, but also hinders the development of collateral coronary vessels that might occur through different mechanisms including angiogenesis and arteriogenesis (Shen et al., 2018). It has been suggested that high-density lipoproteins can rescue impaired angiogenesis of diabetes mellitus by modulating the metabolic reprogramming of endothelial cells (Primer et al., 2020). The risk factors also include the sedentary life commonly associated with hyperlipidemia (Yusuf et al., 2004). Furthermore, excessive alcohol consumption could be a precipitating factor for atheromatous development (Ilic et al., 2018).

Seiler et al. (2013) added that the coronaries have extensive collateral anastomoses, being able to prevent myocardial ischemia during a brief occlusion in about 25% of individuals. Coronary atheromatous block is considered a chronic type if it has persisted for at least 3 months. It affects the main coronary arteries, but differ in their incidence. RCA is affected in 43%-55%, LAD in 24% and finally LCX is affected in 17%-20% of cases of chronic coronary occlusion (Mohammed and Khan, 2022). Development of well-developed collaterals is associated with improved patient survival (Elias et al., 2017). Furthermore, Wustmann et al. (2003) reported in their study of 100 patients that about one-fifth to one-fourth of the population have collaterals to accommodate blood flow in the event of short vascular occlusion.

The anastomoses include three main sites. The first is found in the interventricular septum between the septal branches of LAD and PDA. The second site is located in the posterior interventricular sulcus between the terminal branches of LAD and PDA. The third anastomosis could be found in the posterior aspect of coronary sulcus between the terminations of LCX and RCA (Figs. 2, 6) (Hegazy, 2018). Moreover, the LAD gives anastomosing branch that joins the branch of RCA named conus artery to form a collateral anastomosis. Such anastomosis is called Vieussens' circle (Iaizzo, 2015). However, growth of collateral vessels "arteriogenesis" and formation of new capillaries "angiogenesis" may occur as a life-saving adaptive mechanism in response to arterial occlusion and subsequent ischemia (Schaper and Scholz, 2003).

Well-developed coronary anastomoses form an alternative pathway for blood supply to a part of myocardium that is at risk from ischemia. Therapeutic promotion of the anastomotic collaterals could have clinical value in some patients with CAD who do not benefit from CA by-pass or percutaneous CA intervention (Seiler et al., 2013). This might be achieved through endurance exercise training (Zbinden et al., 2004), external counterpulsation (Gloekler et al., 2010) and therapeutic management using granulocyte-colony-stimulating factor (Meier et al., 2009; Seiler et al., 2013). It has been suggested that exercise programs can enhance coronary collateral growth even for stenosed arteries subject to PCI (Zbinden et al., 2007; Laughlin et al., 2012).

NORMAL CALIBER OF CORONARY ARTERIES

Knowing the normal lumen diameter of the coronaries at a given location is the first step to diagnose condition of blood flow and estimation of severity of coronary diseases. It is considered to be more informative than the traditional method for estimating the percent stenosis that is based on the ratio of a focal diameter to the nearby normal finding (Dodge et al., 1992).

Divia Paul et al (2018) agreed that the CA calibers in males are greater than those found in females. They added that the calibers decrease with increase in body-mass index. Normal caliber of coronary arteries and their major branches have been estimated using catheter angiography. The average range in males is about 4 mm while it is 3 mm in females. It also varies from one artery to another, ranging from a mean of 5 mm in LMCA in males to 2 mm in PDA in females (O'Brien et al., 2007). Dodge et al. (1992) stated that the normal diameter of LMCA is 4.5±0.5 mm; LAD is 3.7+0.4 mm at its proximal part and 1.9+0.4 mm at its distal part; and LCX is ranging from 3.4±0.5 and 4.2±0.6 mm. For RCA, the diameter in proximal part ranges from 3.9±0.6 to 2.8±0.5 mm. Another study showed that the mean values of LMCA are 3.5±0.8 mm diameter and 10.5±5.3 mm length. Its angulation is 75±23° in cases of bifurcation and increased to about 89±21° in presences of RIM, cases called trifurcation (Medrano-Gracia et al., 2016). Regarding diagonal arteries arising from LAD, vessel of a diameter more than 2 mm is regarded as the main one (Zhang et al., 2020). The caliber of the main CA might assist in identifying the dominant artery. In case of left dominance, the caliber of the LCX and LAD is larger than that of RCA. At the same time, the proximal RCA

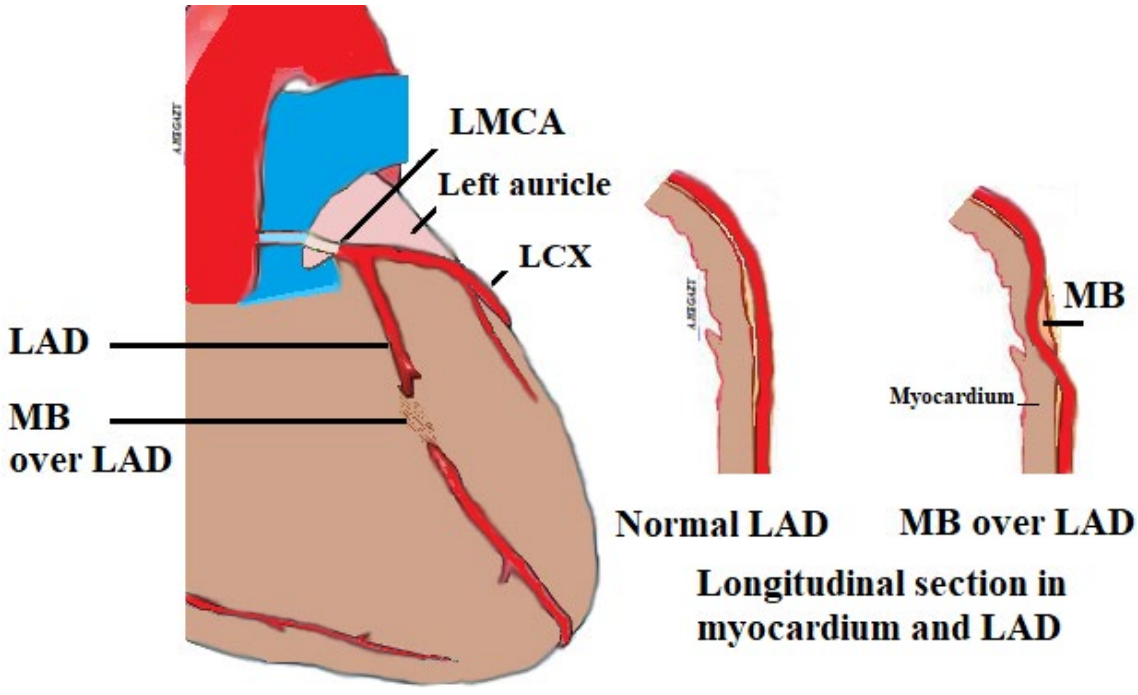

Fig. 6.- Diagrams showing myocardial bridging over a segment of LAD.

diameter is larger than the two terminal branches of LMCA in case of right CA dominance. Detection of small caliber of CA is suggested as an indicator of hypoperfusion in absence of signs of myocardial ischemia. Its evaluation can also reduce false results in the case of ischemia (Pilz et al., 2011).

CORONARY ARTERY ANOMALIES

Coronary artery anomaly is a rare condition. In general, the anomalies of coronaries have been reported to be about 0.3% to 1.3% of healthy population; and discovered incidentally at routine investigations (Angelini et al., 2002; Yildiz et al., 2010). Its incidence has been noticed to be about 0.17% in autopsy investigations (Alexander and Griffith, 1956), 1.2% in angiographically investigated cases (Engel et al., 1975) and 2.33% of population evaluated with multidetector-row computed tomography (Graidis et al., 2015). However, Cademartiri et al. (2008) reported a relatively higher incidence in multi-ethnic Dutch population reaching about 18.4%. Despite the general rare incidence, about one-fifth of such cases could produce life-threatening clinical manifestations such as syncope, arrythmias, myocardial infarction, or even sudden death in young athletes (Maron, 2003; Datta et al., 2005). There is a significant difference in incidence of CA anomalies between both genders. However, the authors reporting gender differences have disagreed regarding who is affected more. Aydar et al. (2011) stated that females are more affected than males. However, others reported the reverse; most of investigated cases of CA anomalies are males (Graidis et al., 2015; Yousif et al., 2019).

Anomalies in origin of main coronary arteries

Despite the uncommon incidence, awareness of the variations in origin of coronaries is important to be remembered and should be put into consideration at CT angiographic investigations to avoid misinterpretations (Kini et al., 2007). The unusual variations of main coronary arteries' origin were found in a percentage of about 0.3% to 0.6% in patients referred to coronary catheterization (Yamanaka and Hobbs, 1990; Harikrishnan et al., 2002; Angelini et al., 2002).

The anomaly of RCA origin is typically from the left sinus of Valsalva (Kini et al., 2007). On the other hand, left CA might arise from the right sinus just above the origin of RCA (Barth and Roberts, 1986; Paolillo et al., 2006). In this case, the LMCA passes anomalously between the two main arteries named the aorta and pulmonary trunk (Fig. 4). This interarterial course of LMCA could be associated with exertional angina and episodes of syncope (Barth and Roberts, 1986). The origin of CA from the unusual aortic sinus with coursing in-between aorta and pulmonary trunk might be responsible for causing sudden death among young athletes with incidence up to about 20% (Basso et al., 2000; Angelini et al., 2002). The CA originating from the opposite sinus might be also intramural "inside wall of aorta", transseptal (or subpulmonic), prepulmonic and retroaortic in its course to reach its dependent area of myocardium (Agarwal et al., 2017). Symptomatic patients undergoing abnormal origin of CA from opposite side might be managed with conservative medical treatment, stent deployment for coronary angioplasty or repair by surgical interference (Angelini, 2007).

Paolillo et al. (2006) also described an origin for RIM early from LMCA before its bifurcation and runs in an unusual course, where it passes to the left side beneath the middle LAD, and emerges epicardially to reach the left free aspect of heart.

However, there are other reported anomalies. In their study of 16,573 patients, the authors stated that the most common abnormality accounting for 0.17% of the total cases and more than 50% of the abnormalities encountered was the abnormal origin of LCX from RCA or the right sinus of Valsalva (Yuksel et al., 2013). Furthermore, the anomalies include a rare case where RCA and other 3 arteries, LCX, LAD and RIM, arise from the right sinus with four separate ostia (Bartorelli et al., 1994; Asciutto et al., 2016; Choudhary et al., 2019). Ludhwani and Woo (2019) reported a case with single RCA arising from right sinus and giving rise to LMCA that passes in a pre- pulmonic course and terminates by trifurcation. Choudhary et al., 2019 stated that none of them pass between the pulmonary trunk and aorta. They found that LCX passes behind aorta, and LAD and RIM run

in an anterior course without causing significant obstructive lesion. However, the course of LAD in-between pulmonary trunk and aorta has been noticed to be associated with increased risk of myocardial ischemia and sudden death (Bartorelli et al., 1994; Asciutto et al., 2016).

On the other hand, some authors reported a case of CAs arising from abnormal single trunk (Barendra et al., 1995). They reported a case of single CA originating from the left sinus of Valsalva. The RCA arises from its proximal portion; while its distal part trifurcates into LAD, RIM and LCX. Similarly, Abdulshakour et al. (2019) recorded a single CA but arising from the right sinus of Valsalva. They added that cases of single CA might represent a difficulty in performing coronary catheterization as all coronaries arise from a single sinus.

Rarely, the coronary arteries might originate from the pulmonary artery. The incidence of CA origin from pulmonary artery instead of the normal arising from aorta is up to 1% of population. The anomalous origins of LMCA and RCA are about 0.25 to 0.5% and 0.002% of all congenital heart anomalies, respectively (Vergara-Uzcategui et al., 2020). In addition to the anomalous origins of LMCA and RCA, this case might occur with LAD or LCX. However, LMCA is the most common of these rare cases. It could lead to death in 90% of cases within the first year of life if not treated (Wesselhoeft et al., 1968; Agarwal et al., 2017).

High take-off CAs is another rare cardiac abnormality with a prevalence of about 0.2%, of cases. In this case, the CA arises above the sinutubular junction with a distance up to 5 cm. High take-off RCA is the most common condition in this category of abnormalities, forming about 85% of total cases (Loukas et al., 2016). Cases of a distance of ≥ one cm are clinically relevant (Loukas et al., 2009). The main clinical concern in high take-off CA is the decreased perfusion that occurs with physical exertion leading to myocardial ischemia. The high take-off CA has been reported to be a cause of sudden cardiac death. Moreover, it is necessary to identify such anomalies to avoid clamping or occluding the CA in interventional therapy or surgery (Deng et al., 2017).

MYOCARDIAL BRIDGING

Myocardial bridging (MB) was first described in the year 1737. It has been defined as one or more segments of epicardial CA that pass through the myocardium "having intramyocardial course" (Mohlenkamp et al., 2002). Although it is frequently silent, it might form a risk factor for coronary artery disease (CAD). This is because the overlying part of the myocardium is prone to compression at the cardiac systole. Its incidence is higher in cases of CADs reaching about 7.4% vs 2.8% in others (Cademartiri et al., 2008). The authors found its prevalence to be 10.9% in their study using computed tomography coronary angiography. On average, the MB affects about one-third of adult populations. The most common site for MB is found in the middle segment of LAD (Fig. 6). It commonly investigated angiographically in LAD at a depth of 1-10 mm with an average length about 10 to 30 mm. The MB also might comprise the marginal and diagonal arteries with an incidence of 40% and 18%, respectively (Mohlenkamp et al., 2002).

CA ANEURYSMS

Local dilatation of an artery to more than 1.5 times diameter of its adjacent part is considered an abnormal finding called aneurysm. If such dilatation is diffuse, it defined as ectasia (O'Brien et al., 2007).

CA aneurysm is a rare anomaly, found in 0.3%–4.9 % of cases undergoing angiography (Swaye et al., 1983; Sheikh et al., 2019). The presence of coronary aneurysm or ectasia is commonly associated with poor outcome irrespective presence of coronary atherosclerosis or not (Warisawa et al., 2015; Doi et al., 2017). Individuals with aneurysms are at risk of developing myocardial ischemia (O'Brien et al., 2007).

The most frequent CA to be affected is the proximal and middle portions of RCA (68%), followed by the proximal segment of LAD (60%) and LCX) (50%). CA aneurysm of the LMCA is rare and occurs in only 0.1% of cases (Swaye et al., 1983; Sheikh et al., 2019).

It might be congenita,l but atherosclerosis is the commonest factor in its incidence in adults.

Cases related to atherosclerosis usually appear at later stages of life than those with congenital or inflammatory etiology (ElGuindy and ElGuindy, 2017). The pathogenesis of CA aneurysm is not clearly understood. However, the sequence might be similar to that occurring in large arteries of other parts of body where there may be weakness of segment of arterial wall either congenital or acquired followed by its progressive dilatation (Sheikh et al., 2019).

CONGENITAL CORONARY ARTERIAL FISTULAS

These are rare abnormal communications between coronary arteries and cardiac chambers or other structures like veins without intervening capillaries (Yun et al., 2018). These cases account about 0.08% to 0.4% of congenital heart anomalies, and 0.3% to 0.8% of indications for catheterization cases (Gowda et al., 2006; Butt et al., 2019).

The majority of cases of coronary fistulas are congenital. However, they might occur following cardiac surgery (Qureshi, 2006). It has been reported that about 90% of cases of fistulas could occur in RCA that joins the RA (Sharland et al., 2016). However, other authors mentioned that the fistulas in the left coronary artery amounted to about 50% of all cases of fistulas, while RCA cases are about 38%, and the remaining 12% occurred in both left coronary artery and RCA. Both RCA and LMCA fistulas mostly drain into the right side of the heart, such as the RA, RV (Fig. 7), pulmonary trunk and coronary sinus (Agarwal et al., 2017).

They are usually asymptomatic in the first two decades, particularly when small. Later on, the incidence of complaints and complications increases. Such complications include coronary steal phenomenon, thrombosis and embolism, atrial fibrillation, rupture, heart failure, endocarditis and arrhythmias. Spontaneous rupture of aneurysmal fistula might occur causing haemopericardium (Skimming and Walls, 1993; Qureshi, 2006). There is often a continuous murmur, and this is highly suggestive of presence of CA fistulas. Its differential diagnosis includes pulmonary or arteriovenous fistulas, persistent ductus arteriosus and ruptured aneurysm of sinus of Valsalva. Its diagnosis depends mainly on coronary angiography but concomitant cardiac catheterization also could help in precise anatomy delineation and assessment of hemodynamics. Treatment of symptomatic patients include surgical repair and transcatheter embolization (Gowda et al., 2006).

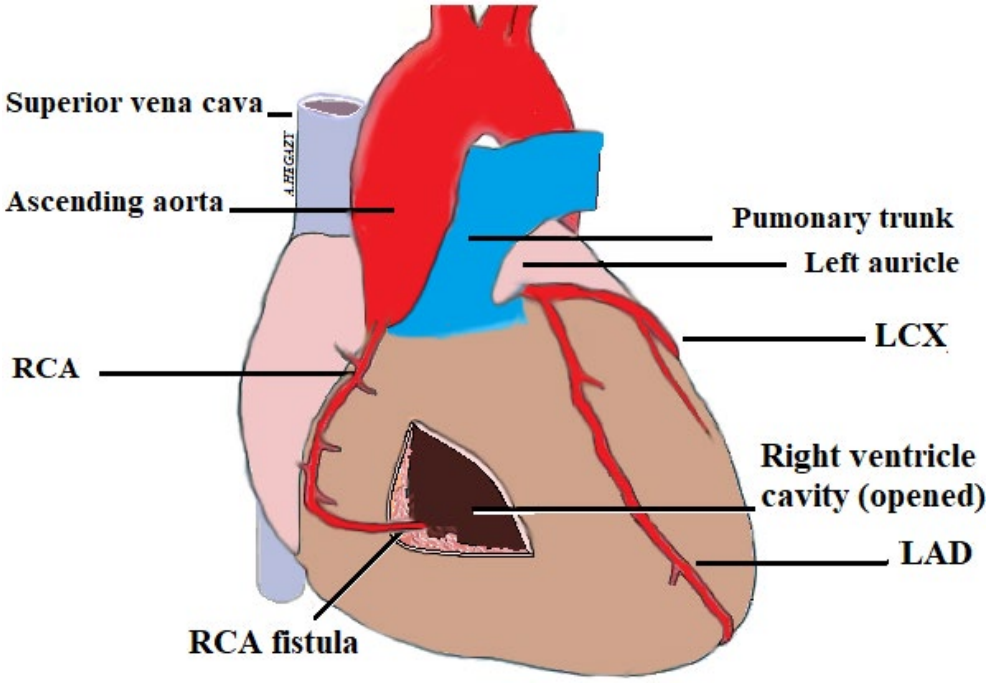

Fig. 7.- Diagram showing RCA fistula into cavity of right ventricle.

CONCLUSIONS

Knowledge of CA anatomy and its differences is critical to the proper diagnosis and treatment of CAD. Although there is an anatomical anastomosis between the terminal branches of the coronary arteries, it lacks the function. Therefore, coronaries are considered functional end-arteries; occlusion in any branch is not compensated by the anastomosis, resulting in the death of the corresponding part of the myocardium. The arteries form an epicardial horizontal ring with a half- loop extending downwards from the ring. The ring is formed by RCA, LMCA and LCX, while the loop comprises the LAD and PDA. Each CA supplies the corresponding side of the heart. In addition, RCA artery gives blood supply to SA node and AV node; and left coronary artery supplies the anterior two-thirds of interventricular septum. The posterior third of interventricular septum is supplied according to the dominance. It is supplied by the RCA in most (about 85%) of populations, a case is called right dominance. On the other hand, the remaining 15% include left dominance where this part is supplied by left coronary artery and codominance supplied by both coronary arteries. The most common variant encountered in this context is trifurcation of LMCA with an additional branch called RIM found to originate in the angle between LAD and LCX. Significant anomalies also include unusual CA origin, myocardial bridging, CA fistula and aneurysm.

Identification of anatomy of CA is recommended before any CA therapeutic intervention. Misinterpretation or misdiagnosis of such variants or anomalies may lead to technical difficulties during coronary angioplasty and interventional procedures or cause significant complications in CA surgery. Furthermore, identification of normal anatomical asymmetry facilitates stent design and selection of the optimal treatment strategy, hence the importance of defining normal and abnormal coronary anatomy.

AUTHORS' CONTRIBUTIONS

All authors share in all steps of the article.

ACKNOWLEDGEMENTS

All diagrams in figures are drawn by the 5th author "AAH".

REFERENCES

ABDULSHAKOUR BM, SAEED M, TAHER MM (2019) Anomalous coronary artery anatomy with a single coronary ostium arising from the right coronary: a case report and literature review. *Int Med Case Rep J*, 12: 135-141.

AGARWAL PP, DENNIE C, PENA E, NGUYEN E, LABOUNTY T, YANG B, PATEL S (2017) Anomalous Coronary Arteries That Need Intervention: Review of Pre- and Postoperative Imaging Appearances. *Radiographics*, 37(3): 740-757.

ALEXANDER RW, GRIFFITH GC (1956) Anomalies of the coronary arteries and their clinical significance. *Circulation*, 14: 800-805.

ANGELINI P (2007) Coronary artery anomalies: an entity in search of an identity. *Circulation*, 115(10): 1296-1305.

ANGELINI P, VELASCO JA, FLAMM S (2002) Coronary anomalies: incidence, pathophysiology, and clinical relevance. *Circulation*, 105(20): 2449-2454.

ASCIUTTO S, LA FRANCA E, CIRRINCIONE G, CARUSO M (2016) Anomalous origin of all three coronary arteries from right sinus of Valsalva. *Indian Heart J*, 68 (Suppl 2): S85-S87.

AYDAR Y, YAZICI HU, BIRDANE A, NASIFOY M, NADIR A, ULUS T, GOKTEKIN O, GORENEK B, UNALIR A (2011) Gender differences in the types and frequency of coronary artery anomalies. *Tohoku J Exp Med*, 225(4): 239-247.

BARENDRA C, CHAN CN, TAN A (1995) Single coronary artery: a case report and review of current literature. *Singapore Med J*, 36(3): 335-337.

BARTH CW, ROBERTS WC (1986) Left main coronary artery originating from the right sinus of Valsalva and coursing between the aorta and pulmonary trunk. *J Am Coll Cardiol*, 7(2): 366-373.

BARTORELLI AL, CAPACCHIONE V, RAVAGNANI P, PEPI M (1994) Anomalous origin of the left anterior descending and circumflex coronary arteries by two separate ostia from the right sinus of Valsalva. *Int J Cardiol,* 44(3): 294-298.

BASSO C, MARON BJ, CORRADO D, THIENE G (2000) Clinical profile of congenital coronary artery anomalies with origin from the wrong aortic sinus leading to sudden death in young competitive athletes. *J Am Coll Cardiol,* 35(6): 1493-1501.

BECKER AE (1995) Congenital coronary arterial anomalies of clinical relevance. *Coron Artery Dis,* 6: 187-193.

BERRY JF, VON MERING GO, SCHALFUSS C, HILL JA, KERENSKY RA (2002) Systolic compression of the left anterior descending coronary artery: a case series, review of literature, and therapeutic options including stenting. *Catheter Cardiovasc Interv*, 56: 58-63.

BUTT K, AGHA A, PARENTE R, LIMBACK J, BURT JR (2019) Anomalous coronary anatomy with fistula diagnosed on coronary computed tomography angiography. *Cureus*, 11(40): e4403.

CADEMARTIRI F, LA GRUTTA L, MALAGO R, ALBERGHINA F, MEIIBOOM WB, PUGLIESE F, MAFFEI E, PALUMBO AA, ALDROVANDI A, FUSARO M, BRAMBILLA V, CORUZZI P, MIDIRI M, MOLLET NR, KRESTIN GP (2008) Prevalence of anatomical variants and coronary anomalies in 543 consecutive patients studied with 64-slice CT coronary angiography. *Eur Radiol,* 18(4): 781-791.

CHOUDHARY R, BATRA A, MALIK V, MAHAJAN K (2019) All four coronary arteries arising separately from the right aortic sinus of Valsalva: rare anomaly. *BMJ Case Rep*, 12(4): e229498.

DATTA J, WHITE CS, GILKESON RC, MEYER CA, KANSAL S, JANI ML, ARILDSEN RC, READ K (2005) Anomalous coronary arteries in adults: Depiction at multidetector row CT angiography. *Radiology*, 235(3): 812-818.

DENG X, HUANG P, CHEN W, YANG X, LIU Q, XIAO Y, HE C (2017) An incidental encounter of a rare high take-off right coronary artery: A case report. *Medicine (Baltimore),* 96(45): e8614.

DIVIA PAUL A, ASHRAF SM, SUBRAMANYAM K, RAMAKRISHNA A (2018) Gender-associated dimensional differences among normal to non-flow limiting coronary artery dimensions. *Indian Heart J*, 70 (Suppl 3): S295-S298.

DODGE JT, BROWN BG, BOLSON EL, DODGE HT (1992) Lumen diameter of normal human coronary arteries. Influence of age, sex, anatomic variation, and left ventricular hypertrophy or dilation. *Circulation*, 86(1): 232-246.

DOI T, KATAOKA Y, NOGUCHI T, SHIBATA T, NAKASHIMA T, KAWAKAMI S, NAKAO K, FUJINO M, NAGAI T, KANAYA T, TAHARA Y, ASAUMI Y, TSUDA E, NAHAI M, NISHIMURA K, ANZAI T, KUSANO K, SHIMOKAWA H, GOTO Y, YASUDA S (2017) Coronary artery ectasia predicts future cardiac events in patients with acute myocardial infarction. *Arterioscler Thromb Vasc Biol,* 37(12): 2350-2355.

ELGUINDY MS, ELGUINDY AM (2017) Aneurysmal coronary artery disease: An overview. *Glob Cardiol Sci Pract*, 2017(3): e201726.

ELIAS J, HOEBERS LPC, VAN DONGEN IM, CLAESSEN BEPM, HENRIQUES JPS (2017) Impact of collateral circulation on survival in ST-segment elevation myocardial infarction patients undergoing primary percutaneous coronary intervention with a concomitant chronic total occlusion. *JACC Cardiovasc Interv*, 10(9): 906-914.

EL-MAASARANY SH, ABOUL-ENEIN FA (2009) Variant distribution of the right coronary artery at the crux of the heart (anatomical and multislice CT imaging study*). FASEB J,* 23: 641-647.

ENGEL HJ, TORRES C, PAGE HL (1975) Major variations in anatomical origin of the coronary arteries: angiographic observations in 4250 patients without congenital heart disease. *Cathet Cardiovasc Diagn*, 1: 157-169.

GLOEKLER S, MEIER P, DE MARCHI SF, RUTZ T, TRAUPE T, RIMOLDI SF, WUSTMANN K, STECK H, COOK S, VOGEL R, TOGNI M, SEILER C (2010) Coronary collateral growth by external counterpulsation: a randomised controlled trial. *Heart,* 96: 202-207.

GOWDA RM, VASAVADA BC, KHAN IA (2006) Coronary artery fistulas: clinical and therapeutic considerations. *Int J Cardiol*, 107(1): 7-10.

GRAIDIS C, DIMITRIADIS D, KARASVVIDIS V, DIMITRIADIS G, ARGYROPOULOU E, ECONOMOU F, GEORGE D, ANTONIOU A, KARAKOSTAS G (2015) Prevalence and characteristics of coronary artery anomalies in an adult population undergoing multidetector-row computed tomography for the evaluation of coronary artery disease. *BMC Cardiovasc Disord,* 15: 112.

HARIKRISHNAN S, JACOB SP, THARAKAN J, TITUS T, KUMAR VKA, BHAT A, SIVASAKARAN S, BIMAL F, MOORTHY KMK, KUMAR RP (2002) Congenital coronary anomalies of origin and distribution in adults: A coronary arteriographic study. *Indian Heart J*, 54: 271-275.

HEGAZY A (2018) *Clinical anatomy of thorax for medical students and doctors*. LAP, Lambert Academic Publishing.

HEGAZY AA (2019) Human anatomy: an inlet of medicine and surgery. *Int J Hum Anat,* 1(4): 1.

HEGAZY AA, HEGAZY MA (2020) Unusual case of absence of suprascapular notch and foramen. *Eur J Anat*, 24(4): 269-272.

HEGAZY MA, MANSOUR KS, ALZYAT AM, MOHAMMAD MA, HEGAZY AA (2022) Pathogenesis and morphology of coronary atheromatous plaque as an inlet for interpretation of diagnostic imaging. *J Cardiovasc Dis Res*, 13(1): 201-218.

IAIZZO PA (2015) *Handbook of Cardiac Anatomy, Physiology, and Devices*. 3rd edition. DOI 10.1007/978-3-319-19464-6. Springer International Publishing Switzerland.

ILIC M, GRUJICIC SIPETIC S, RISTIC B, ILIC I (2018) Myocardial infarction and alcohol consumption: A case-control study. *PLoS One*, 13(6): e0198129.

KASTELLANOS S, AZNAOURIDIS K, VLACHOPOULOS C, TSIAMIS E, OIKONOMOU E, TOUSULIS D (2018) Overview of coronary artery variants, aberrations and anomalies. *World J Cardiol*, 10(10): 127-140.

KIM SY, SEO JB, DO KH, HEO JN, LEE JS, SONG JW, CHOE YH, KIM TH, YONG HS, CHOI SI, SONG KS (2006) Coronary artery anomalies: classification and ECG-gated multi-detector row CT findings with angiographic correlation. *Radiographics*, 26(2): 317-333.

KINI S, BIS KG, WEAVER L (2007) Normal and variant coronary arterial and venous anatomy on high-resolution CT angiography. *AJR Am J Roentgenol*, 188(6): 1665-1674.

KOSAR P, ERGUN E, OZTURK C, KOSAR U (2009) Anatomic variations and anomalies of the coronary arteries: 64-slice CT angiographic appearance. *Diagn Interv Radiol*, 15(4): 275-283.

KUGEL MA (1927) Anatomical studies on the coronary arteries and their branches. I. Arteria anastomotica auricularis magna. *Am Heart J,* 3: 260-270.

KULTIDA CHY, RUEDEEKORN SW, KEERATI HS (2018) Anatomic variants and anomalies of coronary arteries detected by computed tomography angiography in southern Thailand. *Med J Malaysia*, 73(3): 131-136.

LAUGHLIN MH, BOWLES DK, DUNCKER DJ (2012) The coronary circulation in exercise training. *Am J Physiol Heart Circ Physiol*, 302(1): H10-23.

LIBBY P, BURING JE, BADIMON L, HANSSON GK, DEANFIELD J, BITTENCOURT MS, TOKGOZOGLU L, LEWIS EF (2019) Atherosclerosis. *Nat Rev Dis Primers*, 5(1): 56.

LOUKAS M, REBECCA G, ANDALL RG, KHAN AZ, PATEL K, MURESIAN H, SPICER DE, TUBBS RS (2016) The clinical anatomy of high take-off coronary arteries. *Clin Anat*, 29(3): 408-419.

LOUKAS M, WARTMANN CT, TUBBS RS, APAYDIN N, LOUIS RG, EASTER L, BLACK B, JORDAN R (2009) The clinical anatomy of the sinutubular junction. *Anat Sci Int,* 84: 27-33.

LUDHWANI D, WOO V (2019) Anomalous origin of left main coronary artery from right coronary artery in a patient presenting with inferior wall myocardial infarction: a case report and literature review. *Eur Heart J Case Rep*, 3(4): 1-6.

MARON BJ (2003) Sudden death in young athletes. *N Engl J Med*, 349: 1064-1075.

MCALPIN WA (1975) *Heart and coronary arteries: an anatomical atlas for clinical diagnosis, radiological investigation, and surgical treatment*. Springer-Verlag, New York.

MEDRANO-GRACIA P, ORMISTON J, WEBSTER M, BEIER S, YOUNG A, ELLIS C, WANG C, SMEDBY Ö, COWAN B (2016) A computational atlas of normal coronary artery anatomy. *Euro Intervention*, 12(7): 845-854.

MEIER P, GLOEKLER S, DE MARCHI S, INDERMUEHLE A, RUTZ T, TRAUPE T, STECK H, VOGEL R, SEILER C (2009) Myocardial salvage through coronary collateral growth by granulocyte colony-stimulating factor in chronic coronary artery disease: a controlled randomized trial. *Circulation,* 120: 1355-1363.

MICHALOWSKA IM, HRYNIEWIECKI T, KWIATEK P, STOKLOSA P, SWOBODA-RYDZ U, SZYMANSKI P (2016) Coronary artery variants and anomalies in patients with bicuspid aortic valve. *J Thorac Imaging*, 31(3): 156-162.

MOHAMMED M, KHAN MAB (2021) Chronic Coronary Occlusion. 2021 Jul 21. In: StatPearls [Internet]. Treasure Island (FL): *StatPearls Publishing*, 2022. PMID: 32809734.

MOHLENKAMP S, HORT W, GE J, ERBEL R (2002) Update on myocardial bridging. *Circulation*, 106(20): 2616-2622.

NERANTZIS CE, MARIANOU SK, KOULOURIS SN, AGAPITOS EB, PAPAIOANNOU JA, VLAHOS LJ (2004) Kugel's artery: an anatomical and angiographic study using a new technique. *Tex Heart Inst J*, 31(3): 267-270.

O'BRIEN JP, SRICHAI MB, HECHT EM, KIM DC, JACOBS JE (2007) Anatomy of the heart at multidetector CT: what the radiologist needs to know. *Radiographics*, 27(6): 1569-1582.

PAOLILLO V, GASTALDO D, VAUDAANO G (2006) An unusual course of the ramus intermedius: shown by multislice computed tomographic coronary angiography. *Tex Heart Inst J*, 33(3): 406-407.

PAPPANO AJ, WIER WG (2013) *Cardiovascular Physiology* (Tenth edition), Elsevier.

PILZ G, HEER T, GRAW M, ALI E, KLOS M, SCHECK R, ZEYMER U, HOFLING B (2011) Influence of small caliber coronary arteries on the diagnostic accuracy of adenosine stress cardiac magnetic resonance imaging. *Clin Res Cardiol*, 100(3): 201-208.

PRIMER KR, PSALTIS PJ, TAN JTM, BURSILL CA (2020) The role of high-density lipoproteins in endothelial cell metabolism and diabetes-impaired angiogenesis. *Int J Mol Sci*, 21(10): 3633.

QURESHI SA (2006) Coronary arterial fistulas. *Orphanet J Rare Dis*, 1: 51.

RAFIQ S, MOHIUDDIN IN, GAIZAN M (2020) Coronary anomalies and anatomical variants detected by coronary computed tomographic angiography in Kashmir, India. *Int J Res Med Sci*, 8(2): 584.

REAGAN K, BOXT LM, KATZ J (1994) Introduction to coronary arteriography. *Radiol Clin North Am,* 32: 419-433.

REHMAN I, KERNDT CC, REHMAN A (2021) Anatomy, thorax, heart left anterior descending (LAD) artery. 2021 Jul 26. In: *StatPearls [Internet]. Treasure Island (FL)*. StatPearls Publishing.

SCHAPER W, SCHOLZ D (2003) Factors regulating arteriogenesis. *Arterioscler Thromb Vasc Biol,* 23(7): 1143-1151.

SEILER C, STOLLER M, PITT B, MEIER P (2013) The human coronary collateral circulation: development and clinical importance. *Eur Heart J*, 34(34): 2674-2682.

SELCUK E, CEVIRME D, BUGRA O (2020) Prognostic value of coronary dominance in patients undergoing elective coronary artery bypass surgery. *Braz J Cardiovasc Surg*, 35(4): 452-458.

SHARLAND GK, KONTA L, QURESHI SA (2016) Prenatal diagnosis of isolated coronary artery fistulas: progression and outcome in five cases. *Cardiol Young*, 26(5): 915-920.

SHEIKH AS, HAILAN A, KINNAIRD T, CHOUDHURY A, SMITH D (2019) Coronary artery aneurysm: Evaluation, prognosis, and proposed treatment strategies. *Heart Views*, 20(3): 101-108.

SHEN Y, DING FH, DAI Y, WANG XQ, ZHANG RY, LU L, SHEN WF (2018) Reduced coronary collateralization in type 2 diabetic patients with chronic total occlusion. *Cardiovasc Diabetol*, 17(1): 26.

SKIMMING JW, WALLS JT (1993) Congenital coronary artery fistula suggesting a "steal phenomenon" in a neonate. *Pediatr Cardiol*, 14: 174-175.

SUNDARAM B, PATEL S, BOGOT N, KAZEROONI EA (2009) Anatomy and terminology for the interpretation and reporting of cardiac MDCT: part 1, Structured report, coronary calcium screening, and coronary artery anatomy. *AJR Am J Roentgenol*, 192(3): 574-583.

SWAYE PS, FISHER LD, LITWIN P, VIGNOLA PA, JUDKINS MP, KEMP HG, MUDD JG, GOSSELIN AJ (1983) Aneurysmal coronary artery disease. *Circulation*, 67(1): 134-138.

VAHATALO J, HOLMSTROM L, PAKANEN L, KAIKKONEN K, PERKIOMAKI J, HUIKURI H, JUMTTILA J (2021) Coronary artery disease as the cause of sudden cardiac death among victims < 50 years of age. *Am J Cardiol*, 147: 33-38.

VERGARA-UZCATEGUI CE, DAS NEVES B, SALINAS P, FERNANDEZ-ORTIZ A, NUNEZ-GIL IJ (2020) Anomalous origin of coronary arteries from pulmonary artery in adults: a case series. *Eur Heart J Case Rep*, 4(2): 1-5.

WARISAWA T, NAGANUMA T, TOMIZAWA N, FUJINO Y, ISHIGURO H, TAHARA S, KURITA N, NOJO T, NAKAMURA S, NAKAMURA S (2015) High prevalence of coronary artery events and non-coronary events in patients with coronary artery aneurysm in the observational group. *Int J Cardiol Heart Vasc*, 10: 29-31.

WAZIRI H, JORGENSEN E, KELBAEK H, FOSBOL EL, PEDERSEN F, MOGENSEN UM, GERDS TA, KOBER L, WACHTELL K (2016) Acute myocardial infarction and lesion location in the left circumflex artery: importance of coronary artery dominance. *Euro Intervention*, 12(4): 441-448.

WESSELHOEFT H, FAWCETT JS, JOHNSON AL (1968) Anomalous origin of the left coronary artery from the pulmonary trunk: its clinical spectrum, pathology, and pathophysiology, based on a review of 140 cases with seven further cases. *Circulation*, 38(2): 403-425.

WINESKI LE (2019) Snell's Clinical Anatomy. 10th edition. Wolters Kluwer, Philadelphia.

WUSTMANN K, ZBINDEN S, WINDECKER S, MEIER B, SEILER C (2003) Is there functional collateral flow during vascular occlusion in angiographically normal coronary arteries? *Circulation*, 107(17): 2213-2220.

YAMANAKA O, HOBBS RE (1990) Coronary artery anomalies in 126,595 patients undergoing coronary arteriography. *Catheter Cardiovasc Diagn*, 21: 28-40.

YILDIZ A, OKCUN B, PEKER T (2010) Prevalence of coronary artery anomalous in 12,457 adult patients who underwent coronary angiography. *Clin Cardiol*, 33: E60-E64.

YOUSIF N, SHAHIN M, LUSCHER TF, OBEID S (2019) Gender differences in types, frequency, clinical manifestations and atherosclerotic burden of coronary artery anomalies. *Rev Recent Clin Trials*, 14(1): 41-46.

YUAN SM (2014) Anomalous origin of coronary artery: taxonomy and clinical implication. *Rev Bras Cir Cardiovasc*, 29(4): 622-629.

YUKSEL S, MERIC M, SOYLU K, GULEL O, ZENGIN H, DEMIRCAN S, YILMAZ O, SAHIN M (2013) The primary anomalies of coronary artery origin and course: A coronary angiographic analysis of 16,573 patients. *Exp Clin Cardiol*, 18(2): 121-123.

YUN G, NAM TH, CHUN EJ (2018) Coronary artery fistulas: pathophysiology, imaging findings, and management. *Radiographics*, 38(3): 688-703.

YUSUF S, HAWKEN S, OUNPUU S, DANS T, AVEZUM A, LANAS F, MCQUEEN M, BUDAJ A, PAIS P, VARIGOS J, LISHENG L (2004) INTERHEART Study Investigators. Effect of potentially modifiable risk factors associated with myocardial infarction in 52 countries (the INTERHEART study): case-control study. *Lancet*, 364(9438): 937-952.

ZBINDEN R, ZBINDEN S, MEIER P, HUTTER D, BILLINGER M, WAHL A, SCHMID JP, WINDECKER S, MEIER B, SEILER C (2007) Coronary collateral flow in response to endurance exercise training. *Eur J Cardiovasc Prev Rehabil*, 14(2): 250-257.

ZBINDEN R, ZBINDEN S, WINDECKER S, MEIER B, SEILER C (2004) Direct demonstration of coronary collateral growth by physical endurance exercise in a healthy marathon runner. *Heart*, 90: 1350-1351.

ZHANG S, DENG X, YANG W, XIA L, YAO K, LU H, GE L, SHEN L, SUN A, ZOU Y, QIAN J, GE J (2020) The diagonal branches and outcomes in patients with anterior ST-elevation myocardial infarction. *BMC Cardiovasc Disord*, 20(1): 108.

European Journal of Anatomy